



UNIVERSITY OF NAIROBI

**ATMOSPHERIC DISPERSION MODELLING OF
PARTICULATE MATTER AND GASEOUS EMISSIONS
FROM SELECTED CEMENT FACTORIES IN ATHI
RIVER MACHAKOS COUNTY KENYA**

BY

OMULAMI JERMAINE ONYANDO

I56/38808/2020

**A Thesis Submitted in Fulfilment of the Requirements for Award of the
Degree of Master of Science in Industrial Chemistry of the University of
Nairobi**

2023

DECLARATION


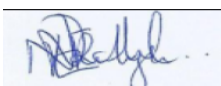

“I declare that this thesis is my original work and has not been submitted elsewhere for examination, award of a degree or publication. Where other people’s work or my work has been used, this has properly been acknowledged and referenced in accordance with the University of Nairobi’s requirements”.

Signature: 

Date: 26-08-2023

Omulami Jermaine Onyando
I56/38808/2020
Department of Chemistry
Faculty of Science and Technology
University of Nairobi

“This thesis is submitted for examination with our approval as research supervisors”.

	Signature	Date
Dr. Patrick K. Tum		01-09-2023
Department of Chemistry University of Nairobi <u>Nairobi, Kenya.</u>	-----	-----
Dr. Rachael E. N. Njogu		01-09-2023
Department of Chemistry University of Nairobi <u>Nairobi, Kenya.</u>	-----	-----
Prof. Dickson M. Andala		27-08-2023
Department of Chemistry Multimedia University of Kenya <u>Nairobi, Kenya</u>	-----	-----

DEDICATION

“I dedicate this thesis to my parents, Mr. and Mrs. R. Omulami for their continuous sacrifice and dedication throughout my entire study”.

ACKNOWLEDGEMENTS

First and foremost, I would like to thank God the almighty for the gift of life, strength and wisdom to carry out this research, for without him, all would not be possible.

Secondly, I would like to express my sincere gratitude to my supervisors and academic advisors, Dr. Patrick K. Tum, Prof. Dickson M. Andala, Dr. Rachael E. N. Njogu and Dr. George O. Oindo for their supervision, advice, guidance and mentorship. Special gratitude goes to Prof. Dickson M. Andala for introducing me to the field of air quality, dispersion and modelling in addition to continuously encouraging me to learn.

Thirdly, I am grateful to the Department of Chemistry, University of Nairobi for the opportunity to undertake this research work.

I greatly appreciate the two cement factories in Athi River for allowing me to access the facilities to carry out sampling. The staff were supportive; especially the operational manager who guided me throughout the sampling period and explained the production process. I am extremely grateful to CSI International Ltd and its entire community for the provision of instruments and manpower to carry out sampling and analysis.

Most sincere appreciation goes to my father and mentor, Mr. Robert M. Omulami for his financial support and advice. The beginning and completion of my master's program would not have been possible without his input. I would also like to thank my mother, Mrs. Beatrice Omulami for always supporting and praying for me. I am also grateful to Miss Juliet Wakhu and my siblings, Mr. Mangira, Miss Ahono and Miss Whitney for continuously uplifting my spirit with words of encouragement.

Lastly, many thanks go to my course mates for their assistance, support and positive criticism.

ABSTRACT

Cement manufacturing industries play a vital role in economic development through the development of infrastructure and the creation of employment opportunities. However, cement manufacturing results in the emission of particulate matter (Total Suspended Particles (TSP), coarse particles (PM₁₀) and fine particles (PM_{2.5})) and flue gases (carbon monoxide (CO), carbon dioxide (CO₂), sulphur dioxide (SO₂) and nitrogen oxides (NO_x)). These emissions cause air pollution which is unfavourable to human health. Exposure to air pollution results in adverse health effects such as pulmonary and cardiovascular diseases. In the current study, two cement factories in Athi River, Machakos County in Kenya were selected to determine the concentrations of particulate matter and flue gases emitted into the atmosphere and their subsequent downwind dispersion. Cement Factory 1 (CF1) contained one sampling point (Stack 1 with a height of 35 m) and Cement factory 2 (CF2) contained two points (Stack 2a with a height of 39 m and 2b with a height of 45 m). Particulate matter was sampled isokinetically using an isokinetic source sampler-XC-572-V and its concentration determined gravimetrically. Flue gas sampling and determination of concentration were done using an emission analyser E6000-5SC. The sampling procedure was based on the United States Environmental Protection Agency (EPA) standard methods. The stack emission concentrations were subsequently used to model the downwind dispersion of the pollutants in the atmosphere using the American Meteorological Society/Environmental Protection Regulatory Model (AERMOD). The findings show that except for carbon dioxide from CF1, stack emission concentration and modelling results of particulate matter, carbon monoxide, sulphur dioxide and nitrogen oxides from both cement factories were below the permissible limits as stipulated by the Environmental Management and Coordination (Air Quality) Regulations and World Health Organization air quality Guidelines. The average stack emission concentration of carbon dioxide was 24062 ± 3340 mg/Nm³, the 8-hour mean maximum concentration was 8.809 ± 1.570 mg/m³ and the 1-hour mean maximum concentration was 32.715 ± 4.362 mg/m³. Negligible concentrations of CO, SO₂ and NO_x were detected in Stack 2a and Stack 2b.

TABLE OF CONTENTS

DECLARATION	ii
DEDICATION	iii
ACKNOWLEDGEMENTS	iv
ABSTRACT	v
TABLE OF CONTENTS	vi
LIST OF TABLES	x
LIST OF FIGURES	xi
LIST OF APPENDICES	xiii
LIST OF ABBREVIATIONS/ACRONYMS AND SYMBOLS	xiv
CHAPTER ONE	1
1 INTRODUCTION	1
1.1 Background of Study	1
1.1.1 Air Pollution from Cement Manufacturing Industries	1
1.1.2 Health and Environmental Effects of Air Pollution	2
1.1.3 Atmospheric Dispersion	2
1.1.4 Legal Framework Regulating Air Quality in Kenya	3
1.2 Statement of the Problem	4
1.3 Objectives	4
1.4.1 General Objective	4
1.4.2 Specific Objectives	4
1.4 Justification and Significance of the Study	5
CHAPTER TWO	6
2 LITERATURE REVIEW	6
2.1 Atmospheric Pollution	6
2.2 Cement Manufacturing Process	7
2.2.1 Emissions from the Cement Manufacturing Process	9
2.2.2 Pollution Control Technologies	9
2.3 Particulate Matter (PM)	10
2.3.1 Isokinetic Sampling of Particulate Matter	11
2.3.2 Isokinetic Source Sampler-XC-572-V	13

2.4	Gaseous Emissions.....	14
2.4.1	Oxides of Carbon	15
2.4.2	Sulphur dioxide (SO ₂).....	16
2.4.3	Nitrogen Oxides (NO _x).....	17
2.4.4	Formation and Effects of Acid Deposition	18
2.4.5	Analysis of Gaseous Emissions	20
2.4.6	Emission Analysis.....	21
2.5	Atmospheric Dispersion Modelling.....	22
2.5.1	Sources of Air Pollution.....	23
2.5.2	Dispersion of Pollutants	23
2.5.3	Pollution Receptor.....	24
2.6	American Meteorological Society/Environmental Protection Regulatory Model (AERMOD).....	24
2.6.1	Terrain Pre-processor (AERMAP).....	25
2.6.2	Meteorological Data Pre-processor (AERMET).....	26
CHAPTER THREE		27
3	MATERIALS AND METHODS.....	27
3.1	Materials	27
3.1.1	Sample Collection	27
3.1.2	Sampling Sites.....	27
3.1.3	Map of Sampling Area	27
3.1.4	Sampling Duration and Frequency.....	28
3.1.5	Sampling Procedure	29
3.1.6	Reagents and Chemicals.....	29
3.1.7	Apparatus	29
3.1.8	Instrumentation and Software	30
3.2	Methods.....	30
3.2.1	Particulate Matter Analysis	30
3.2.2	Gaseous Emissions Analysis.....	38
3.2.3	Dispersion Modelling of Particulate Matter and Gaseous Emissions	38
CHAPTER FOUR.....		43

4	RESULTS AND DISCUSSION	43
4.1	Stack Emission of Particulate Matter Analysis.....	43
4.1.1	Determination of the Number of Traverse Points	43
4.1.2	Determination of Stack Gas Velocity and Volumetric Flow Rate	44
4.1.3	Determination of Molecular Weight, Dry Basis	45
4.1.4	Determination of Stack Gas Volume and Wet Molecular Weight.....	45
4.1.5	Determination of Percentage Isokinetic	46
4.1.6	Stack Emission Concentration of Total Suspended Particulates.....	47
4.1.7	Stack Emission Concentration of PM ₁₀ and PM _{2.5}	49
4.2	Stack Emission of Gaseous Emissions Analysis	50
4.2.1	Stack Emission Concentration of Carbon Dioxide	50
4.2.2	Stack Emission Concentration of Carbon Monoxide	51
4.2.3	Stack Emission Concentration of Sulphur Dioxide.....	52
4.2.4	Stack Emission Concentration of Nitrogen Oxides.....	53
4.3	Modelling Input Data Analysis	54
4.3.1	Wind Speed and Direction	54
4.3.2	Source Emission Rate.....	55
4.3.3	Terrain and Building Data.....	56
4.4	Dispersion Modelling.....	57
4.4.1	Total Suspended Particles	57
4.4.2	Particulate Matter (PM ₁₀)	62
4.4.3	Particulate Matter (PM _{2.5})	66
4.4.4	Carbon Dioxide	70
4.4.5	Carbon Monoxide.....	74
4.4.6	Sulphur Dioxide	77
4.4.7	Nitrogen Oxides	80
4.4.8	Effect of Stack Height on Carbon Dioxide Mean Maximum Concentration	83
	CHAPTER FIVE	85
5	CONCLUSIONS AND RECOMMENDATIONS	85
5.1	Conclusions.....	85
5.2	Recommendations.....	86

References.....	87
Appendix.....	99

LIST OF TABLES

Table 2-1: US EPA methods for determination of particulate matter concentration -----	12
Table 3-1: Location of sampling sites -----	27
Table 3-2: Reagents and Chemicals -----	29
Table 3-3: Apparatus-----	29
Table 3-4: Instruments and Software -----	30
Table 3-5: Discrete Receptors -----	41
Table 4-1: Determination of Traverse Points-----	43
Table 4-2: Stack gas velocity and volumetric flow rate -----	44
Table 4-3: Dry molecular weight -----	45
Table 4-4: Mass of liquid collected in impingers -----	45
Table 4-5: Molecular weight, wet basis -----	46
Table 4-6: Percentage isokinetic (Validatory procedure)-----	47
Table 4-7: Mass of particulate matter collected-----	47
Table 4-8: Stack emission concentration of Total Suspended Particles -----	48
Table 4-9: Stack emission concentration of PM ₁₀ and PM _{2.5} -----	49
Table 4-10: Percentage concentration of carbon dioxide -----	50
Table 4-11: Concentration of carbon dioxide -----	50
Table 4-12: Concentration of carbon monoxide -----	51
Table 4-13: Concentration of Sulphur dioxide-----	52
Table 4-14: Concentration of Nitrogen oxides -----	53
Table 4-15: Emission Source Data – Cement Factory1 (CF1), Stack 1 -----	55
Table 4-16: Emission Source Data – Cement Factory 2 (CF2), Stack 2a -----	55
Table 4-17: Emission Source Data – Cement Factory 2 (CF2), Stack 2b -----	56
Table 4-18: Buildings and Structures Surrounding CF1 and CF2-----	57
Table 4-19: Annual and 24-hour maximum concentration of Total Suspended Particles (TSP) -	60
Table 4-20: Discrete receptor annual and 24-hour average concentration of PM (TSP)-----	61
Table 4-21: Annual and 24-hour Maximum Concentration of PM ₁₀ -----	65
Table 4-22: Discrete receptor annual and 24-hour average concentration of PM ₁₀ -----	66
Table 4-23: Annual and 24-hour Maximum Concentration of PM _{2.5} -----	69
Table 4-24: Discrete receptor annual and 24-hour average concentration of PM _{2.5} -----	70
Table 4-25: 8-hour and 1-hour Maximum Concentration of carbon dioxide -----	73
Table 4-26: Discrete receptor 8-hour and 1-hour average concentration of carbon dioxide -----	74
Table 4-27: 8-hour and 1-hour maximum concentration of carbon monoxide -----	76
Table 4-28: Discrete receptor 8-hour and 1-hour average concentration of carbon monoxide ---	77
Table 4-29: Annual and 24-hour maximum concentration of sulphur dioxide-----	79
Table 4-30: Discrete receptor annual and 24-hour average concentration of sulphur dioxide----	80
Table 4-31: Annual and 24-hour maximum concentration of nitrogen oxide -----	82
Table 4-32: Discrete receptor annual and 24-hour average concentration of nitrogen oxides ----	83
Table 4-33: Effect of stack height on the mean maximum concentration-----	84

LIST OF FIGURES

Figure 2-1: Cement manufacturing process -----	7
Figure 2-2: Rotary kiln -----	8
Figure 2-3: Isokinetic Sampling-----	12
Figure 2-4: Isokinetic source sampling train -----	14
Figure 2-5: Typical isokinetic source sampling train -----	14
Figure 2-6: E6000-5SC hand-held emission analyser-----	22
Figure 2-7: AERMOD schematic diagram -----	23
Figure 2-8: Gaussian plume-----	25
Figure 3-1: Map of the study area-----	28
Figure 3-2: Determination of the number of traverse points (sampling points)-----	30
Figure 3-3: S-type Pitot tube with an inclined manometer -----	31
Figure 3-4: Filter papers contained in Petri dishes -----	36
Figure 3-5: Land use -----	40
Figure 4-1: Percentage Isokinetic (%)-----	47
Figure 4-2: Stack emission – dry standard concentration of total suspended particles-----	48
Figure 4-3: Stack emission – dry standard emission (A) PM ₁₀ and (B) PM _{2.5} concentration -----	50
Figure 4-4: Stack emission – concentration of carbon dioxide -----	51
Figure 4-5: Stack emission – concentration of carbon monoxide -----	52
Figure 4-6: Stack emission – concentration of sulphur dioxide from Stack 1 -----	52
Figure 4-7: Stack emission – concentration of nitrogen oxides -----	53
Figure 4-8: Wind Class frequency distribution -----	54
Figure 4-9: Wind-Rose -----	54
Figure 4-10: Terrain-----	56
Figure 4-11: Annual ambient concentration of TSP from (a) CF1, S1; (b) CF1, S2; (c) CF1, S3; (d) CF2, S1; (e) CF2, S2; (f) CF2, S3 -----	58
Figure 4-12: 24-hour ambient concentration of TSP from (a) CF1, S1; (b) CF1, S2; (c) CF1, S3; (d) CF2, S1; (e) CF2, S2; (f) CF2, S3 -----	59
Figure 4-13: A graph of the (A) annual and (B) 24-hour maximum concentration of Total Suspended Particles -----	61
Figure 4-14: The (A) annual and (B) 24-hour discrete receptor concentration of Total Suspended Particles -----	62
Figure 4-15: Annual ambient concentration of PM ₁₀ from (a) CF1, S1; (b) CF1, S2; (c) CF1, S3; (d) CF2, S1; (e) CF2, S2; (f) CF2, S3 -----	63
Figure 4-16: 24-hour ambient concentration of PM ₁₀ from (a) CF1, S1; (b) CF1, S2; (c) CF1, S3; (d) CF2, S1; (e) CF2, S2; (f) CF2, S3 -----	64
Figure 4-17: A graph of the (A) annual and (B) 24-hour maximum concentration of PM ₁₀ -----	65
Figure 4-18: The (A) annual and (B) 24-hour discrete receptor concentration of PM ₁₀ -----	66
Figure 4-19: Annual ambient concentration of PM _{2.5} from (a) CF1, S1; (b) CF1, S2; (c) CF1, S3; (d) CF2, S1; (e) CF2, S2; (f) CF2, S3 -----	67

Figure 4-20: 24-hour ambient concentration of PM _{2.5} from (a) CF1, S1; (b) CF1, S2; (c) CF1, S3; (d) CF2, S1; (e) CF2, S2; (f) CF2, S3 -----	68
Figure 4-21: The (a) annual and (b) 24-hour maximum concentration of PM _{2.5} -----	69
Figure 4-22: The (A) annual and (B) 24-hour discrete receptor concentration of PM _{2.5} -----	70
Figure 4-23: 8-hour ambient concentration of carbon dioxide from (a) CF1, S1; (b) CF1, S2; (c) CF1, S3; (d) CF2, S1; (e) CF2, S2; (f) CF2, S3-----	71
Figure 4-24: 1-hour ambient concentration of carbon dioxide from (a) CF1, S1; (b) CF1, S2; (c) CF1, S3; (d) CF2, S1; (e) CF2, S2; (f) CF2, S3-----	72
Figure 4-25: The (A) 8-hour and (B) 1-hour maximum concentration of carbon dioxide-----	73
Figure 4-26: The (A) 8-hour and (B) 1-hour discrete receptor concentration of carbon dioxide -	74
Figure 4-27: 8-hour ambient concentration of CO from (a) CF1, S1; (b) CF1, S2; (c) CF1, S2; and 1-hour ambient concentration of CO from (d) CF1, S1; (e) CF1, S2; (f) CF1, S3--	75
Figure 4-28: The (A) 8-hour and (B) 1-hour maximum concentration of CO-----	76
Figure 4-29: The (A) 8-hour and (B) 1-hour discrete receptor concentration of carbon monoxide -----	77
Figure 4-30: Annual ambient concentration of SO ₂ from (a) CF1, S1; (b) CF1, S2; (c) CF1, S2; and 24-hour ambient concentration of SO ₂ from (d) CF1, S1; (e) CF1, S2; (f) CF1, S2; -----	78
Figure 4-31: A graph of the (A) annual and (B) 24-hour ambient maximum concentration of sulphur dioxide -----	79
Figure 4-32: The (A) annual and (B) 24-hour discrete receptor ambient concentration of sulphur dioxide -----	80
Figure 4-33: Annual ambient concentration of NO _x from (a) CF1, S1; (b) CF1, S2; (c) CF1, S2; and 24-hour ambient concentration of SO ₂ from (d) CF1, S1; (e) CF1, S2; (f) CF1, S2; -----	81
Figure 4-34: The (A) annual and (B) 24-hour maximum ambient concentration of nitrogen dioxide -----	82
Figure 4-35: The (A) annual (B) 24-hour ambient discrete receptor concentration of nitrogen dioxide -----	83
Figure 4-36: Effect of Stack height on (A) 8-hour and (B) 1-hour mean maximum concentration -----	84

LIST OF APPENDICES

Appendix I: Gaseous emissions – Cement Factory 1, Stack 1, Sample 1	99
Appendix II: Gaseous emissions – Cement Factory 2, Stack 2a, Sample 1	100
Appendix III: Gaseous emissions – Cement Factory 2, Stack 2b, Sample 1	101
Appendix IV: Gaseous emissions – Cement Factory 1, Stack 1, Sample 2.....	102
Appendix V: Gaseous emissions – Cement Factory 2, Stack 2a, Sample 2	103
Appendix VI: Gaseous emissions – Cement Factory 2, Stack 2b, Sample 2.....	104
Appendix VII: Gaseous emissions – Cement Factory 1, Stack 1, Sample 3	105
Appendix VIII: Gaseous emissions – Cement Factory 2, Stack 2a, Sample 3	106
Appendix IX: Gaseous emissions – Cement Factory 2, Stack 2b, Sample 3.....	107
Appendix X: Cement Factory 1 – Stack 1 average data	108
Appendix XI: Cement Factory 2 – Stack 2a average data	109
Appendix XII: Cement Factory 2 – Stack 2b average data	110
Appendix XIII: Particulate matter run summaries – Cement Factory 1 Stack 1	111
Appendix XIV: Particulate matter run summaries – Cement Factory 2 Stack 2a	112
Appendix XV: Particulate matter run summaries – Cement Factory 2 Stack 2b	113
Appendix XVI: Particulate matter calculation equations	114
Appendix XVII: Statistical analysis (P-test).....	115
Appendix XVIII: Discrete receptor sample run (Annual and 24-hour concentrations).....	116
Appendix XIX: Discrete receptor sample run (8-hour and 1-hour concentrations)	117

LIST OF ABBREVIATIONS/ACRONYMS AND SYMBOLS

AEOLIUSF	Assessing the Environmental of Locations in Urban Streets Full version
AERMOD	American Meteorological Society/Environmental protection Agency Regulatory Model
AUSPLUME	Australia Plume Dispersion Model
BPIP	Building Input Profile Program
CALINE	California Line Source Dispersion Model
CALPUFF	California Puff Model
CF1 S1	Cement Factory 1 Sample 1
CF1 S2	Cement Factory 1 Sample 2
CF1 S3	Cement Factory 1 Sample 3
CF1	Cement Factory 1
CF2	Cement Factory 2
CF2 S1	Cement Factory 2 Sample 1
CF2 S2	Cement Factory 2 Sample 2
CF2 S3	Cement Factory 2 Sample 3
COVID 19	Coronavirus Disease 2019
CTDMPLUS	Complex Terrain Dispersion Model Plus Algorithms for Unstable Situations
DGM	Dry Gas Meter
EGR	Exhaust Gas Recycling
EMCA	Environmental Management Coordination Act
ESRL	Earth System Research Laboratories
GeoTIFF	Geographic Tagged Image File Format
GEP	Good Engineering Practices
ISC3	Industrial Source Complex, Version 3
ISCST3	Industrial Source Complex Short-Term, Version 3
ISCST3	Industrial Source Complex Short-Term, Version 3
JKIA	Jomo Kenyatta International Airport
KS	Kenya Standards

MOS	Metal Oxide Semiconductor
NCDC	National Climatic Data Centre
NCEI	National Centres for Environmental Information
NDIR	Non-Dispersive Infrared Analyser
NEMA	National Environmental Management Authority
NLCD	National Land Cover Database
NOAA	National Oceanic and Atmospheric Administration
OCD	Offshore and Coastal Dispersion
PM	Particulate Matter
SARS-COV-2	Severe Acute Respiratory Syndrome Coronavirus 2
SDGs	Sustainable Development Goals
STRM	Shuttle Radar Topography Mission
S-type pitot	Stausscheibe type Pitot tube
TSP	Total Suspended Particles
US EPA	United States Environmental Protection Agency
USGS	United States Geological Survey
UTM	Universal Transverse Mercator
UV	Ultra-Violet
VOCs	Volatile Organic Compounds
VRM	Vertical Roller Mill
WHO	World Health Organization
WMO	World Meteorological Organization

CHAPTER ONE

1 INTRODUCTION

1.1 Background of Study

In recent years, air quality degradation has developed to be a global crisis, with the World Health Organization (WHO) reporting over four million premature deaths annually (Li *et al.*, 2019; Sen *et al.*, 2023). Air pollution is recognised as a global concern as it plays a vital role in attaining the Sustainable Development Goals (SDGs) (Longhurst *et al.*, 2018). With Kenya striving to attain Vision 2030 aimed at transforming herself into an industrialized, middle-income country, degradation of air quality is likely to increase if not properly monitored. Industrial development involves an increase in the utilization of fossil fuels which in turn increases atmospheric emissions (Jittra *et al.*, 2015). Common air pollutants include volatile organic compounds (VOCs) such as benzene and toluene, carbon monoxide (CO), nitrogen oxides (NO_x), carbon dioxide (CO₂), particulate matter (PM₁₀ and PM_{2.5}), sulphur dioxide (SO₂), ozone (O₃) and heavy metals such as arsenic, lead and mercury (Manisalidis *et al.*, 2020).

1.1.1 Air Pollution from Cement Manufacturing Industries

In Kenya, the cement manufacturing industry is growing at a very fast rate due to the continuous increase in demand. The sector provides a means of better housing and creates employment opportunities, facilitating economic growth (Devi *et al.*, 2017; Eshikumo and Odock, 2017). Most of the cement industries in Kenya are located in Athi River in Machakos County. This is attributed to the availability of raw materials such as volcanic ash used to manufacture commercial Portland Pozzolana Cement (PPC) (Marangu, 2020). The cement manufacturing industries in Athi River include East Africa Portland Cement, Blue Triangle Cement, Savannah Cement, Arm Cement, Ndovu Cement, Mombasa Cement and Bamburi Cement. Athi River also is home to low and middle-income residential areas such as Kitengela, Mlolongo, Syokimau and Athi River. Cement manufacturing involves the burning of limestone-based raw materials which releases carbon dioxide gas as a by-product (Ali *et al.*, 2011). Some common emissions emitted by the cement manufacturing industry include CO, NO₂, SO₂, PM₁₀ and PM_{2.5} (Ali *et al.*, 2011). In addition to calcination, grinding, milling and the use of fossil fuels in kilns and dryers also lead to the release of emissions (Etim *et al.*, 2021).

1.1.2 Health and Environmental Effects of Air Pollution

Air pollution poses adverse health risks to the general population. Air pollution accounts for approximately 19000 premature deaths in Kenya as reported by the State of the Global Air (2019) Report (deSouza, 2020). The State of Global (2020) Report ranked air pollution as the fourth highest cause of premature deaths (Bai *et al.*, 2022). The health effect of air pollution depends on the type of pollutant, time and concentration of exposure, the age of the individual and underlying health effects (Kampa and Castanas, 2008; Makri and Stilianakis, 2008). The most vulnerable groups include the elderly, children, expectant mothers together with a foetus and people with underlying cardiovascular and lung diseases (Chen *et al.*, 2022). Poor health negatively impacts the individual's productivity thereby affecting economic growth (Jittra *et al.*, 2015). Air pollution has been linked to lung cancer, chronic obstructive pulmonary diseases, stroke, acute respiratory infections and heart diseases which increase mortality rates (Ibrahim *et al.*, 2012; WHO, 2019). Particulate matter includes airborne solid and liquid particles with aerodynamic diameters less than 10 μm (PM_{10}) and 2.5 μm ($\text{PM}_{2.5}$). Fine particles can penetrate the bloodstream and affect multiple body organs such as the heart, liver, lungs and kidney (Chen *et al.*, 2022). In the bloodstream, the particles can initiate oxidative stress and inflammation causing respiratory infections such as asthma and lung diseases (Horak *et al.*, 2002).

Air pollution also negatively affects the environment. Particulate matter in the air reduces visibility through the reflection of light (Vallero, 2014). Carbon dioxide and ozone are greenhouse gases that cause global warming which in return leads to climate change. Climate change leads to increasing threats of the number of natural disasters, food insecurity and difficulty in accessing clean water and sanitation (Onoja *et al.*, 2011). Nitrogen oxides and sulphur dioxide form acid rain which damages buildings and cultural monuments (Gandhi *et al.*, 2017), affects aquatic life adversely by reducing the pH of the water bodies (Vallero, 2014), leaching of nutrients in the soil and enabling the availability of toxic metal compounds of aluminium and mercury (Gandhi *et al.*, 2017).

1.1.3 Atmospheric Dispersion

Atmospheric dispersion models are mathematical formulas that provide the relationship between the source of air pollution and the recipients. It predicts the downwind dispersion of specific

pollutants and the ambient concentration of the atmospheric emissions at a given receptor (Schnelle and Brown, 2001). The extent of downwind dispersion of air pollutants is influenced by the topography and meteorological conditions of the area (Turner, 1994), the height of the emitting stack and the existing nearby buildings and structures (Schnelle and Brown, 2001). By combining these factors, modelling can be used to determine the pollutant concentrations in various regions and determine the affected recipients (Schnelle and Brown, 2001). Modelling can not only be used to determine the extent of air pollution by existing industries but also to predict the effects of future industrial projects (Barratt, 2001). Some examples of atmospheric dispersion modelling tools are the American Meteorological Society/Environmental Protection Regulatory Model (AERMOD) and the California Puff Model (CALPUFF).

In Kenya, AERMOD has been used to predict future concentrations of hydrogen sulphide (H_2S) from a proposed Geothermal Plant site in Menengai (Ndetei, 2010; Nyairo and Onyancha, 2018). The investigation concluded that the concentration of hydrogen sulphide emitted from the power plant were within the World Health Organisation (WHO) permitted guidelines of $150 \mu\text{gm}^{-3}$.

According to Kiano, (2018), the study on the health effects of industrial pollution of the pulp and paper industry in Webuye on the residents living in the area reported the mean emission rate of particulate matter in Webuye town at $102.17 \mu\text{gm}^{-3}$. Additional results showed that there was a significant variation in respiratory tract infections among the residents between the periods when emissions were being released between 2007 and 2009 and the post-emission period, from 2014 to 2015. In addition, seven out of ten respondents had a persistent cough during the emission period (Kiano, 2018).

1.1.4 Legal Framework Regulating Air Quality in Kenya

The main law for prevention and control of air pollution is the Environmental Management and Co-ordination Act (EMCA) (Air Quality) Regulation, 2014. Air Quality Regulation, 2014 provides guidelines on the permissible limits of various pollutants. The act also provides the procedure for obtaining an emission licence and carries out inspections to ensure that air quality regulations are being followed. The act requires industrial plants to carry out stack emission monitoring quarterly (deSouza, 2018). Other relevant laws related to air quality regulation in Kenya include Environmental Policy, 2013, Kenya Standards Act, Cap 496, Kenya Standard (KS 1515): Code of

Practice on Inspection of road vehicles, Occupational Safety and Health Act No. 15 of 2007, Public Health Act, cap 242, National Transport and Safety Act, 2012 and Energy Act, 2006.

1.2 Statement of the Problem

The cement manufacturing industry plays an important role as Kenya strives to be an industrialized, middle-income country through the development of infrastructure. However, the cement manufacturing process releases emissions into the atmosphere which causes air pollution and climate change. According to Environmental Protection Agency 2022, in addition to particulate matter, cement manufacturing contributes more than 500,000 tonnes of oxides of nitrogen, carbon monoxide and sulphur dioxide per year. These emissions cause air pollution which affects the health of the general population, negatively affecting economic growth. The Global Air Report of 2019 reported that air pollution causes approximately 19000 premature deaths in Kenya. In the report released a year later, air pollution was ranked as the fourth highest cause of premature deaths worldwide. Increased emissions from industries have resulted in increased health burdens that include cardiovascular diseases, pulmonary diseases and premature deaths for the communities living around the industrial plants and some distance downwind. Exposure to PM_{2.5} and NO_x causes reduced lung function and dry coughing in children living around industrial zones. Despite the various reports, little research has been done in Kenya on the emissions released from the stationary points and their subsequent dispersion in ambient air.

1.3 Objectives

1.3.1 General Objective

To evaluate the source concentration and downwind dispersion of particulate matter and gaseous emissions from selected cement factories.

1.3.2 Specific Objectives

- i. To determine the source concentration of emitted particulate matter in a gas stream.
- ii. To determine the source concentration of emitted gaseous emissions in a gas stream.
- iii. To establish downwind dispersion of particulate matter from the gas stream.
- iv. To establish downwind dispersion of gaseous emissions from the gas stream.

1.4 Justification and Significance of the Study

Maintaining a balance between environmental sustainability and economic development is very important. However, this has proven to be a challenge in Kenya because of inadequate data on air quality measurements and simulations. It is important to understand how various emissions from stationary sources interact with the environment, their dispersion and the affected recipients to develop sustainable and effective legislations and policies that would reduce health burden and environmental degradation. The expected findings would inform cement factories, urban and physical planners, potential investors and the County Government of Machakos on the dispersion of emissions, the most likely affected regions, the modes of mitigating the effects and where future industrial structures can be located.

CHAPTER TWO

2 LITERATURE REVIEW

2.1 Atmospheric Pollution

Atmospheric pollution is caused by the release of harmful substances in gaseous form and finely divided solids or liquid aerosols into the atmosphere by both natural phenomena such as forest fires and human activities such as industrialization. Air pollution not only causes climatic change such as global warming but also affects human health (Manisalidis *et al.*, 2020). Some common air pollutants include heavy metals, particulate matter (PM₁₀ and PM_{2.5}), nitrogen oxides (NO_x), volatile organic compounds (VOCs), ozone (O₃), carbon dioxide (CO₂), sulphur dioxide (SO₂) and carbon monoxide (CO) (Schnelle and Brown, 2001). Air pollution causes respiratory infections such as pulmonary diseases, asthma, lung cancer, bronchitis and cardiovascular diseases (Manisalidis *et al.*, 2020). Industrial development results in increased demand for fossil fuels to meet energy requirements. Common fossil fuels include petroleum, diesel, natural gas, shale oil and bitumen (Chmielewski, 1999). The burning of fossil fuels to generate energy is accompanied by the release of pollutants such as NO_x which cause formation of smog and acid rain (Najjar, 2011), SO₂ resulting from burning sulphur-containing fuels, CO, CO₂, and PM (Chmielewski, 1999).

Effective air pollution prevention and control requires the availability of air quality data as it enables one to identify sources of pollution, study the trend of pollutants in the air (Lee *et al.*, 2007) and determine the health effects caused by specific pollutants (Samet *et al.*, 2000). Data on air quality can be obtained using ground monitoring (deSouza, 2020) and satellite monitoring of the various air pollutants (Duncan *et al.*, 2014). In addition to monitoring, modelling is also used to assess air quality by predicting the dispersion of various pollutants from volume, line and point sources (Schnelle and Brown, 2001). However, like most developing countries, air quality monitoring and modelling systems in Kenya are not highly advanced (deSouza, 2020). This makes it a challenge to balance air pollution control strategies and economic development (Omanga *et al.*, 2014).

2.2 Cement Manufacturing Process

The cement manufacturing industry is a very important sector in Kenya's economic development. The cement industry is a growing industrial sector due to the increasing road construction and various government and non-government housing projects (Eshikumo and Odock, 2017). Apart from providing a means of better housing, the cement manufacturing industry also provides a source of employment (Devi *et al.*, 2017).

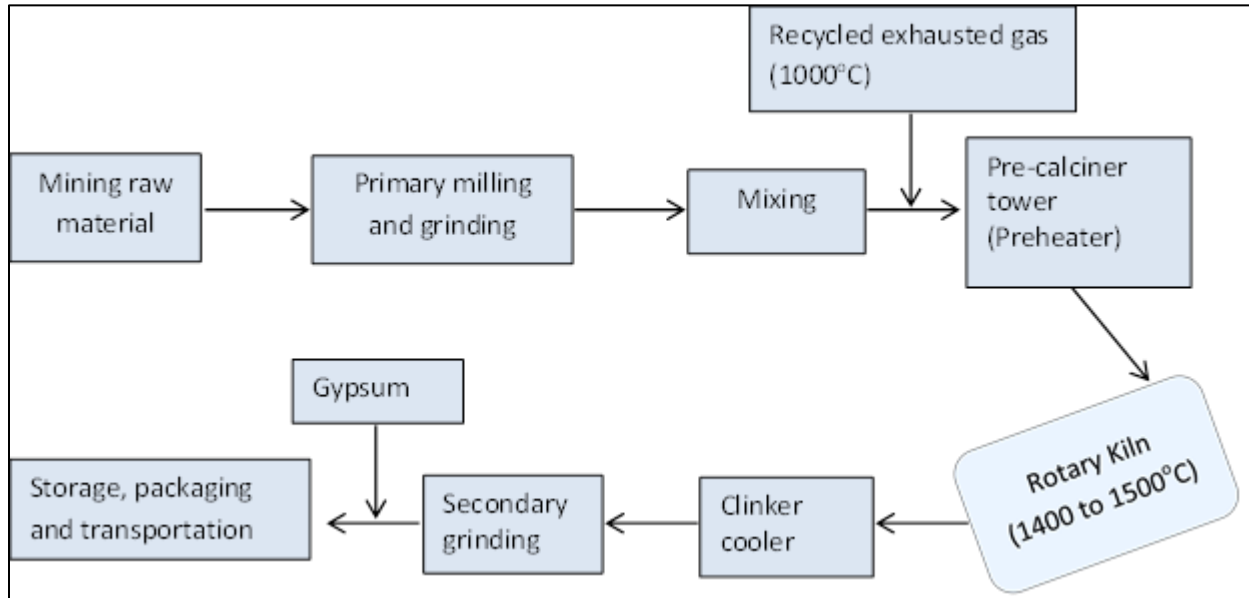


Figure 2-1: Cement manufacturing process
(Source: author)

Cement manufacturing involves three main stages; (i) mining and grinding from the earth's crust to obtain the raw material, (ii) calcination of raw materials to produce clinker and (iii) secondary milling and grinding of the clinker (Ali *et al.*, 2011) as shown in Figure 2-1. The raw material for the production of cement is composed of limestone, clay, shale and chalk (Devi *et al.*, 2017). The initial stage of cement production involves the extraction of limestone-based raw material through drilling and blasting using explosives (Jankovic *et al.*, 2004). The extracted raw material is then loaded into trucks and transported to the manufacturing site.

There are various processes in cement production which vary depending on the amount of water to be added to the raw feed. These processes include the dry process, semi-dry process and wet process. In the dry process, the raw material obtained is first dried before feeding into the pre-

calciner. Instead of drying, water can also be added to the raw material to form slurry or pellets in wet and semidry processes (Ali *et al.*, 2011; Devi *et al.*, 2017).

The extracted raw material is grounded, milled to smaller sizes and mixed to produce a uniform mixture (Kakali and Tsvilis, 1993). After milling, the homogenised raw material is conveyed to a pre-calciner tower where the raw material is mixed with collected exhaust gas at temperatures of around 1000 °C. Mixing with exhaust gas enables energy saving, provides the temperature required for the initiation of the chemical process of cement production and reduces the emissions released into the atmosphere (Jankovic *et al.*, 2004). The pre-heated feed is then moved to the kiln where the complete chemical processes progress to completion. In the kiln, the calcium carbonate decomposes to form lime (calcium oxide) and carbon dioxide (Devi *et al.*, 2017) shown in Equation (1). The formed lime further combines with silica and alumina to form alite (C₃S), belite (C₂S) and tricalcium aluminate (C₃A) (Kääntee *et al.*, 2004).

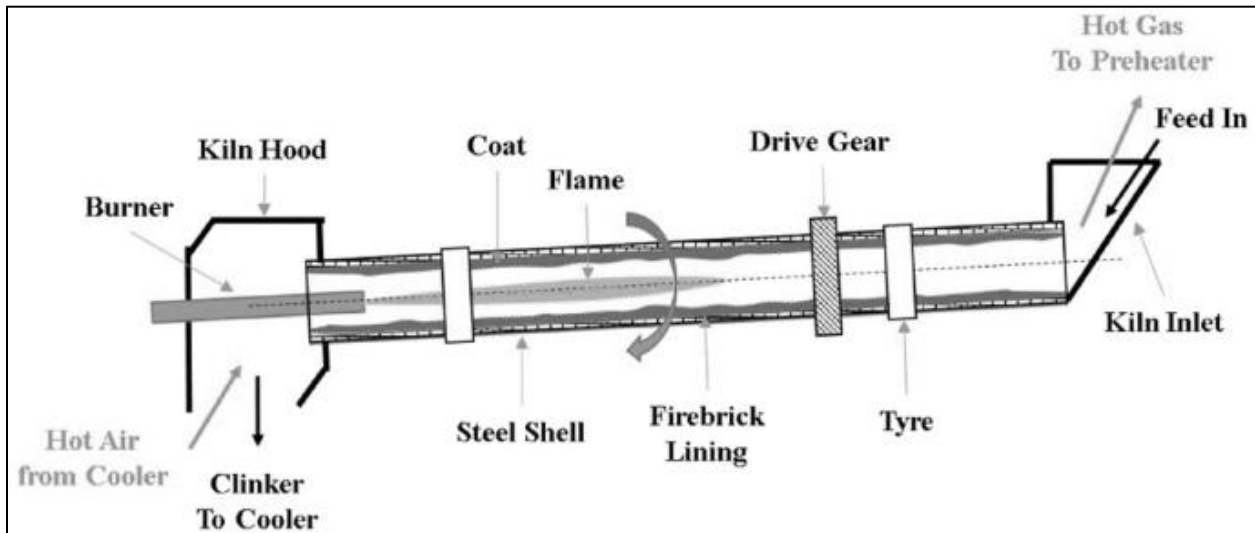


Figure 2-2: Rotary kiln
(Yang *et al.*, 2018)

The cement kiln is made of steel and firebrick lining as shown in Figure 2-2. The fire bricks enable energy conservation in the kiln because of their low thermal conductivity (Aramide and Seidu, 2013). The kiln is positioned in a slightly inclined position and the pre-calcined mill is fed from the upper end (Okoji *et al.*, 2018) and the product is released from the lower end as a clinker. The

temperature in the mill (1400-1500°C) allows for the calcium carbonate to decompose into calcium oxide.

The formed clinker is transported for secondary grinding and milling to produce a fine product. In the secondary milling process, gypsum and other additives are added and mixed to form cement. A ball mill or a vertical roller mill can be used to facilitate the secondary grinding stage. A vertical roller mill is a high-energy-saving device that can crush, grind, classify and dry the clinker in one unit (Altun *et al.*, 2017; Pareek and Sankhla, 2021). In the secondary grinding process, gypsum is added to adjust the cement setting time. Adjusting the setting time provides adequate time for placing the concrete before hardening (Papageorgiou *et al.*, 2005). The cement can then be packed in various sizes and ready for transportation (Devi *et al.*, 2017; Ibrahim *et al.*, 2012).

2.2.1 Emissions from the Cement Manufacturing Process

Cement manufacturing is associated with the release of various emissions into the atmosphere. These emissions are grouped into PM (TSP, PM₁₀ and PM_{2.5}) and gaseous emissions (SO₂, CO₂, CO and NO_x) (Ali *et al.*, 2015b; Devi *et al.*, 2017). During the formation of clinker, the calcium carbonate is decomposed to produce carbon dioxide. Carbon dioxide is a greenhouse gas responsible for global warming and climate change (Ali *et al.*, 2011). Cement production accounts for approximately 7% of the total anthropogenically produced carbon dioxide (Devi *et al.*, 2017). Apart from cement production, the calcination process leads to the production and release of sulphur dioxide, nitrogen oxides and particulate matter. The type of fuel used also contributes to the emissions released (Ibrahim *et al.*, 2012). Fuel containing sulphur-bound chemicals results in the production of SO₂ (Ali *et al.*, 2011). The oxides of nitrogen are produced by the reaction of nitrogen in the air with oxygen at extreme temperatures (Devi *et al.*, 2017). Apart from the calcination process, particulate matter is also produced from grinding and milling processes (Ibrahim *et al.*, 2012).

2.2.2 Pollution Control Technologies

Pollution control systems in industries help reduce the impact of air pollution on human health and environmental effects (Kwiatkowski *et al.*, 2019). The six processes used in the control of emissions listed in the EPA Handbook include absorption, adsorption, condensation, thermal

incineration, catalytic incineration and use of flares (Schnelle and Brown, 2001). Incineration is used in the control of VOCs and hydrocarbons by converting them to carbon dioxide and water (Vaart *et al.*, 2012).

Scrubbers, both wet and dry are one of the most common techniques used to control flue gases. Wet scrubbers and dry scrubbers use absorption and adsorption principles (Schnelle and Brown, 2001). Absorption and adsorption techniques are based on mass transfer separation into solvent and solid adsorbent materials (Hu and Xu, 2020). Acidic gases such as sulphur dioxide and nitrous oxides can be separated from a gas stream by use of an alkali medium such as ammonium hydroxide, and potassium hydroxide (Schnelle and Brown, 2001). Potassium hydrogen carbonate and sodium hydrogen carbonate can be used to remove carbon dioxide. Scrubbers can provide an efficiency of up to 95% (Yang *et al.*, 2021). Particulate matter can also be controlled by the use of wet scrubbers containing water and dry scrubbers such as electrostatic precipitators (Schnelle and Brown, 2001; Umar *et al.*, 2006)

Exhaust Gas Recycling (EGR) is used in the control of nitrous oxides, carbon monoxide and unburnt hydrocarbons. Paykani *et al.*, 2012 reported a reduction of NO_x, CO and unburnt hydrocarbons by 21%, 24% and 31%. EGR also increases thermal efficiency (Abd-Alla, 2002).

2.3 Particulate Matter (PM)

Particulate matter is a liquid and solid aerosol mixture present in the atmosphere (Yadav and Devi, 2019). Particulate matter comprises a cluster of molecules which may be similar or vary in their chemical and physical composition. The sources of particulate matter can be divided into natural sources and anthropogenic sources. Natural sources include dust storms, micro-organisms and wind pollen (Ukaogo *et al.*, 2020; Vallero, 2014) while anthropogenic sources including industrial processes, fuel combustion and vehicle emissions (Anderson *et al.*, 2012). Secondary particulate matter is formed in the atmosphere through various complex chemical reactions of the water vapour and atmospheric gases such as sulphur dioxide, nitrogen oxides and ammonia gas (Karagulian *et al.*, 2015). Particulate matter differs in its chemical properties depending on the sources and the chemical reactions they undergo (Anderson *et al.*, 2012). Being airborne, particulate matter can be transported over a long distance from its source and the effects are observed in locations away from the source (Vallero, 2014). The main chemical constituents

include elemental carbon, organic compounds, inorganic ions, metallic compounds and crystal substances such as carbonates (Vallero, 2014).

Particulate matter is mainly classified based on aerodynamic diameter. Large particles such as soot, smoke, dirt or dust are easily visualized due to their large size or dark colour (Ibrahim *et al.*, 2012), unlike smaller ones which can only be observed by the use of an electron microscope (Tuvjargal *et al.*, 2019). The particles with aerodynamic diameter below ten microns, PM₁₀ and PM_{2.5} easily enter the human bloodstream through the respiratory system and cause adverse health complications (Vallero, 2014). Particulate matter can initiate oxidative stress and inflammation leading to respiratory infections such as asthma and lung diseases. In addition, PM₁₀ and PM_{2.5} affect lung development and lung function in children (Horak *et al.*, 2002). Prolonged exposure can eventually lead to death (Anderson *et al.*, 2012; Schnelle and Brown, 2001). Increased particulate matter in the atmosphere increases the rate of viral transmission such as COVID-19 (Sharma and Balyan, 2020). Studies have shown that the SARS-CoV-2 virus remains infectious in aerosol suspensions during the hours of study (van Doremalen *et al.*, 2020). Chen *et al.*, (2017) observed that there was a significant increase in measles infections with increasing particulate concentration.

Particulate matter control can be achieved by using various mechanisms including impaction, diffusion, interception, electrostatic attraction, gravity, centrifugal force and thermophoresis (Schnelle and Brown, 2001). Some of the common techniques used to control particulate matter include dry and wet scrubbers, cyclone separators, electrostatic precipitators and fabric filters (Umar *et al.*, 2006). Cyclone separators are used to control heavy dust loads by employing centrifugal force (Schnelle and Brown, 2001).

2.3.1 Isokinetic Sampling of Particulate Matter

Environmental Protection Agency (EPA) method 5 is the standard procedure for isokinetic stack sampling and analysis of particulate matter. This involves sampling at a velocity equal to the gas flow rate using a probe in a stack (EPA, 2018). To ascertain the validity of particulate matter sampling, percentage isokinetic is used. Percentage isokinetic is a mode of comparing the sampling velocity and the velocity of the gas stream. The sampling velocity should be equal to the velocity of the gas stream to obtain a representative sample (Nicklin and Darabkhani, 2022). A higher

sample velocity causes the diversion of the excess gas stream towards the probe while a lower sampling velocity diverts excess gas away from the probe (Schnelle and Brown, 2001). Particles of sufficient momentum, however, continue travelling in a straight line shown in Figure 2-3. This results in lower and higher particulate concentrations respectively (Schnelle and Brown, 2001).

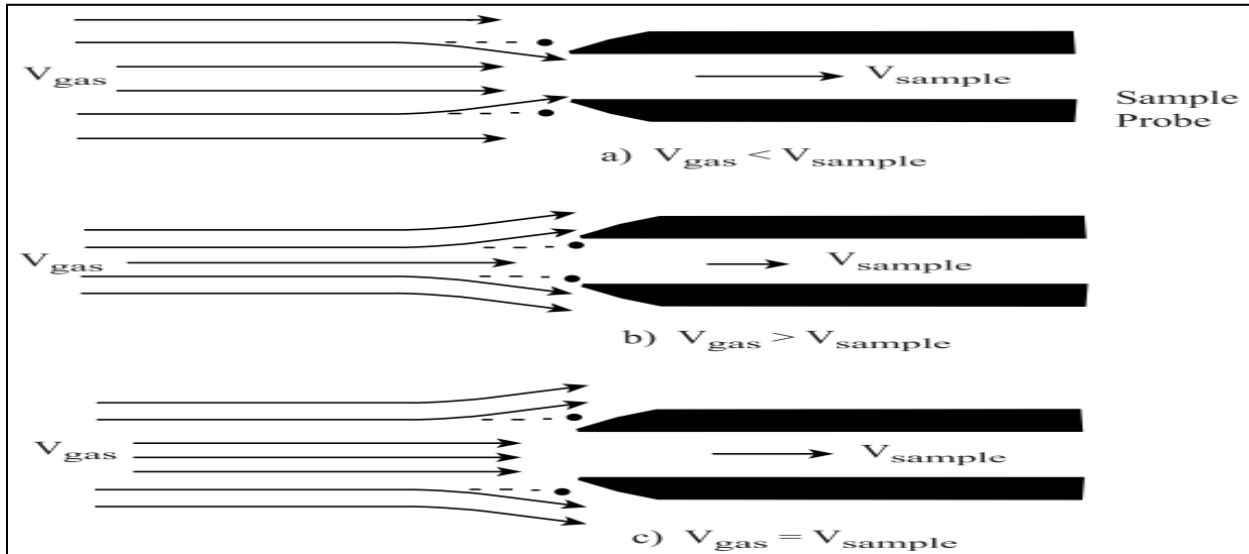


Figure 2-3: Isokinetic Sampling (Schnelle and Brown, 2001)

Sampling and analysis of particulate matter in stack emission can be determined using Standard EPA method 5 (EPA, 2020b). EPA Method 5 involves the sampling of gas samples isokinetically using a probe. During sampling, the particulate matter is collected on a glass fibre filter and its concentration is determined gravimetrically (EPA, 2020b). Gas velocity and particulate matter distribution vary with location across the stack. US EPA Standard Method 1 is first used to determine transverse positions where the sample probe is positioned to obtain a representative sample (EPA, 2018). In addition to method 1, data from method 2 to 4 is important when carrying out method 5 shown in Table 2-1. To carry out Method 1 to 5, an isokinetic source sampler is used.

Table 2-1: US EPA methods for determination of particulate matter concentration

US EPA Standard Method	Parameter determined
Method 1	Location and number of traverse points
Method 2	Volumetric flow rate and stack gas velocity
Method 3	Dry molecular weight
Method 4	Moisture content of the gas stream
Method 5	Particulate matter sampling

Environmental Protection Agency method 2 is used to determine the volumetric flow rate and velocity of the stack gas stream. These parameters are subject to temperature, differential pressure and molecular weight of the gas stream. The differential pressure is measured using an S-type ((Stausscheibe or reverse) Pitot tube (EPA, 2017e). The dry and wet molecular weight of the gas stream are determined by EPA methods 3 and 4. Dry molecular weight is calculated based on molecular weight and concentration of oxygen, carbon dioxide, carbon monoxide, nitrogen and moisture content in the gas stream (EPA, 2017d). Wet molecular weight is a factor of the molecular weight of the moisture content in the gas stream (EPA, 2017f).

2.3.2 Isokinetic Source Sampler-XC-572-V

An isokinetic source sampler is standard equipment that enables the sampling of a gas sample isokinetically in a gas stream. This sampling system can be used to determine a wide range of pollutants including polycyclic aromatic hydrocarbons, dioxins, metals, particulate size distributions, polychlorinated biphenyls and furans from a stationary source (Apex Instruments, 2016). A typical isokinetic source sampler contains a probe assembly, a modular sample case, an umbilical cable, a meter console and an external pump shown in Figure 2-4 and Figure 2-5.

The probe assembly is composed of the sampling nozzle used to collect the gas sample, an S-type Pitot tube for measuring stack velocity, a tube heater and a stack and heater-type K thermocouple used to heat the probe to prevent water vapour from condensing before reaching the condenser and Orsat line (Apex Instruments, 2016). The particulate matter sampled is collected at the modular sample case. The modular sample case contains a filter assembly containing a filter holder, filter temperature sensor and filter heating system used to filter out particulate matter from the gas sample collected from the probe. In addition, it contains impinge glassware where moisture is pulled out from the gas stream (EPA, 2020b). The metering console is composed of a dry gas meter, temperature controller, thermocouple plugs, flow control valves with an orifice flow meter and a dual-column manometer. The meter console is contained in a polyethylene case, an ultra-high molecular weight, light and weather-resistant material. It is used to control and monitor pressure, temperature, sample and gas velocities. The metering console is connected to the source sample console and the external pump through umbilical cords. The external pump enables the sampling of the gas sample from the gas stream (EPA, 2020b).

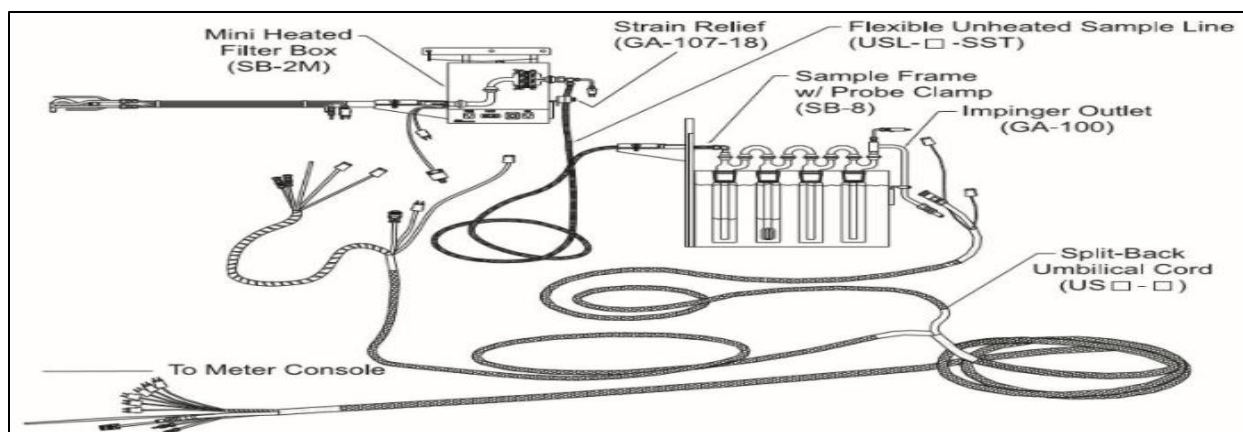


Figure 2-4: Isokinetic source sampling train
(Apex Instruments, 2016)



Figure 2-5: Typical isokinetic source sampling train
(Source: author)

2.4 Gaseous Emissions

Combustion as an industrial process involves the burning of fossil fuel to produce energy used in boilers, furnaces and engines (Obaidullah, 2016). The burning of fossil fuels results in the release of carbon dioxide and water as primary products. Carbon monoxide is produced when a low amount of oxygen is supplied into the combustion process (Rahman *et al.*, 2018). It can also be produced when air has not completely mixed with the fuel during burning (Manahan, 2017).

Sulphur dioxide is produced when sulphur-containing fuel is used to produce energy and nitrogen oxides result in the reaction of nitrogen in the air with oxygen at elevated temperatures (Ali *et al.*, 2011; Devi *et al.*, 2017). Other gaseous emissions produced during industrial processes include ozone, ammonia, chlorine, hydrogen fluoride, hydrogen chloride and hydrogen sulphide (Manahan, 2017). Combustion as a process causes the release of pollutants which have adverse effects on the surrounding environment (Rahman *et al.*, 2018).

2.4.1 Oxides of Carbon

Carbon monoxide and carbon dioxide are produced primarily during the combustion of fossil fuels (Chen *et al.*, 2007). The formation of either gas is dependent on the amount of oxygen supplied in the system. Carbon monoxide is produced when a limited amount of oxygen is supplied during the combustion process (Rahman *et al.*, 2018).

As a pollutant, carbon monoxide is a poisonous gas associated with various health issues such as dizziness, headache, nausea and loss of consciousness (Rahman *et al.*, 2018). In the human body, carbon monoxide combines with haemoglobin to form stable carboxyhaemoglobin (Thurston, 2008), depriving the body of oxygen and this causes ischemia, hypoxia and cardiovascular diseases (Mansoor *et al.*, 2019). Prolonged exposure in a closed environment causes loss of consciousness and even death (Raub *et al.*, 2000).

Carbon dioxide is a greenhouse gas produced mainly through the combustion of fuel (Rahman *et al.*, 2018). Greenhouse gases keep the earth warm by absorbing the infrared radiation emitted by the earth's surface, maintaining life on earth (Kweku *et al.*, 2018). Other greenhouse gases include water vapour, methane, nitrous oxide, and ozone (Błaszczak, 1999). An increase in the concentration of greenhouse gases as a result of anthropogenic activities causes global warming (Florides and Christodoulides, 2009). Global warming increases the overall temperatures which in return causes increased wildfires and loss of species, increased infectious diseases such as malaria and dengue fever and climate change (Kurane, 2010; Onoja *et al.*, 2011; Peters, 1990). Climate change leads to increasing threats of the number of natural disasters, food insecurity and difficulty in accessing clean water and sanitation (Onoja *et al.*, 2011).

Carbon dioxide control can be achieved by the use of wet scrubbers containing alkali solutions such as K_2CO_3 (Schnelle and Brown, 2001). The use of carbon capture and storage controls carbon dioxide in the atmosphere by capturing the gas from exhaust gas or ambient air using membranes or cryogenic distillation, transporting and utilizing storing. The gas can be reused in the manufacture of fertilizers and polymer processing (Rajabloo *et al.*, 2023).

2.4.2 Sulphur dioxide (SO_2)

Sulphur dioxide, a major pollutant in the oxides of the sulphur group (Jittra *et al.*, 2015), is a common air pollutant mainly produced by burning fossil fuels containing sulphur (Manahan, 2017). Other anthropogenic sources include locomotives utilising sulphur-containing fuel and metal processing and smelting facilities (Zandaryaa and Buekens, 2009). In the cement manufacturing industry, sulphur dioxide is also produced from sulphur compounds in the raw material during the calcination process (Ali *et al.*, 2011; Devi *et al.*, 2017).

Sulphur dioxide causes respiratory health issues such as difficulty in breathing especially in children and individuals with underlying cardiovascular and pulmonary infections (Ali *et al.*, 2011). Prolonged exposure to sulphur dioxide can cause premature deaths (Manahan, 2017). Sulphur dioxide also causes the decolourization of green leaves and the stunting of leaf tissues (Lee *et al.*, 2017; Pastuszka, 2016).

Sulphur trioxide (SO_3) is also produced alongside sulphur dioxide but in very low concentrations (Zandaryaa and Buekens, 2009). Sulphur dioxide also undergoes oxidation to form sulphur trioxide in the presence of particulate catalysts in flue gas and the atmosphere (Dean, 2001). Sulphur trioxide readily dissolves in water vapour resulting in acid deposits that damage buildings, and affect aquatic life and plant growth (Gandhi *et al.*, 2017; Thurston, 2008). Sulphur trioxide can react with ammonia and other gaseous chemicals in the atmosphere to form sulphate particles. These particles have a very low aerodynamic diameter and they can scatter light hindering visibility (Vallero, 2014). These particles cause cardiovascular and respiratory health issues (Gandhi *et al.*, 2017).

The control of sulphur dioxide is achieved either through the prevention of emissions or the treatment of flue gas before being released into the atmosphere (Zandaryaa and Buekens, 2009).

Since sulphur dioxide is mainly produced through the burning of sulphur-containing fuel, the best solution would be to use an alternative fuel with low sulphur content (Jafarinejad, 2022). Alternatively, desulphurization can also be done to reduce sulphur levels in fuel. Generally, all conventional fuels contain sulphur compounds, either organic or inorganic (Zandaryaa and Buekens, 2009). Solid fuels such as coal can be mechanically milled and washed to reduce the concentration of sulphur (Schnelle and Brown, 2001). In the case of liquid and gaseous fuels, scrubbing using an appropriate absorption liquor, and capturing the gases or reactive solid adsorbents such as iron oxides can be used to lower sulphur content (Zandaryaa and Buekens, 2009). Flue gas treatment involves the use of chemical compounds that chemically interact with sulphur dioxide reducing its concentration. The compounds used include sodium hydroxide, sodium carbonate or calcium carbonate (Schnelle and Brown, 2001). The use of a sulphur recovery unit can also aid in the removal of hydrogen sulphide by converting it to elemental sulphur (Jafarinejad, 2022).

2.4.3 Nitrogen Oxides (NO_x)

Nitrogen can react with oxygen to form different oxides of nitrogen due to its wide range of ionization i.e. (+1 to +5). Some oxides that form include; nitrous oxide (N₂O), nitric oxide (NO), dinitrogen dioxide (N₂O₂), dinitrogen trioxide (N₂O₃), nitrogen dioxide (NO₂), dinitrogen tetroxide (N₂O₄) and dinitrogen pentoxide (N₂O₅) (Blaszczak, 1999).

Nitrous oxide (N₂O) is a greenhouse gas that can cause the depletion of ozone. The gas is mainly biogenic and can persist in the atmosphere for hundreds of years (Khalil and Rasmussen, 1992). Dinitrogen trioxide (N₂O₃), dinitrogen tetroxide (N₂O₄) and dinitrogen pentoxide (N₂O₅) are present in small amounts in flue gases (Blaszczak, 1999). The most prevalent gases in the oxides of nitrogen are NO₂ and NO (Jittra *et al.*, 2015).

The oxides of nitrogen in the atmosphere formed mainly as a result of the combustion process at very high temperatures (Boningari and Smirniotis, 2016). During the combustion process, the nitrogen in the atmosphere combines with oxygen forming nitrogen dioxide and nitric oxide shown in Equations (2) and (3). In cement production, this reaction takes place during the calcination and drying stages (Ali *et al.*, 2011; Devi *et al.*, 2017; Ibrahim *et al.*, 2012).



Inhaling nitrogen dioxide causes health problems such as respiratory disorders (Ibrahim *et al.*, 2012). Nitrogen dioxide undergoes various reactions in the atmosphere to form secondary pollutants that include acid rain, particulate matter and ozone (Jittra *et al.*, 2015). In the presence of VOCs and UV light, the oxides of nitrogen readily react to produce ozone. The VOCs are responsible for the oxidation of nitric oxide to nitrogen dioxide (Finlayson-Pitts and Pitts, 2012). The general chemical reactions for the formation of ozone are shown in Equations (4) below.



One of the major constraints in ozone control results from the ability of primary pollutants to travel over a long distance downwind before the ozone formation takes place (Blaszczak, 1999). As a pollutant, ozone causes various health problems such as difficulty in breathing and asthma, impairment in the functioning of the lungs, damage of the cell airways and lining fluids through oxidation and premature death, especially in children (Finlayson-Pitts and Pitts, 2012). Additionally, ozone as a greenhouse gas readily contributes to global warming and climate change (Blaszczak, 1999; Zhang *et al.*, 2019). Sulphur dioxide and nitrogen oxides readily dissolve in water to form weak acid depositions through complex chemical reactions (Mohajan, 2018).

Reducing the combustion temperatures by the injection of water or steam, cooled oxygen-depleted flue gas or by regulating the fuel to oxygen mixture readily reduces the oxide of nitrogen emissions (Blaszczak, 1999). The emissions can also be significantly reduced by chemically eliminating the NO_x using selective catalytic and non-catalytic reduction techniques (Han *et al.*, 2019; Javed *et al.*, 2007) or by the installation of a wet scrubber (Schnelle and Brown, 2001).

2.4.4 Formation and Effects of Acid Deposition

Acid deposition is a secondary pollutant formed when rainwater combines with sulphuric acid and nitric acid to form a deposition with a $\text{pH} < 5.6$ (Mohajan, 2018). Acid depositions develop as either wet deposits such as rain and snow or dry deposits such as aerosols, gas and dry particles (Gandhi *et al.*, 2017). Sulphur dioxide and nitrogen oxides readily react with water in the atmosphere to form a weak solution of sulphuric acid and nitric acid (Vallero, 2014).

In the air, sulphur dioxide is first converted to sulphur trioxide which readily combines with water in the atmosphere to form sulphuric acid as shown in Equations (5) and (6) (Mohajan, 2018). The oxidation process is catalysed by the presence of nitrogen dioxide in the air (Pastuszka, 2016).



Nitrogen oxide in the atmosphere causes the formation of nitric acid as shown in Equations (7) to (11). The formation of the acid is catalysed by UV radiation which promotes the formation of ozone and an oxygen radicle from nitrogen dioxide. The oxygen radicle formed oxidises water in the atmosphere to hydroxyl ions which in turn combine with nitric oxide and nitrogen dioxide to form nitrous acid and nitric acid. The nitrous acid formed is further oxidised to nitric acid (Mohajan, 2018)



The formation of acid rain adversely affects the environment. Hydrogen ions (H^+) readily react with calcium carbonate, CaCO_3 in cement to form soluble calcium hydrogen carbonate, $\text{Ca}(\text{HCO}_3)_2$ which is easily washed away with rainwater. This process severely damages buildings and cultural monuments (Gandhi *et al.*, 2017). Apart from buildings, acid rain affects aquatic life adversely. Acid rain reduces the pH of the water bodies and this causes the death of some species (Vallero, 2014). Due to the interdependence among aquatic species, the death of one will affect the other, thereby affecting the entire ecosystem (Gandhi *et al.*, 2017). In the soil, acid rain causes the leaching of nutrients such as magnesium (Gandhi *et al.*, 2017). In addition, it enables the formation and availability of toxic metal compounds of aluminium and mercury through cation exchange and partial dissolution (Gandhi *et al.*, 2017; Kim *et al.*, 2010) which are easily absorbed by plant species. Acid rain also washes away the toxic elements into water bodies affecting the aquatic species (Mohajan, 2018).

2.4.5 Analysis of Gaseous Emissions

Analysis of gaseous emissions involves measurements and monitoring of flue gas concentrations. In addition to monitoring the concentrations of undesirable gaseous products, emission analysis in industries and vehicles also enables the tuning of the combustion process to take place at maximum efficiency economizing on fuel consumption (Zaporozhets, 2019). The gases monitored during this process include oxygen, carbon dioxide, carbon monoxide, sulphur dioxide, nitrogen oxide, nitrogen dioxide and hydrocarbon (Rahman *et al.*, 2018). The concentration of oxygen, carbon dioxide and carbon monoxide during analysis is used to determine the efficiency of the combustion process (Santoleri, 2003). For a complete and efficient combustion process, the concentration of carbon monoxide should be minimised. Carbon monoxide is an undesirable product that is produced when the oxygen supply is inadequate (Vakkilainen, 2017; Vallero, 2019). The presence of oxygen during the combustion process also indicates more oxygen was supplied into the system and should be reduced to the optimum level required. Excess oxygen in the system is undesirable as it dilutes the carbon dioxide produced. Emission analysis, therefore, enables monitoring of the system to ensure the optimization of the combustion process (Rahman *et al.*, 2018).

In addition to the concentrations of oxygen, carbon monoxide and carbon dioxide, the emission analyser also monitors the concentrations of sulphur dioxide, nitrogen oxides (nitric oxide and nitrogen dioxide) and hydrocarbons (Rahman *et al.*, 2018). The presence of sulphur dioxide during analysis shows that the fuel used contains sulphur (Manahan, 2017). The sulphur dioxide content can be reduced by using either low-sulphur fuel or desulphurization of the fuel before usage (Zandaryaa and Buekens, 2009). High nitrogen oxide concentration indicates the process takes place at very high temperatures (Blaszczak, 1999; Francis and Peters, 1980). The high concentration may also be due to the presence of nitrogen-bound compounds in the fuel (Ali *et al.*, 2015a). The presence of hydrocarbons indicates incomplete combustion (Rahman *et al.*, 2018).

Apart from the concentrations of the various gaseous emissions, flue gas analysis also monitors gas temperature and draft. High exhaust gas temperature indicates heat loss which in turn indicates a lower level of fuel efficiency (Rahman *et al.*, 2018). Heat loss from the flue gas is determined by subtracting the temperature of the supply air from the exhaust gas temperature. A low draft results in the build-up of the emissions in the chamber while a high draft causes turbulence and prevents complete combustion. Flue gases can also be vented indoors when the draft is low (Craig and McMahan, 1996).

2.4.6 Emission Analysis

In stack emission analysis, the concentrations of gaseous emissions can be determined using a wide range of wet chemical-based standard methods. However, a portable emission analyser is often used (EPA, 2018). Emission analysers contain an in-built sampling pump used to draw in a representative stack gas sample through the gas-sampling probe. The gas sample drawn is filtered before entering the sensor. The sensors use various principles depending on the gas being analysed. The most common types of sensors used include electrochemical sensors, Metal Oxide Semiconductors (MOS) and non-dispersive infrared (NDIR) (Price, 2019).

Electrochemical sensors contain three electrodes, the working, counter and reference electrodes (Shinwari *et al.*, 2010). When the gas sample reaches the electrodes, a redox reaction takes place at the working electrode, initiating the flow of electrons and this generates an electric current. The electric current generated is proportional to the gas sample concentration (Koz, 2021). Nitrogen oxides, sulphur dioxide and carbon monoxide analysis are mainly based on electrochemical analysis (Beard *et al.*, 1979). Electrochemical sensors have low detection limits and require less energy (Price, 2019).

Non-dispersive infrared (NDIR) sensors analyse flue gases based on the principle that molecules absorb light of a specific wavelength that is characteristic of their structural composition and proportionality, either linear or nonlinear to their concentration (El-Azazy, 2019; Schnelle and Brown, 2001). This technique is best used to determine the concentration of carbon dioxide. Carbon dioxide absorbs infrared radiation at a wavelength of 4.26 μm . Non-dispersive infrared (NDIR) has a fast response time and requires limited calibration. In addition, unlike electrochemical sensors, NDIR has a prolonged lifespan. The gas pumped enters the sample chamber where infrared radiation is directed from the source towards the detector (Price, 2019).

In Metal Oxide Semiconductors (MOS), the gas pumped alters the resistance of the metal oxide during interaction (Rahman *et al.*, 2018). The difference in the resistance is used to calculate the concentration of the gas using a nonlinear correlation. Metal oxide semiconductors are low-cost semiconductors as compared to electrochemical sensors albeit other gases tend to interfere with the signal generated (McDermott, 2004).



Figure 2-6: E6000-5SC hand-held emission analyser (Apex Instruments, 2016)

Figure 2-6 shows a handheld E6000-5SC emission analyser used to determine the concentration, draft and exhaust temperature of stack emission. The analyser can determine the concentrations of oxygen, carbon monoxide, sulphur dioxide, nitric oxide and nitrogen dioxide using electrochemical sensors (Kuo *et al.*, 2019). The concentrations of carbon dioxide and nitrogen oxides are calculated. In addition, the analyser also can determine the concentration of hydrocarbons, the exhaust temperature and draft and exit velocity.

2.5 Atmospheric Dispersion Modelling

The atmospheric dispersion model is a mathematical simulation used to determine the ambient concentration of pollutants downwind from the emission source. Atmospheric modelling can be used to predict the impact of new and existing sources (Turner, 1994). With an increase in industrial development and population, atmospheric dispersion modelling is an important tool that can be used for monitoring and preventing future deterioration of air quality (Schnelle and Brown, 2001). Atmospheric dispersion modelling studies the dispersion of pollutants from the source to the receptors. The extent of dispersion is determined by the meteorological conditions and topography of the area (Turner, 1994). Source, receptor, meteorological, topographical and building parameters form the primary input to a dispersion model (Johnson, 2022) shown in Figure 2-7.

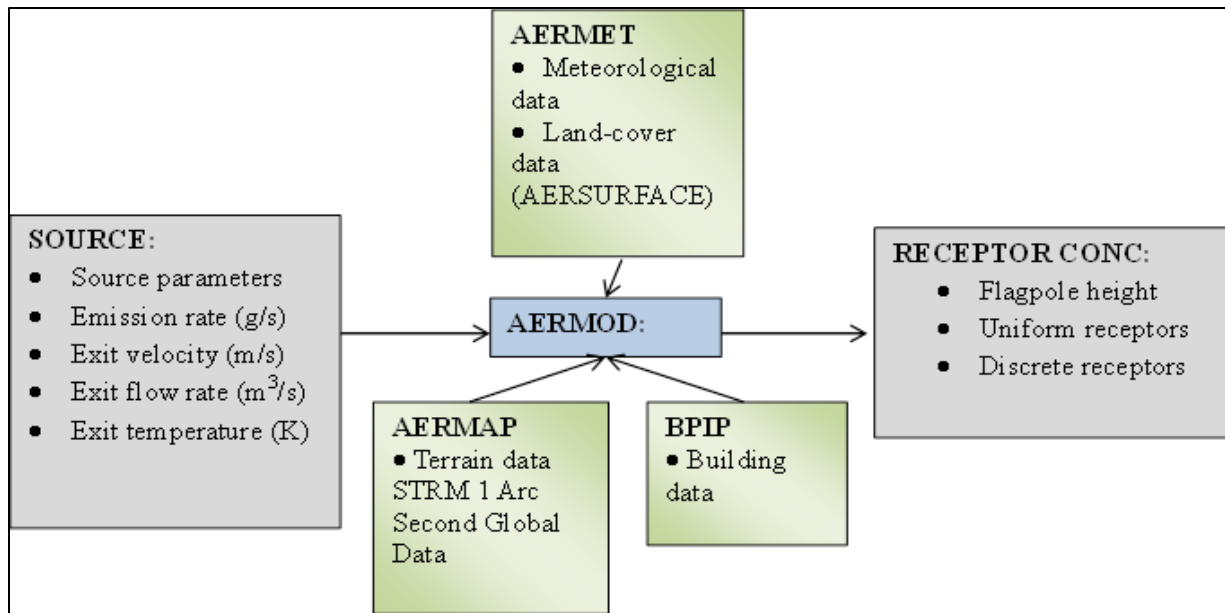


Figure 2-7: AERMOD schematic diagram

2.5.1 Sources of Air Pollution

The sources of air pollution can be divided into two general classes; point sources and non-point sources (Schweitzer and Noblet, 2018). The sources can also be further classified into stationary sources such as an industrial setup and moving sources such as motor vehicles using fossil fuel or steam engines (Schnelle and Brown, 2001). In the dispersion model, some of the source information required includes; source location coordinates, stack gas velocity, stack gas temperature, stack diameter, pollution emission rates, effective emission height, composition, concentration and density of emission (Turner, 1994).

2.5.2 Dispersion of Pollutants

The dispersion of pollutants from a source to receptors is governed by atmospheric characteristics and topographical conditions. Meteorological conditions such as wind direction and speed, turbulence and temperature inversion determine atmospheric stability (Turner, 1994) and the transportation and dispersion of pollutants. In dispersion models, the meteorological data used are averaged on an hourly basis (Schnelle and Brown, 2001). In urban centres, the presence of tall buildings influences the extent of pollutant dispersion as they cause a downwash effect (Schnelle and Brown, 2001). The speed and direction of the wind determine the extent and direction in which pollutants will travel and the dilution of the pollutants (Turner, 1994). Turbulence, both

mechanical and buoyant generation also affects the dispersion and mixing of air pollutants. Wind blowing past vegetation or structures generates mechanical turbulence while buoyant turbulence is due to heating and cooling of air close to the earth's surface (Turner, 1994). Buoyant generation turbulence often causes temperature inversion (Schnelle and Brown, 2001), a phenomenon that causes the atmosphere to stabilize and reduce vertical dispersion (Turner, 1994).

2.5.3 Pollution Receptor

Dispersion modelling aims to predict or determine the concentration of a specific pollutant at the receptor location thereby predicting the adverse effects the receptor is likely to experience. The ambient concentration at the receptor is determined by various factors affecting air quality and emission rates (Schnelle and Brown, 2001). Emission rates of various air pollutants should be in such a way that the pollutants do not accumulate over time and cause adverse effects at the receptor location (Turner, 1994). Receptor location and elevation are important inputs in analysing air dispersion modelling of particulate matter and gaseous pollutants (Turner, 1994).

2.6 American Meteorological Society/Environmental Protection Regulatory Model (AERMOD)

AERMOD is a Gaussian plume modelling system (Visscher, 2013) based on the assumption that pollutants released from a point source at a constant emission rate, Q (Turner, 1994), the wind blowing at a constant speed, u in the x -direction (Brusca *et al.*, 2016) causes the plume formed to spread vertically (z -direction) and perpendicularly (y -direction) as it moves in the x -direction to assume a Gaussian concentration profile (Visscher, 2013) as shown in Figure 2-8. The concentration $c(x, y, z)$ at any point in space is given by Equation (12) (Brusca *et al.*, 2016).

$$c(x, y, z) = \frac{Q}{2\pi\sigma_y\sigma_z u} \exp\left(-\frac{y^2}{2\sigma_y^2}\right) \left(\frac{1}{2\pi\sigma_z}\right) \exp\left(-\frac{(z-H)^2}{2\sigma_z^2}\right) \quad (12)$$

Where,

σ_z = extent to which the plumes move vertically

σ_y = extent to which the plumes move in a perpendicular direction

H = stack height

Gaussian plume models require little computation and are highly efficient. Examples of models developed based on this principle are AERMOD, ISC, CALINE, CTDMPPLUS, AEOLIUSF and OCD (Johnson, 2022; Visscher, 2013).

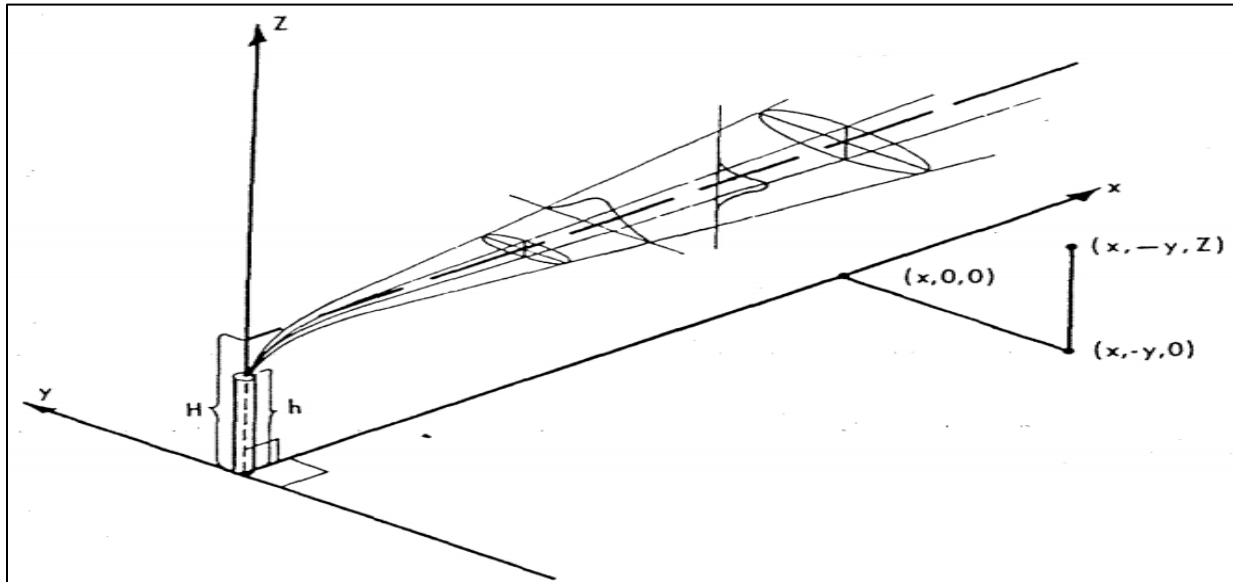


Figure 2-8: Gaussian plume (Visscher, 2013)

AERMOD is a new-generation modelling technique that has been developed as a supplement to Industrial Source Complex Short-Term, Version 3, ISCST3 (Schnelle and Brown, 2001). ISCST3 is best used as a screening model (Visscher, 2013) for non-reactive pollutants within a 16 km radius (Schnelle and Brown, 2001). AERMOD is recommended by the United States EPA for application within 50km from the source to the receptor (Jittra *et al.*, 2015). AERMOD is made of two data input pre-processors; AERMAP and AERMET.

2.6.1 Terrain Pre-processor (AERMAP)

Terrain data pre-processor (AERMAP) is used to characterize terrain and receptor grids and define the elevation of the area of study (Jittra *et al.*, 2015). As input, AERMAP requires gridded digital terrain, source and boundary layer data and receptor information (Zade and Ingole, 2015). The terrain data can be sourced from the United States Geological Survey (USGS) Earth Explorer databases. The global terrain data obtained is the Shuttle Radar Topography Mission (STRM) 1 Arc-Second Global data (EPA, 2018).

2.6.2 Meteorological Data Pre-processor (AERMET)

Meteorological data pre-processor (AERMET) is used to calculate boundary parameters (Zade and Ingole, 2015) such as surface heat balance, friction velocity, convective velocity scale and the Obukhov length (Visscher, 2013). These parameters are used to determine atmospheric stability by calculating the minimum angle of solar radiation required to generate sufficient heat to overcome temperature inversion (Schnelle and Brown, 2001; Visscher, 2013). Atmospheric stability determines whether heat is transferred from the surface to the atmosphere or vice versa, a phenomenon called temperature inversion (Turner, 1994).

As input, AERMET requires upper air sounding data and hourly surface meteorological data which comprises; relative humidity, temperature, wind speed and direction, surface pressure and cloud cover (Zade and Ingole, 2015). AERMET also contains a land cover data processor called AERSURFACE used to estimate land surface characteristics including Bowen ratio, surface roughness and Albedo (Pongprueksa and Chatchupong, 2016). A rough surface causes mechanical turbulence and mixing of the pollutants and subsequent pollutant deposition. Albedo, commonly known as surface reflectivity affects the amount of heat that a surface absorbs and releases to the atmosphere and the Bowen ratio indicates the amount of moisture in the atmosphere. This in turn causes convective turbulence. These parameters are used to determine the stability of the boundary layer (Visscher, 2013).

CHAPTER THREE

3 MATERIALS AND METHODS

3.1 Materials

3.1.1 Sample Collection

Samples were collected from two cement processing factories in Athi River, Machakos County in Kenya. The obtained samples comprised particulate matter (TSP, PM₁₀ and PM_{2.5}) and gaseous emissions (SO₂, NO_x, CO and CO₂). The particulate matter samples were collected under isokinetic conditions following EPA sampling protocols.

3.1.2 Sampling Sites

Two cement factories were selected for sample collection and analysis. The main processing operations in the two cement factories were grinding and milling raw materials. The cement factories were labelled as Cement Factory 1 (CF1) and Cement Factory 2 (CF2). CF1 and CF2 had a production capacity of 2.0 and 3.0 million metric tons per year. Cement manufacturing in CF1 involves milling and drying using a diesel-powered vertical roller mill (VRM) dryer while CF2 is a dry grinding facility that grinds and mills the readymade clinker with 5% gypsum using an electric-powered ball mill. The UTM coordinates and elevation of CF1 and CF2 are shown in Table 3-1.

Table 3-1: Location of sampling sites

Cement Factory	UTM Coordinates	Elevation (m)
Cement Factory 1 (CF1)	(37S 273285.26 mE 9841629.32 mS)	1539
Cement Factory 2 (CF2)	(37S 273268.57 mE 9841687.44 mS)	1512

3.1.3 Map of Sampling Area

Athi River is a town within Mavoko Sub-county in Machakos County that forms part of the greater Nairobi Metropolitan area located in the Universal Transverse Mercator coordinates (37S 275033.42 mE 9838954.72 mS). The town is relatively industrialised containing cement factories, chewing gum factories, oil refineries and steel manufacturing industries. Athi River also is home to low and middle-income residential areas such as Kitengela, Mlolongo, Syokimau and Athi River. Figure 3-1 below shows the map of the study area.

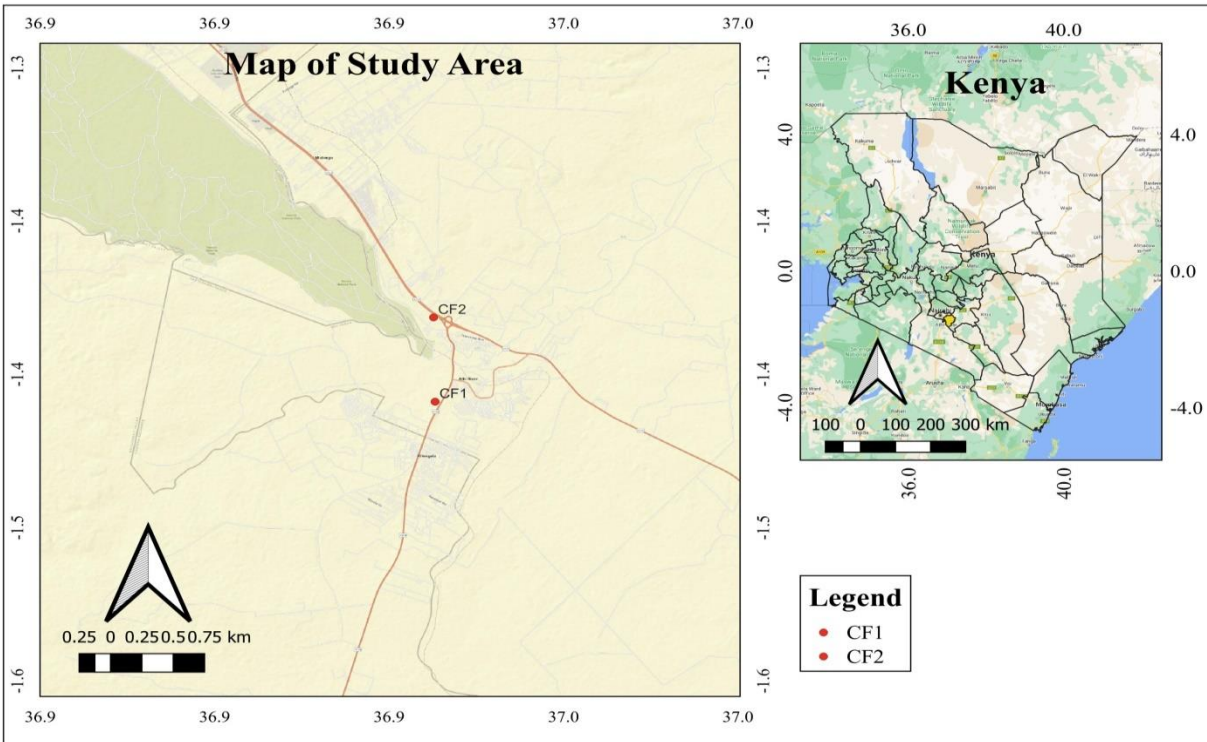


Figure 3-1: Map of the study area
(Source: Author)

3.1.4 Sampling Duration and Frequency

Sampling was done from the stationary sources in the selected cement factories. Cement Factory 1 comprised of one stationary source, labelled as Stack 1 releasing emissions from the drying and grinding process while Cement Factory 2 comprised of two stationary sources, Stack 2a and Stack 2b releasing emissions from the cement milling and grinding process.

Sampling from each of the three stacks in the two selected cement factories was carried out in April 2022, July 2022 and September 2022. Sampling was done in triplicate for each sampling run, i.e. Run 1, Run 2 and Run 3. The average of the triplicate sampling data; Sample 1, Sample 2 and Sample 3 for the samplings done in April, July and September was calculated from the triplicate sampling data and used to calculate the stack concentrations of the emitted pollutants (particulate matter and gaseous emissions).

3.1.5 Sampling Procedure

3.1.5.1 Particulate Matter

Sampling and analysis of particulate matter were carried out following the United States Environment Protection Agency (US EPA) standard methods 1, 2, 3, 4 and 5 (EPA, 2017d, 2017e, 2017f, 2020b) using an Isokinetic Source Sampler-XC-572-V as described in sections 3.2.1.1 to 3.2.1.5.

3.1.5.2 Gaseous Emissions

Gaseous emissions analysis was done using an E6000 emission analyser using US EPA methods 3A (CO₂), 6C (SO₂), 7E (NO_x) and 10 (CO) (EPA, 2017b, 2017c, 2017a, 2020a) described in sections 3.2.2.1 and 3.2.2.2.

3.1.6 Reagents and Chemicals

The list of chemicals and reagents used in the study is shown in Table 3-2

Table 3-2: Reagents and Chemicals

Item No.	Chemical	Amount/Size	Manufacturer
1	Acetone (>99% purity)	5 litres	FINAR
2	Silica Gel	1kg	FINAR
3	Distilled water	20 litres	FINAR
4	Ice cubes	10 kg	Prepared at the lab

3.1.7 Apparatus

The list of apparatus used in the study is shown in Table 3-3

Table 3-3: Apparatus

Item No.	Apparatus	Size	Manufacturer
1	Plastic wash bottles	500 ml	FINAR
2	Graduated glass cylinders	250 ml	FINAR
3	Petri dishes (plastic)	27 pairs	FINAR
4	Binder-less glass microfiber filter media in Petri-dishes	27 (1.47µm)	Lab-Exact
5	Nylon bristle brushes	520 mm length	FINAR
6	Rod	4 m	--
7	Ceramic fibre blanket	1 m	Kerui Refractory Co., Ltd
8	Blade	--	--
9	Surveyor tape measure	50 m	Hongzer Dev. Co., Ltd
10	Sample storage container	100 ml	FINAR

3.1.8 Instrumentation and Software

The instruments and the software used in this study are shown in Table 3-4

Table 3-4: Instruments and Software

Item No.	Instrument	Model (Version)
1	Isokinetic Sampler	Sampler-XC-572-V
2	Emission analyser	E6000 5SC handheld
3	AERMOD Modelling software	Web Lakes (Version 8.9.0)
4	Analytical balance	Sartorius Practum124

3.2 Methods

3.2.1 Particulate Matter Analysis

3.2.1.1 Determination of the Number of Traverse Points (EPA Method 1)

Standard EPA method 1 was used to determine the sampling points (EPA, 2020b). Into the stack, a long rod was inserted until it touched the other side of the wall. The point of entrance was marked before removing the rod. The length of the rod marked was measured using a tape measure and recorded as the length L_1 . Using the tape measure, the distance near the wall to the port nipple was also measured and recorded as length L_2 . The diameter of the stack was determined by the difference between the two lengths measured.

Horizontal measurements from the port to the nearest disturbance were also measured and recorded. This was done for both downstream (A) and upstream (B). Using the data obtained in the above procedures, the number of ‘duct diameters’ downstream and upstream were determined by dividing the distance A and distance B by the diameter, D. The number of traverse points was determined as illustrated in Figure 3-2.

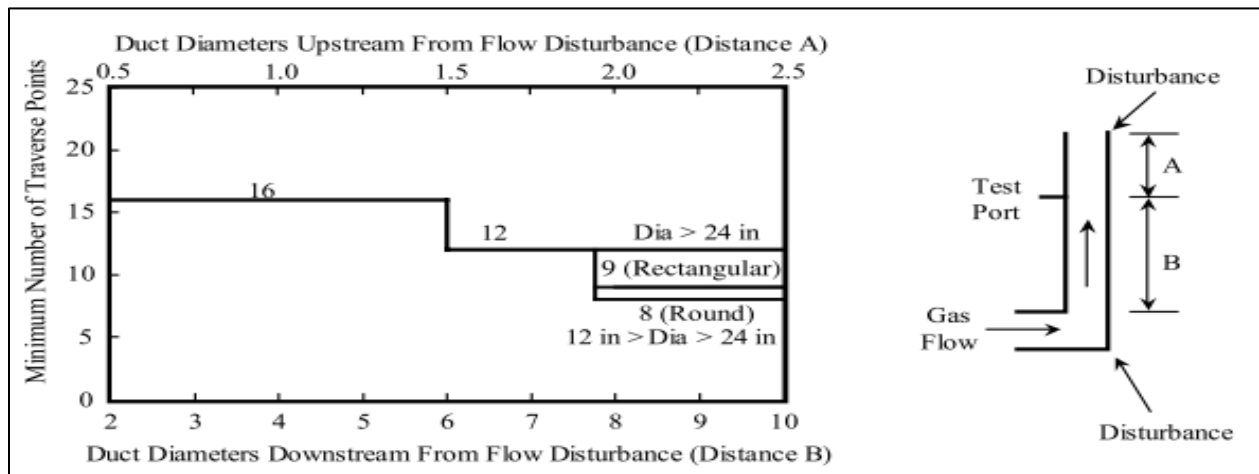


Figure 3-2: Determination of the number of traverse points (sampling points) (Schnelle and Brown, 2001)

3.2.1.2 Determination of Stack Gas Velocity and Volumetric Flow Rate (EPA Method 2)

Determination of the volumetric flow rate and velocity of sample gas was done based on standard EPA method 2 (EPA, 2017e). This involved the measurement of the stack gas temperature, velocity head and static gas pressure using an S-type pitot shown in Figure 3-3

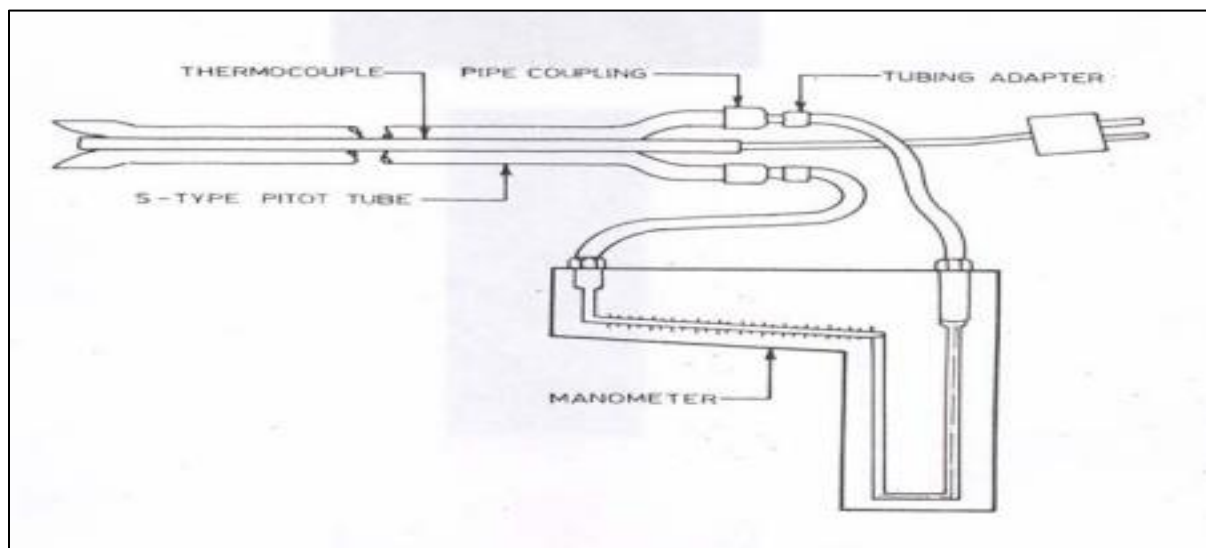


Figure 3-3: S-type Pitot tube with an inclined manometer

Source: (EPA, 2020b)

A pre-test leak-check: Into the S-type pitot impact opening, air was blown through until the 7.6 cm H₂O velocity head read on the manometer. The pressure (± 2.5 mm H₂O) was then observed for at least 15 seconds if it remained stable. This was repeated using suction for the static pressure side to obtain a minimum of 7.6 cm H₂O. In addition, the manometer was levelled and zeroed. Periodic checks were made between the runs to ensure the manometer level did not drift.

Stack Gas Temperature (T_s): An S-type Pitot tube was placed into the stack, starting with the furthest traverse. The sampling port was completely sealed off using a high-temperature silica cloth at the opening of the stack to prevent the ambient air effect. The temperature was allowed to stabilize before recording it as the absolute stack gas temperature (T_s). This was done at each traverse point, and the average of the absolute stack gas temperature ($T_{s(avg)}$) was calculated.

Determination of Velocity Head (ΔP): An S-type pitot tube was used to determine the velocity head. An S-type pitot tube was placed into the stack in such a way that one leg pointed in the direction of the flow and the other in the opposite direction. The leg pointing into the direction of the flow measured the impact pressure (P_i) and the other the wake pressure (P_w). The velocity pressure head (ΔP) in cm H₂O was then calculated by getting the difference between the impact

pressure and the wake pressure. This was done at each traverse point. The square root of the velocity head ($\sqrt{\Delta P}$) for each point was determined and the average of the square root of the velocity heads ($(\sqrt{\Delta P})_{avg}$) calculated.

Static Gas Pressure (P_g): An S-type pitot tube was placed into the stack and then rotated until the manometer reading was zero. The positive side was disconnected from the manometer and the oil deflection was read and recorded as a negative static pressure (P_g). If the oil travelled passed the zero mark, the positive end was connected and the negative end disconnected. The oil deflection was read and recorded as a positive static pressure (P_g). A post-test leak check was then carried out as illustrated in the pre-test procedure. The static pressure (P_g) in mm Hg was then used to calculate the absolute stack gas pressure (P_s) in mm Hg using Equation (13);

$$P_s = P_{bar} + \frac{P_g}{13.6} \quad (13)$$

Stack Gas Velocity: The average of the square root of the velocity heads ($(\sqrt{\Delta P})_{avg}$), absolute stack gas temperature (T_s) in Kelvin and absolute stack gas pressure (P_s) in mmHg, as measured and calculated, were used to determine the stack gas velocity using Equation (14);

$$v_s = K_p C_p (\sqrt{\Delta P})_{avg} \sqrt{\frac{T_{S(avg)}}{P_s M_s}} \quad (14)$$

Where,

K_p = velocity constant and is given by 34.97.

C_p = pitot tube coefficient and is given by 0.83, dimensionless.

M_s = molecular weight of the stack gas stream in g/g-mole, wet basis obtained in Method 4.

Volumetric Flow Rate: Using the stack gas velocity obtained above, the volumetric flow rates (actual, standard and dry standard) were calculated using Equations (15), (16) and (17);

$$\text{Actual volumetric flow rate, (m}^3/\text{min), } Q_a = 60 v_s A_s \quad (15)$$

$$\text{Standard volumetric flow rate, (sm}^3/\text{min), } Q_s = K_s v_s A_s \frac{P_s}{T_s} \quad (16)$$

$$\text{Dry standard volumetric flow rate, (dsmm}^3/\text{min), } Q_{std} = K_s (1 - B_{ws}) v_s A_s \frac{P_s}{T_s} \quad (17)$$

Where,

v_s = average stack gas velocity in m/sec.

A_s = area of the stack in m^2 .

K_s = a constant of 21.553 used to convert P/T to standard conditions and time to minutes.
 P_s = absolute stack gas pressure in mm Hg.
 T_s = absolute average stack gas temperature in K.
 B_{ws} = water vapour in the gas stream as determined in US EPA method 4, dimensionless.

3.2.1.3 Determination of Dry Molecular Weight (EPA Method 3)

A Portable Extractive Chemical Cell Analyser was used to determine the percentage concentrations of the gaseous pollutants based on US EPA methods 3A (oxygen and carbon dioxide) (EPA, 2017b).

A sampling probe was first connected to the cell analyser before switching it on. The cell analyser was allowed to idle for one minute to allow for calibration in ambient air. The probe was then inserted into the stack to draw out the gaseous mixture in the stack. The sampling port was completely sealed off using a high-temperature silica cloth at the opening of the stack to prevent the ambient air effect. After ten minutes, the gas concentrations were recorded. The analyser gave the percentage concentration of oxygen (%O₂) and carbon dioxide (%CO₂). The percentage concentration of nitrogen gas, N₂ and carbon dioxide (CO) was determined and used to calculate the dry molecular weight of the emission from the stack using Equations (18) and (19).

$$\%(\text{N}_2+\text{CO})=100-(\%\text{O}_2+\%\text{CO}_2) \quad (18)$$

$$M_d=0.32(\%\text{O}_2)+0.44(\%\text{CO}_2)+0.28(\%\text{CO}+\%\text{N}_2) \quad (19)$$

3.2.1.4 Determination of Moisture Content Rate (EPA Method 4)

The sampling procedure was based on standard US EPA method 4 (EPA, 2017f). Silica gel, 300g was placed into Impinger (4) and water, approximately 100 mL poured into Impingers (1) and (2). Impinger (3) was left empty. Each impinger and its contents were carefully measured and initial weights were recorded. Ice cubes were placed into an ice bath to facilitate condensation.

An appropriate probe length was selected based on the stack diameter. The probe tip was positioned at the first traverse point determined in Method 1. The pump was immediately turned on and the flow rate was adjusted to the desired rate.

After sampling, the impingers were measured and recorded as the final weights. The amount of liquid collected, M_w calculated by the differences in mass of the impingers, was used to calculate

the total moisture content by volume. Stack gas moisture content was obtained by calculating the ratio of gas moisture volume to the total volume of the sample gas and the gas moisture content.

$$\text{Stack gas moisture content, } B_{ws} = \frac{V_{wc(std)}}{V_{wc(std)} + V_{m(std)}} \quad (20)$$

In Equation (20),

$V_{m(std)}$ = sample gas volume, m^3 .

$V_{wc(std)}$ = gas moisture volume, m^3 .

The sample gas volume and the gas moisture volume were calculated using Equations (21) and (22).

$$\text{Sample gas volume, } V_{m(std)} = K_3 Y \Delta V_m \frac{\left(P_{bar} + \frac{\Delta H}{13.6} \right)}{T_m} \quad (21)$$

$$\text{Gas moisture volume, } V_{wc(std)} = K_2 (M_w) \quad (22)$$

In Equations (21) and (22),

$K_3 = 0.3858 \text{ } ^\circ\text{K/mm Hg}$,

Y = dry gas meter calibration factor and is given by 0.9965.

ΔV_m = dry gas volume measured by the dry gas meter, m^3 .

P_{bar} = barometric pressure at the measurement site, mm Hg.

ΔH = average orifice tube pressure during sampling in mm H_2O .

T_m = dry gas meter (DGM) absolute temperature in K.

$K_2 = 0.001335 \text{ } m^3/\text{g}$

M_w = amount of liquid collected in g

The dry gas volume represents the total amount of effluent gas sampled from the gas stream. The volume of gas sampled was used to determine the concentration in mg/m^3 of analysed constituents.

The stack gas moisture content B_{ws} and the dry molecular weight M_d in $\text{g}/\text{g-mole}$ were then used to calculate the molecular weight, wet basis, and M_s in $\text{g}/\text{g-mole}$ of the gas stream using Equation (23).

$$M_s = M_d(1 - B_{ws}) + 18(B_{ws}) \quad (23)$$

3.2.1.5 Determination of Total Suspended Particles (TSP) Concentration (EPA Method 5)

The sampling procedure was based on standard US EPA method 5 (EPA, 2020b). The filter heating system and the probe heater were turned on and set to temperatures of $120 \pm 14 \text{ } ^\circ\text{C}$ and allowed to

stabilize to prevent water vapour from condensing before reaching the condenser. Nozzle size was selected based on the range of velocity heads in such a way as to ensure isokinetic sampling was maintained.

During sampling, a probe was inserted into the stack through the ports and placed at each of the traverse points determined in US EPA method 1. To avoid disturbance from ambient air, the sampling port was completely sealed using a high-temperature silica cloth. At each traverse point, sampling was done for 5 minutes starting from the most distant traverse point.

A sample gas was pumped through a probe fitted with filter paper in a holder and particulate matter collected. The probe system contained a heating system that prevented the cooling of moisture contained in the gas stream. The filter media used were binder-less borosilicate glass microfibers with a diameter of 8.26 cm and 1.47 μ m pore size. The volume of the gas sample obtained from the gas stream was measured and recorded. The volume of the gas collected enabled the calculation of concentration in mg/m³. Sampling at each stationary point was done in triplicate for a sampling time of 60 minutes for each run.

After sampling, the probe was allowed to cool before dismantling the sample train. The openings were then capped to prevent leakage and the components were transported to the clean-up area. At the clean-up area, the filter paper was carefully removed using tweezers and placed in a Petri dish container. Using a sharp blade, the remaining particulate matter and filter fibres were scrapped onto a petri dish. The petri dish was covered and labelled “sample type 1” shown in Figure 3-4. This was done for each of the sample runs.

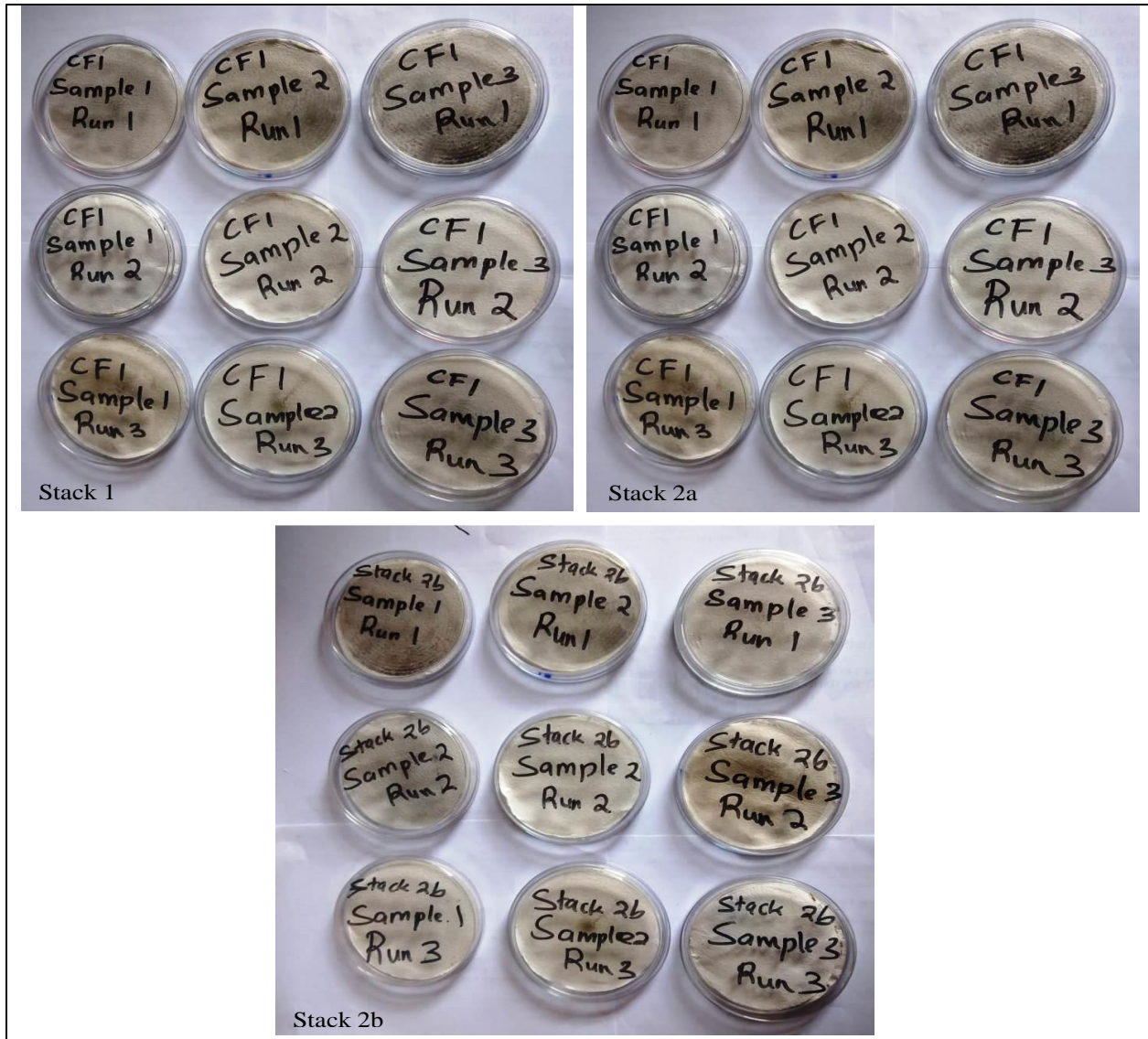


Figure 3-4: Filter papers contained in Petri dishes

The probe and the filter holder were then rinsed using acetone and a nylon bristle brush. This was done until the acetone rinse showed no visible particulate matter. The acetone was collected and placed in a container and labelled “sample type 2”. The level of the liquid in the containers was marked to determine whether any leakage took place during transportation to the laboratory. Unused acetone of equal volume to that of “sample type 2” was transferred into a separate container, sealed and labelled “acetone blank”.

In the laboratory, the filter paper contained in “sample type 1” was measured and recorded. The mass obtained was recorded as the final mass of the filter paper. The mass of particulate in “sample

type 1” was determined by subtracting the initial mass from the final mass of the filter paper. “Sample type 2” and “acetone blank” were observed to ensure no leakage took place during transportation then measured and the initial weights were recorded. The acetone was evaporated at ambient temperature and pressure and the mass of the containers was measured. The mass of the particulate in the probe was then determined by subtracting the final mass of “sample type 2” from the initial mass less the acetone blank.

The total weight of particulate matter (M_p) in mg was then calculated by adding the mass of particulate matter obtained in “sample Type 1” and “sample Type 2” less the acetone blank. The concentration of the particulate matter was then determined by dividing it by the sample gas volume as shown in Equations (24) and (25).

$$\text{Dry standard TSP concentration, } c_{\text{dry}} = \frac{M_p}{V_{m(\text{std})}} \quad (24)$$

$$\text{Normal wet TSP concentration, } c_{\text{wet}} = \frac{M_p}{V_{\text{wc}(\text{std})} + V_{m(\text{std})}} \quad (25)$$

3.2.1.6 Determination of Particulate Matter (PM₁₀, PM_{2.5}) Concentration

The concentration of PM₁₀ and PM_{2.5} were determined by multiplying the results obtained in Equation (24) in Section 3.2.1 concentration by 0.85 and 0.45.

3.2.1.7 Determination of Percentage Isokinetic Conditions

Using the data obtained in the US EPA Methods 1 to 5, the percentage isokinetic was then calculated using Equation (26) to determine the validity of the runs.

$$\text{Percentage isokinetic} = \frac{K_4 T_s V_{m\text{std}}}{P_s v_s A_n \theta (1 - B_{\text{ws}})} \quad (26)$$

In Equation (26),

$K_4 = 4.320$ mmHg

A_n = cross-sectional area of the nozzle in m^2 .

θ = sampling time in minutes.

3.2.2 Gaseous Emissions Analysis

Before sampling, the emission analyser was first switched on and then allowed to stand for one minute to calibrate in ambient air. The probe was then connected to the analyser. No oxygen reference was used.

3.2.2.1 Determination of Carbon Dioxide concentration (%)

The probe connected to the emission analyser was placed into the stack at the sampling port. After about twenty minutes, the carbon dioxide gas concentration was recorded in percentage units. The percentage concentrations were converted to mg/Nm³ using Equation (27) (EMCA, 2014).

$$c(\text{mg/m}^3) = c(\text{ppm}) \times \frac{\text{MW}}{22.4} \times \frac{273}{T(\text{K})} \times \frac{p}{101.3} \quad (27)$$

In Equation (27),

MW = molecular weight of carbon dioxide

T (K) = stack temperature in Kelvins

p = pressure in KPa

The concentration in ppm was obtained by multiplying the percentage concentration by 10000. All readings were recorded at atmospheric pressure p=101.3KPa.

3.2.2.2 Determination of Carbon Monoxide, Sulphur Dioxide and Nitrous Oxides concentration (mg/m³)

The probe connected to the emission analyser was placed into the stack at the sampling port. After about twenty minutes, the concentration of carbon monoxide, sulphur dioxide and nitrous oxides was recorded in mg/m³.

3.2.3 Dispersion Modelling of Particulate Matter and Gaseous Emissions

The model simulation was done using AERMOD. Modelling was done for each of the sample runs performed for each pollutant (TSP, PM₁₀, PM_{2.5}, CO, CO₂, SO₂ and NO_x).

The position of the cement manufacturing industrial site was first defined using the Universal Transverse Mercator (UTM) projection. The Cement Factories, CF1 and CF2 were located in the UTM Coordinates (37S 273285.26mE 9841629.32mS) and (37S 273268.57mE 9841687.44mS). The pollutant type depending on the run and averaging time was defined in a rural-based setup.

3.2.3.1 Meteorological Data

Meteorological data obtained contained surface hourly data and upper air sounding data. Hourly surface data was obtained from the National Centre for Environmental Information (NCEI) formerly the National Climatic Data Centre (NCDC) as reported by Kenya Ports Authority at Jomo Kenyatta International Airport (JKIA). Jomo Kenyatta International Airport weather station has station number 637400-99999 as assigned by the World Meteorological Organization (WMO). The data obtained was dated between 1st January 2018 and 31st December 2020. The hourly surface data included the measurement hour, day, month and year, relative humidity, temperature, opaque sky cover, wind speed and direction, cloud cover and surface pressure.

Upper air sounding data (height of measurement and temperature and pressure) was obtained from the National Oceanic and Atmospheric Administration Earth System Research Laboratories (NOAA/ESRL) database as reported by the Dagoretti weather meteorological station. Dagoretti meteorological weather station has station number 637410-99999 as assigned by the World Meteorological Organization (WMO). The hourly surface meteorological data and the upper air sounding data obtained were processed using the AERMET pre-processor.

3.2.3.2 Land Use Data

The land use cover at the hourly surface meteorological site was classified according to the National Land Cover Database (NLCD-1992). The area was classified into open water (11), low (21) and high-intensity residential areas (22), commercial/industrial and transportation (23), scrubland (51) and urban/recreational grasses (85) as shown in Figure 3-5.

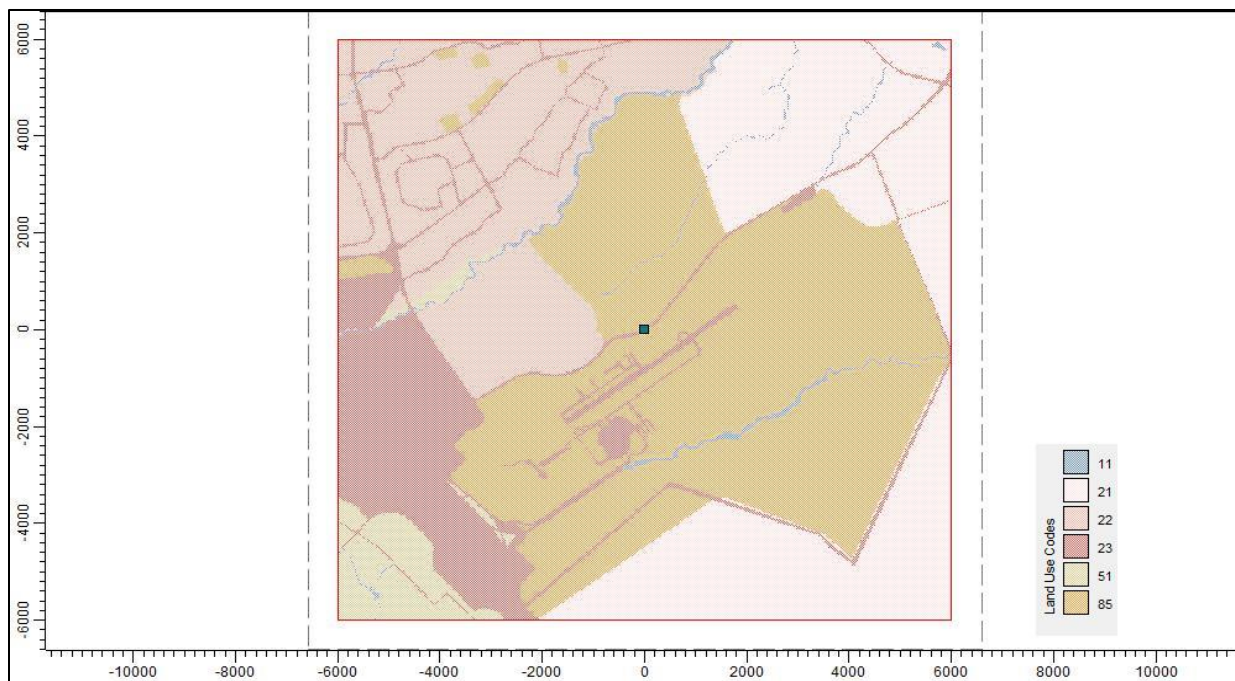


Figure 3-5: Land use

The land use data in GeoTIFF format were processed using an AERSURFACE pre-processor to obtain surface roughness, Albedo and Bowen ratio. A domain distance of 1 km radius relative to the measurement site was used to determine surface roughness. Albedo and Bowen's ratios were determined using a domain distance of 10 km by 10 km square distance centred at the measurement site.

3.2.3.3 Source Data

The source data included source location and release parameters. The source location details including stack location coordinates and stack elevation were obtained from Google Earth, which provided the above satellite imagery and 3D terrain of the study area. Source release parameters included stack height, stack diameter, stack gas exit velocity and temperature, stack gas flow rate, and emission rates. The source release parameters were obtained from the determination of stack emission concentration of particulate matter and gaseous emissions. The emission rate in mass per unit time (g/s) was calculated from the concentration of particulate matter and gaseous emissions obtained in Sections 3.2.1 and 3.2.2 using Equation (28).

$$\text{Emission Rate } \left(\frac{\text{g}}{\text{s}}\right) = \frac{\text{Actual Volumetric flow rate } \left(\frac{\text{m}^3}{\text{s}}\right) \times \text{Concentration } \left(\frac{\text{mg}}{\text{m}^3}\right)}{10^3} \quad (28)$$

3.2.3.4 Terrain and Building Data

Terrain data was obtained from the USGS as STRM 1-Arc second global digital elevation data. For the selected buildings found around the study area, the data required included the building tier heights and their elevations. The terrain and buildings' data were processed using AERMAP and BPIP respectively to obtain the elevation in metres of the surrounding area, including the defined buildings, point sources and receptors points.

3.2.3.5 Receptor Data

Modelling was done at a square distance of 10 km by 10 km centred at each of the point sources. The concentrations were simulated at a flagpole height of 1.50 m, the approximate breathable height. Uniform Cartesian Grid with a grid resolution of 50 m by 50 m within the first 5 km by 5km square distance and 200 m by 200 m up to the 10 km by 10 km square distance centred at the point source totalling to 10201 and 2601 uniform receptor points. Selected Discrete receptors (8) were also defined including schools and hospitals. The discrete receptors (A, B, C, D, E, F, G and H) selected included schools and hospitals shown in Table 3-5. The total number of receptor points, including both uniform and discrete receptors was 12810.

Table 3-5: Discrete Receptors

Discrete Receptor	Distance from CF1 (km)	Distance from CF2 (km)
A	2.2	2.1
B	2.6	0.5
C	2.4	4.3
D	1.3	4.3
E	2.4	3.6
F	1.9	3.7
G	3.5	6.2
H	1.7	3.4

3.2.3.6 Output

After feeding the data above (pre-processed meteorological data, land use data, terrain data, building data, source data, and receptor data) AERMOD software was allowed to run. The concentration of each receptor was represented as a contour plot file for the 1st highest 24-hour

and annual period for particulate matter, sulphur dioxide and nitrogen oxides and the 1st highest 1-hour and 8-hour period for carbon dioxide and carbon monoxide. The mean maximum concentration as predicted by the model and the location were recorded. The concentrations observed at the selected discrete receptor boundaries were also recorded. The above concentrations were compared with the ambient tolerance limits stipulated under EMCA, 2014 and WHO Air Quality Guidelines, 2021.

3.2.3.7 Effect of Stack Height on Mean Maximum Concentration of Carbon Dioxide
For the pollutants with the mean maximum concentration above the ambient tolerance limits stipulated under EMCA, 2014 and WHO Air Quality Guidelines, 2021, AERMOD simulations were carried out using the stack heights recommended according to good engineering practices and its average emission rate. The mean maximum concentrations from the current height and those from the predicted height were compared.

CHAPTER FOUR

4 RESULTS AND DISCUSSION

4.1 Stack Emission of Particulate Matter Analysis

4.1.1 Determination of the Number of Traverse Points

The number of traverse points as determined using US EPA method 1 is shown in Table 4-1.

Table 4-1: Determination of Traverse Points

	CF1	CF2	
	Stack 1	Stack 2a	Stack 2b
Shape	Circular	Circular	Circular
Diameter, D (m)	1.8	1.5	1.5
Upstream distance, A (m)	20	16	27
Downstream distance, B (m)	10	14	9
Upstream Duct Diameter (A/D)	11.11	10.67	16
Downstream Duct Diameter (B/D)	6	9	6
Meets Requirements*	YES	YES	YES
Number of traverse Points	12	12	12

* For circular stationary points with diameters greater than 0.6 m and downstream and upstream duct diameters greater than 8 and 2 respectively, the number of traverse points should be 12.

From Table 4-1, the total number of traverse points was 12 for each of the sampling points. The number of traverse points in each of the stationary points in the cement factories was calculated based on the shape and duct diameters (geometric configuration) of the stack. The diameters of the stationary points were 1.8 m for Stack 1 and 1.5 m for Stack 2a and Stack 2b. The upstream and downstream duct diameters were calculated by dividing the upstream distance and the downstream distance by the diameter. The upstream and downstream duct diameters calculated were 11.11 and 6 for Stack 1, 10.67 and 9 for Stack 2a and 16 and 6 for Stack 2b. Given that each of the stationary points was circular with diameters greater than 0.6 m and duct diameters greater than eight and two for upstream and downstream respectively; the number of traverse points for each of the stationary points was 12. Sampling at the traverse points is essential because the particulate matter is not evenly distributed within the gas stream. A sampling port position that meets the above requirement ensures that the gas sampled represents the total or a known portion of the emissions released from the source (Schnelle and Brown, 2001).

4.1.2 Determination of Stack Gas Velocity and Volumetric Flow Rate

Table 4-2 shows the absolute stack gas pressure, the stack gas velocity (V_s) and the volumetric flow rate; actual (Q_a), standard (Q_s) and dry standard (Q_{std}).

Table 4-2: Stack gas velocity and volumetric flow rate

		Sample 1	Sample 2	Sample 3	Average
Stack 1	P_s (mmHg)	764.3±0.001	764.3±0.0026	764.3±0.0082	764.3±0.006
	V_s , (m/sec)	3.972±0.016	4.057±0.023	4.123±0.086	4.051±0.076
	Q_a , (m ³ /min)	606.4±1.098	619.4±3.573	629.6±3.696	618.5±11.583
	Q_s , (sm ³ /min)	500.5±1.098	505.5±3.573	517.0±3.696	507.7±8.440
	Q_{std} , (dsm ³ /min)	476.5±1.248	490.8±2.066	503.9±4.000	490.1±13.313
Stack 2a	P_s (mmHg)	680.5±0.0005	680.5±0.0018	680.5±0.0011	680.5±0.001
	V_s , (m/sec)	6.472±0.020	6.441±0.085	6.493±0.029	6.469±0.026
	Q_a , (m ³ /min)	686.2±2.133	682.9±9.059	688.5±3.086	685.9±2.818
	Q_s , (sm ³ /min)	496.8±0.851	495.1±2.491	488.9±1.749	493.6±4.205
	Q_{std} , (dsm ³ /min)	473.6±1.443	469.2±3.032	464.9±0.662	469.1±4.571
Stack 2b	P_s (mmHg)	680.5±0.000	680.5±0.000	680.5±0.000	680.5±0.000
	V_s , (m/sec)	7.424±0.0071	7.141±0.1273	6.463±0.1047	7.009±0.494
	Q_a , (m ³ /min)	787.1±0.0125	757.1±13.50	685.3±11.10	743.2±52.31
	Q_s , (sm ³ /min)	564.1±0.7556	543.8±4.144	489.2±6.437	532.4±38.76
	Q_{std} , (dsm ³ /min)	539.9±1.244	521.6±2.840	460.7±4.468	507.4±41.50

* P_s – Absolute Stack Gas Pressure, V_s – Stack gas velocity; Q_a – Volumetric flow rate; Q_s – Volumetric flow rate; Q_{std} – Volumetric flow rate dry Q_{std}

Table 4-2 shows the average absolute stack gas pressure was (Stack1 = 764.3±0.006 mmHg; Stack 2a = 680.5±0.001 mmHg; Stack 2b = 680.5±0.000 mmHg). The absolute stack gas pressure was used to determine the stack gas velocity (V_s) and the volumetric flow rate; actual (Q_a), standard (Q_s) and dry standard (Q_{std}). The stack velocity for the stationary points was (Stack 1 = 4.051±0.076 m/s; Stack 2a = 6.469±0.026 m/s; Stack 2b = 7.009±0.494 m/s). The actual volumetric flow rates were (Stack 1 = 618.5±11.583 m³/min; Stack 2a = 685.9±2.818 m³/min; Stack 2b = 743.2±52.31 m³/min). The standard volumetric flow rates calculated were (Stack 1 = 507.7±8.440 m³/min; Stack 2a = 493.6±4.205 m³/min; Stack 2b = 532.4±38.76 m³/min). The standard volumetric flow rate provides the reading at standard temperature (273K) and pressure (100 kPa).

Stack gas velocity and volumetric flow rates describe the rate of emission released from the stack into the atmosphere (Geršl *et al.*, 2018). The stack gas velocity was below the recommended velocity of 12 to 20 m/s according to Patel, 2022. Low stack velocity results in low momentum

force and lower plume rise (Bhargava, 2016; Carson and Moses, 2012). Lower plume rise results in higher ground-level concentrations of the pollutant within the gas stream (Westbrook, 1999).

4.1.3 Determination of Molecular Weight, Dry Basis

The dry molecular weights, calculated from the percentage concentration of oxygen, carbon dioxide, carbon monoxide and nitrogen of the gas stream in the three stationary points are shown in Table 4-3.

Table 4-3: Dry molecular weight

		Sample 1	Sample 2	Sample 3	Average
Stack 1	O ₂ (%)	19.81±0.040	19.5±0.079	19.3±0.324	19.53±0.257
	CO ₂ (%)	1.7±0.794	1.3±0.608	1.5±0.265	1.5±0.2
	N ₂ + CO, (%)	78.49±0.832	79.2±0.594	79.2±0.171	78.963±0.410
	M _d (g/g-mole)	29.06±0.129	28.99±0.097	29.01±0.032	29.021±0.039
Stack 2a	O ₂ (%)	19.98±0.040	19.87±0.324	18.91±0.079	19.589±0.589
	CO ₂ (%)	0.02±0.794	0.01±0.265	0.01±0.608	0.013±0.006
	N ₂ + CO, (%)	80.00±0.832	80.119±0.171	81.08±0.594	80.40±0.592
	M _d (g/g-mole)	28.80±0.129	28.80±0.032	28.76±0.097	28.79±0.024
Stack 2b	O ₂ (%)	19.98±0.330	19.87±0.671	18.91±0.390	19.589±0.589
	CO ₂ (%)	0.02±0.010	0.01±0.000	0.01±0.000	0.013±0.006
	N ₂ + CO, (%)	80.00±0.339	80.12±0.671	81.08±0.390	80.40±0.592
	M _d (g/g-mole)	28.80±0.015	28.80±0.027	28.76±0.016	28.79±0.024

*M_d – Dry Molecular Weight

The dry molecular weights of the gas stream in the stack were 29.021±0.039 g/g-mole for CF1 Stack 1 and 28.79±0.024 g/g-mole for both Stacks 2a and 2b in CF2. The dry molecular weight of a gas stream is used to determine the volumetric flow rate of a gas stream as discussed in Sections 4.1.2 and 4.1.4 (EPA, 2017d).

4.1.4 Determination of Stack Gas Volume and Wet Molecular Weight

The wet molecular weight of the stack gas stream was determined by the mass of condensed moisture collected at the impinger as shown in Table 4-4 below

Table 4-4: Mass of liquid collected in impingers

	Sample 1 (g)	Sample 2 (g)	Sample 3 (g)	Average (g)
Stack 1	35.0±1.097	21.0±5.31	20.3±1.42	25.43±8.292
Stack 2a	31.9±1.097	33.94±0.026	32.79±0.009	32.70±1.023
Stack 2b	33.3±0.015	31.94±0.040	40.62±0.015	32.29±4.670

From Table 4-4, the average mass of the liquid (M_w) collected in the three average sample runs for each of the stationary points, Stacks 1, 2a and 2b were 25.43 ± 8.292 g, 32.70 ± 1.023 g and 32.29 ± 4.669 g. The mass of the moisture obtained was used to determine the standard volume of the gas stream and the stack gas moisture content (B_{ws}) as described in section 4.1.4 which was then used to calculate the molecular weight, wet basis in Table 4-5.

Table 4-5: Molecular weight, wet basis

	CF1, Stack 1				
		Sample 1	Sample 2	Sample 3	Average
Stack 1	V_m (std), m^3	0.926 ± 0.014	0.933 ± 0.163	0.981 ± 0.025	0.9467 ± 0.0298
	V_{wc} (std), m^3	0.047 ± 0.001	0.028 ± 0.007	0.027 ± 0.002	0.0340 ± 0.0110
	B_{ws}	0.048 ± 0.002	0.029 ± 0.007	0.027 ± 0.002	0.0347 ± 0.0116
	M_s , g/gmol	28.53 ± 0.102	28.67 ± 0.131	28.72 ± 0.048	28.64 ± 0.0947
Stack 2a	V_m (std), m^3	0.869 ± 0.129	0.820 ± 0.038	0.834 ± 0.112	0.8408 ± 0.0250
	V_{wc} (std), m^3	0.043 ± 0.001	0.045 ± 0.000	0.044 ± 0.000	0.0439 ± 0.0014
	B_{ws}	0.047 ± 0.005	0.052 ± 0.002	0.049 ± 0.005	0.0493 ± 0.0029
	M_s , g/gmol	28.30 ± 0.176	28.23 ± 0.043	28.22 ± 0.149	28.25 ± 0.0413
Stack 2b	V_m (std), m^3	0.993 ± 0.057	1.004 ± 0.138	0.877 ± 0.165	0.9579 ± 0.0707
	V_{wc} (std), m^3	0.044 ± 0.000	0.043 ± 0.000	0.054 ± 0.000	0.0471 ± 0.0062
	B_{ws}	0.043 ± 0.002	0.041 ± 0.006	0.058 ± 0.011	0.0473 ± 0.0096
	M_s , g/gmol	28.34 ± 0.024	28.36 ± 0.073	28.13 ± 0.108	28.28 ± 0.1255
* V_m (std) – Sample Gas Volume; V_{wc} (std) – Gas Moisture Volume; B_{ws} – Stack gas moisture content; M_s – Wet Molecular weight					

The dry average standard volume, V_m (std) of the gas stream were (Stack 1 = 0.9467 ± 0.0298 m^3 ; Stack 2a = 0.8408 ± 0.0250 m^3 ; Stack 2b = 0.9579 ± 0.0707 m^3) and the gas moisture volume in the gas streams were (Stack 1 = 0.0340 ± 0.0110 m^3 ; Stack 2a = 0.0439 ± 0.0014 m^3 ; Stack 2b = 0.0471 ± 0.0062 m^3). The wet molecular weight of gas stream, M_s were (Stack 1 = 28.64 ± 0.0947 g/gmol; Stack 2a = 28.25 ± 0.0413 g/gmol; Stack 2b = 28.28 ± 0.1255 g/gmol). This was calculated from the average stack gas moisture content, B_{ws} of (Stack 1 = 0.0347 ± 0.0116 , Stack 2a = 0.0493 ± 0.0029 ; Stack 2b = 0.0471 ± 0.0062) from the Stacks 1, 2a and 2b.

4.1.5 Determination of Percentage Isokinetic

To validate the isokinetic conditions during sampling, the percentage isokinetic was calculated from the averages obtained from each run. The results are shown in Table 4-6 and Figure 4-1.

Table 4-6: Percentage isokinetic (Validatory procedure)

	Sample 1	Sample 2	Sample 3	Average	Comment
CF1, Stack 1	97.31	95.23	97.64	96.73±1.32	Valid
CF2, Stack 2a	100.0	95.34	97.96	97.77±2.36	Valid
CF2, Stack 2b	100.3	105.0	103.8	103.03±2.44	Valid

*Key: A valid run should have the percentage isokinetic calculation in the range of 90% to 110% (EPA, 2020b)

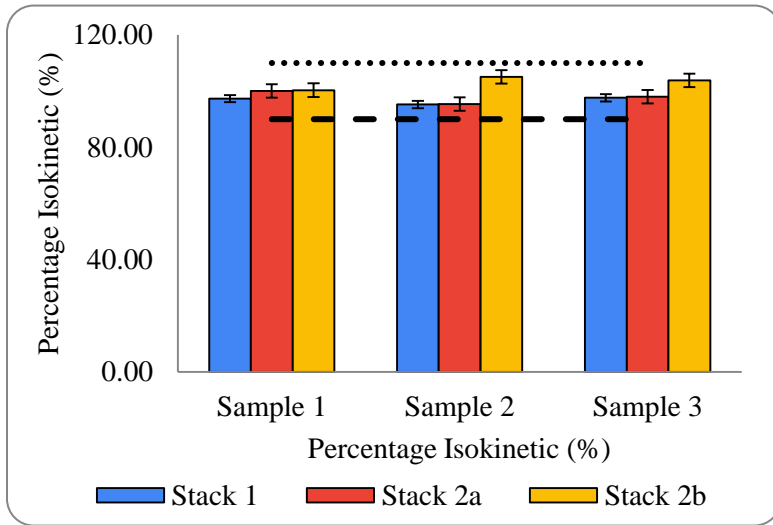


Figure 4-1: Percentage Isokinetic (%)

Figure 4-1 shows that the sampling runs were within the required percentage range of 90% to 110%, indicating that the sampling process was done under isokinetic conditions. The samples collected formed a fairly representative portion of the gas stream within the stack. A higher or lower sample velocity causes lower or higher than expected particulate concentrations respectively (Schnelle and Brown, 2001).

4.1.6 Stack Emission Concentration of Total Suspended Particulates

The mass of collected particulate matter was determined gravimetrically by calculating the mass of particulate matter accumulated on the filter paper (sample type 1) and the probe catch (sample type 2) less the acetone blank. The mass is shown in Table 4-7.

Table 4-7: Mass of particulate matter collected

Weight of Particulate, mass g	Sample 1	Sample 2	Sample 3	Average
Stack 1	0.0052±0.0003	0.0059±0.0004	0.0047±0.0003	0.0053±0.0006
Stack 2a	0.0041±0.0014	0.0054±0.0001	0.0048±0.0006	0.0048±0.0007
Stack 2b	0.007±0.0007	0.0065±0.0001	0.0068±0.0003	0.0068±0.0003

The average mass of the particulate matter collected and used to calculate its concentration was (Stack 1 = 0.005267 g; Stacks 2a = 0.004767 g; Stack 2b = 0.006767 g).

The standard dry (C_d) and wet (C_w) concentrations of Total Suspended Particles sampled from Stack 1, Stack 2a and Stack 2b are shown in Table 4-8 and Figure 4-2.

Table 4-8: Stack emission concentration of Total Suspended Particles

Conc. in mg/Nm ³		Sample 1	Sample 2	Sample 3	Average	Standard Limit
Stack 1	C_d	5.613	6.324	4.791	5.576±0.767	50
	C_w	5.343	6.140	4.663	5.382±0.739	
Stack 2a	C_d	4.721	6.586	5.755	5.687±0.934	
	C_w	4.500	6.241	5.468	5.403±0.872	
Stack 2b	C_d	7.050	6.472	7.758	7.093±0.644	
	C_w	6.748	6.208	7.306	6.754±0.549	

*The standard limits are under EMCA, 2014

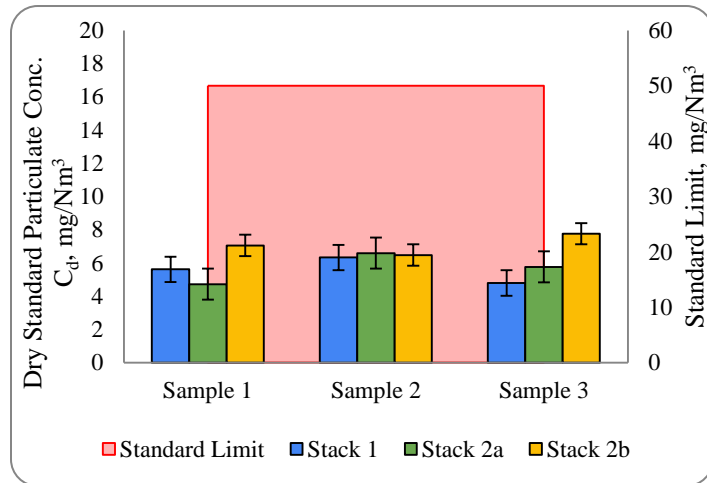


Figure 4-2: Stack emission – dry standard concentration of total suspended particles

The concentration of the Total Suspended Particles was determined by dividing the mass collected by the standard gas volume, i.e. dry and wet concentration. The average dry standard concentration of the Total Suspended Particles was (Stack 1 = 5.576±0.767 mg/Nm³; Stack 2a = 5.687±0.934 mg/Nm³; Stack 2b = 7.093±0.644 mg/Nm³). Wet particulate matter concentration was calculated by considering the gas moisture volume. The average wet concentration of Total Suspended Particles was (Stack 1 = 5.382±0.739 mg/Nm³; Stack 2a = 5.403±0.872 mg/Nm³; Stack 2b = 6.754±0.549 mg/Nm³) shown in Table 4-8. The results show that there was a minimal change in difference ($P>0.05$) in the source concentrations of Total Suspended Particles in the three

stationary sources. Figure 4-2 shows that the dry standard concentrations of Total Suspended Particles were within the standard limit of 50 mg/Nm³ for cement factories as stipulated under EMCA, 2014. The low concentrations of Total Suspended Particles were attributed to the baghouse filters installed as the emission control technology. Bag house filters are effective in controlling coarse (greater than 10 µm) particulate matter with an efficiency of up to 99% (Gupta *et al.*, 2012).

4.1.7 Stack Emission Concentration of PM₁₀ and PM_{2.5}

The concentration of PM₁₀ and PM_{2.5} was calculated from the Total Suspended Particles. The concentration of PM₁₀ and PM_{2.5} form a fraction of the Total Suspended Particles (Ciobanu *et al.*, 2021). The concentration of PM₁₀ and PM_{2.5} from Stack 1, 2a and 2b are shown in Table 4-9 and Figure 4-3.

Table 4-9: Stack emission concentration of PM₁₀ and PM_{2.5}

Conc. in mg/Nm ³		Sample 1	Sample 2	Sample 3	Average	Standard Limit	
PM ₁₀	Stack 1	C _d	4.771	5.376	4.073	4.740±0.652	50
		C _w	4.542	5.219	3.963	4.575±0.513	
	Stack 2a	C _d	4.013	5.598	4.892	4.834±0.794	
		C _w	3.825	5.305	4.648	4.593±0.605	
	Stack 2b	C _d	5.992	5.501	6.594	6.029±0.547	
		C _w	5.736	5.277	6.210	5.741±0.381	
PM _{2.5}	Stack 1	C _d	2.526	2.846	2.156	2.509±0.345	Np
		C _w	2.404	2.763	2.098	2.422±0.272	
	Stack 2a	C _d	2.124	2.964	2.590	2.559±0.420	
		C _w	2.025	2.808	2.461	2.431±0.320	
	Stack 2b	C _d	3.172	2.912	3.491	3.192±0.290	
		C _w	3.036	2.794	3.288	3.039±0.202	

*The standard limits are under EMCA, 2014 (EMCA, 2014); Np – not provided

From Table 4-9, the average dry standard concentration of PM₁₀ was (Stack 1 = 4.740±0.652 mg/Nm³; Stack 2a = 4.834±0.794 mg/Nm³; Stack 2b = 6.029±0.547 mg/Nm³) and the average normal wet concentration was (Stack 1 = 4.575±0.513 mg/Nm³; Stack 2a = 4.593±0.605 mg/Nm³; Stack 2b = 5.741±0.381 mg/Nm³). The average dry standard concentration of PM_{2.5} was (Stack 1 = 2.509±0.345mg/Nm³; Stack 2a = 2.559±0.420mg/Nm³; Stack 2b = 3.192±0.290 mg/Nm³) and the average normal wet concentration was (Stack 1 = 2.422±0.272mg/Nm³; Stack 2a = 2.431±0.320mg/Nm³; Stack 2b = 3.039±0.202 mg/Nm³). The results show that there was a

minimal change in the difference ($P>0.05$) in the source concentrations of the PM_{10} and $PM_{2.5}$ from the three stationary sources

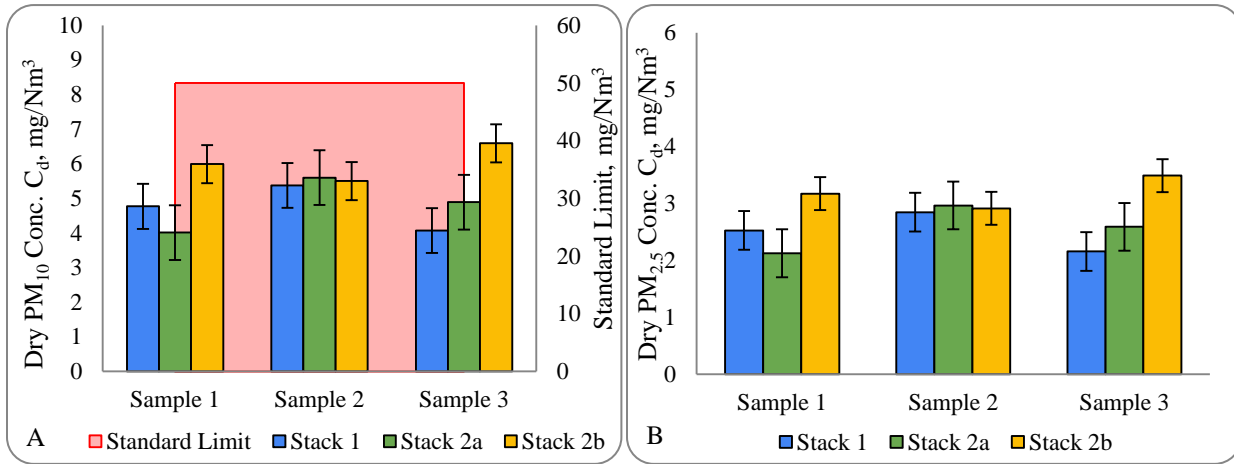


Figure 4-3: Stack emission – dry standard emission (A) PM_{10} and (B) $PM_{2.5}$ concentration

Figure 4-3 shows that the concentration of PM_{10} and $PM_{2.5}$ could be compared to each of the stationary points. The concentrations of PM_{10} were within the standard limit of 50 mg/Nm^3 for cement factories as stipulated under EMCA, 2014. The limits for $PM_{2.5}$ were not provided.

4.2 Stack Emission of Gaseous Emissions Analysis

4.2.1 Stack Emission Concentration of Carbon Dioxide

The percentage of concentration of carbon dioxide from the three stacks is shown in Table 4-10.

Table 4-10: Percentage concentration of carbon dioxide

	Sample 1 (%)	Sample 2 (%)	Sample 3 (%)	Average (%)
CF1 Stack 1	1.7 ± 0.79	1.3 ± 0.26	1.5 ± 0.26	1.5 ± 0.163
CF2 Stack 2a	0.02	0.01	0.01	0.013 ± 0.005
CF2 Stack 2b	0.02 ± 0.012	0.01	0.01	0.013 ± 0.005

The concentrations of carbon dioxide were (Stack 1 = $1.5 \pm 0.163\%$; Stack 2a = $0.013 \pm 0.005\%$; Stack 2b = $0.0133 \pm 0.005\%$). The concentrations of carbon dioxide converted to mg/Nm^3 are shown in Table 4-11 and Figure 4-4.

Table 4-11: Concentration of carbon dioxide

	Sample 1	Sample 2	Sample 3	Average	Standard Limit
CF1 Stack 1 (mg/Nm^3)	27404.3	20724.1	24058.5	24062.3 ± 3340	500
CF2 Stack 2a (mg/Nm^3)	317.65	159.05	155.76	210.82 ± 92.53	500
CF2 Stack 2b (mg/Nm^3)	314.45	157.56	156.59	209.53 ± 90.86	500

*The standard limits are under EMCA, 2014 (EMCA, 2014)

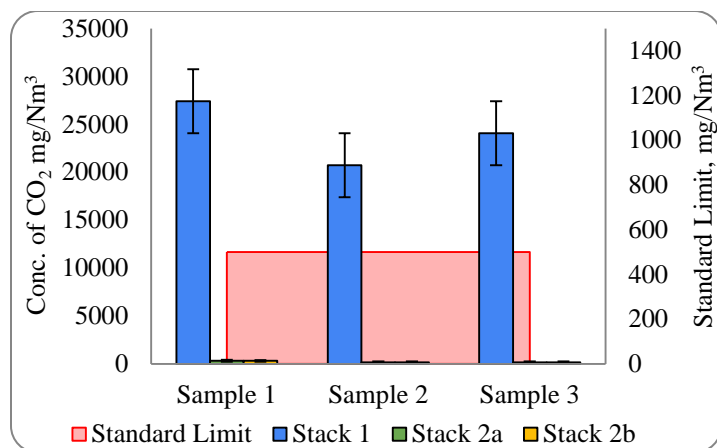


Figure 4-4: Stack emission – concentration of carbon dioxide

The average concentrations of carbon dioxide were (Stack 1 = 24062.3 ± 3340 mg/Nm³; Stack 2a = 210.82 ± 92.53 mg/Nm³; Stack 2b = 209.53 ± 90.86 mg/Nm³) as shown in Table 4-11. The results in Figure 4-4 indicate that the carbon dioxide concentration released from Stack 1 was higher than that released from Stack 2a and Stack 2b. The concentration of carbon dioxide released from Stack 1 in CF1 exceeded the standard limit of 500 mg/Nm³ set for cement factories under EMCA, 2014. The concentration of carbon dioxide was also significantly higher ($P < 0.05$) in Stack 1 compared to Stack 2a and Stack 2b. The higher concentration could be attributed to the combustion of diesel to produce energy for drying operations in CF1. Diesel as a fossil fuel readily burns in the air to produce carbon dioxide and water (Chmielewski, 1999). The concentration of carbon dioxide in Stack 2a and Stack 2b in CF2 was below the standard limits stipulated under EMCA, 2014.

4.2.2 Stack Emission Concentration of Carbon Monoxide

The stack emission concentration of carbon monoxide from Stack 1 is shown in Table 4-12 and Figure 4-5.

Table 4-12: Concentration of carbon monoxide

	Sample 1	Sample 2	Sample 3	Average
CF1 Stack 1 (mg/Nm ³)	0.760 ± 0.29	0.810 ± 0.26	0.620 ± 0.20	0.730 ± 0.098

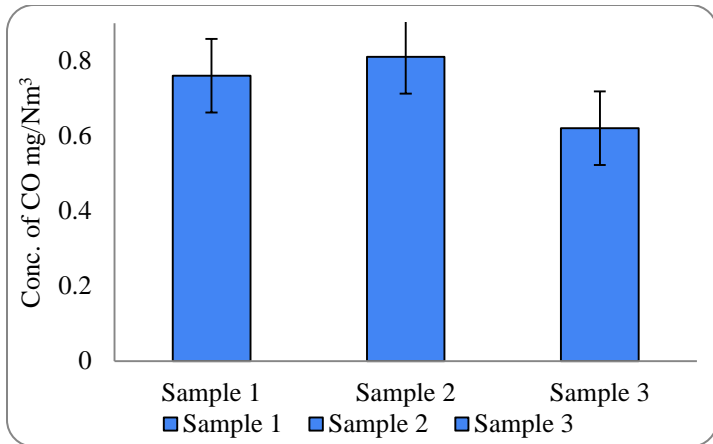


Figure 4-5: Stack emission – concentration of carbon monoxide

The average concentration of carbon monoxide from stack 1 was 0.730 ± 0.098 mg/Nm³. The presence of carbon monoxide from stationary sources indicates inefficiencies in the combustion process or poor mixing of air with diesel (Manahan, 2017; Rahman *et al.*, 2018). The concentration of carbon monoxide in CF2 was below the detection limit of the emission analyser.

4.2.3 Stack Emission Concentration of Sulphur Dioxide

The stack emission concentration of sulphur dioxide from Stack 1 is shown in Table 4-13 and Figure 4-6.

Table 4-13: Concentration of Sulphur dioxide

	Sample 1	Sample 2	Sample 3	Average	Standard Limit
CF1 Stack 1 (mg/Nm ³)	6.390 ± 1.90	5.510 ± 2.22	4.120 ± 0.30	5.340 ± 1.145	400

*The standard limits are under EMCA, 2014 (EMCA, 2014)

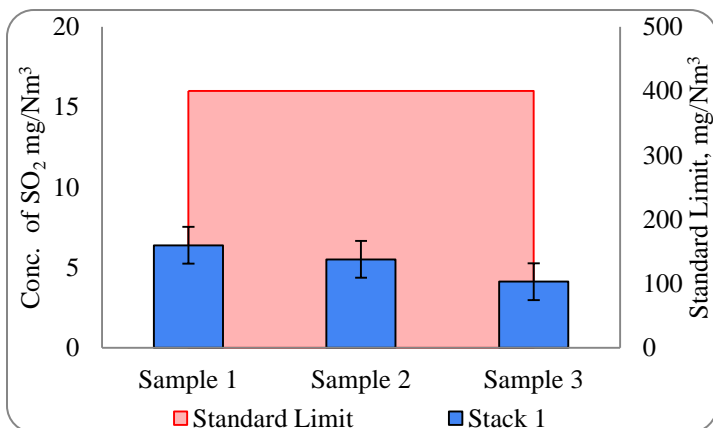


Figure 4-6: Stack emission – concentration of sulphur dioxide from Stack 1

The average concentration of sulphur dioxide from stack 1 was 5.340 ± 1.145 mg/Nm³. Figure 4-6 shows that the concentration of sulphur dioxide from Stack 1 was below the set standard limit of 400 mg/Nm³ for cement processing factories according to EMCA, 2014. The concentration of sulphur dioxide was below the detectable limit of the emission analyser used in Stack 2a and 2b. The presence of sulphur dioxide in the emission stream is an indication of traces of sulphur-containing compounds in the diesel used (Rahman *et al.*, 2018).

4.2.4 Stack Emission Concentration of Nitrogen Oxides

The stack emission concentration of nitrogen oxides from Stack 1 is shown in Table 4-14 and Figure 4-7.

Table 4-14: Concentration of Nitrogen oxides

	Sample 1	Sample 2	Sample 3	Average	Standard Limit
CF1 Stack 1 (mg/Nm ³)	18.92±1.17	18.71±3.12	22.12±3.43	19.92±1.911	1500

*The standard limits are under EMCA, 2014 (EMCA, 2014)

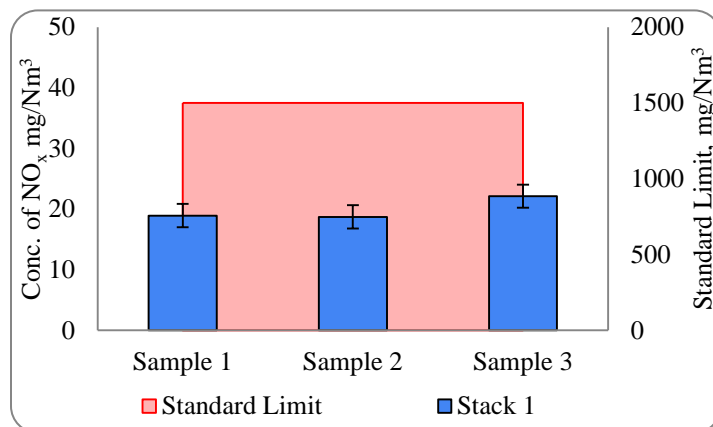


Figure 4-7: Stack emission – concentration of nitrogen oxides

The average concentration of nitrogen oxides from Stack 1 was 19.92 ± 1.911 mg/Nm³. The concentration of nitrogen oxides was below the standard limit of 1500 mg/Nm³ for cement factories according to the EMCA, 2014. The concentration of nitrogen oxides was below the detectable limit of the emission analyser used in Stack 2a and 2b. Nitrogen oxides within the stack mainly form when atmospheric oxygen combines with nitrogen at elevated temperatures (Ali *et al.*, 2011; Rahman *et al.*, 2018).

4.3 Modelling Input Data Analysis

4.3.1 Wind Speed and Direction

The wind frequency distribution and wind rose in Figure 4-8 and Figure 4-9 show the speed and direction of the wind. The wind speed and direction data were from the study area. Wind speed and direction influence the transportation and dispersion of emissions (Turner, 1994).

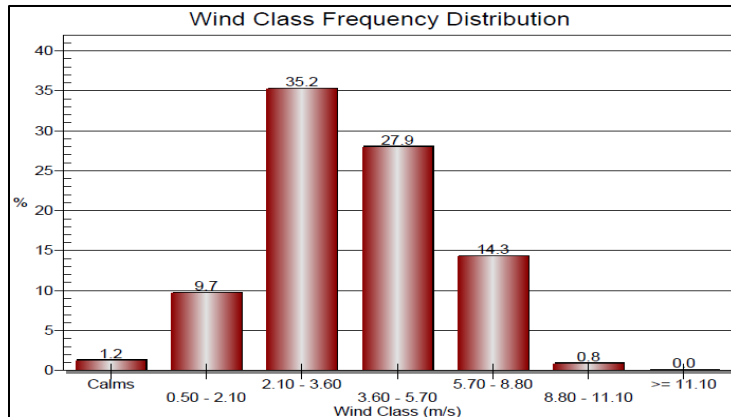


Figure 4-8: Wind Class frequency distribution

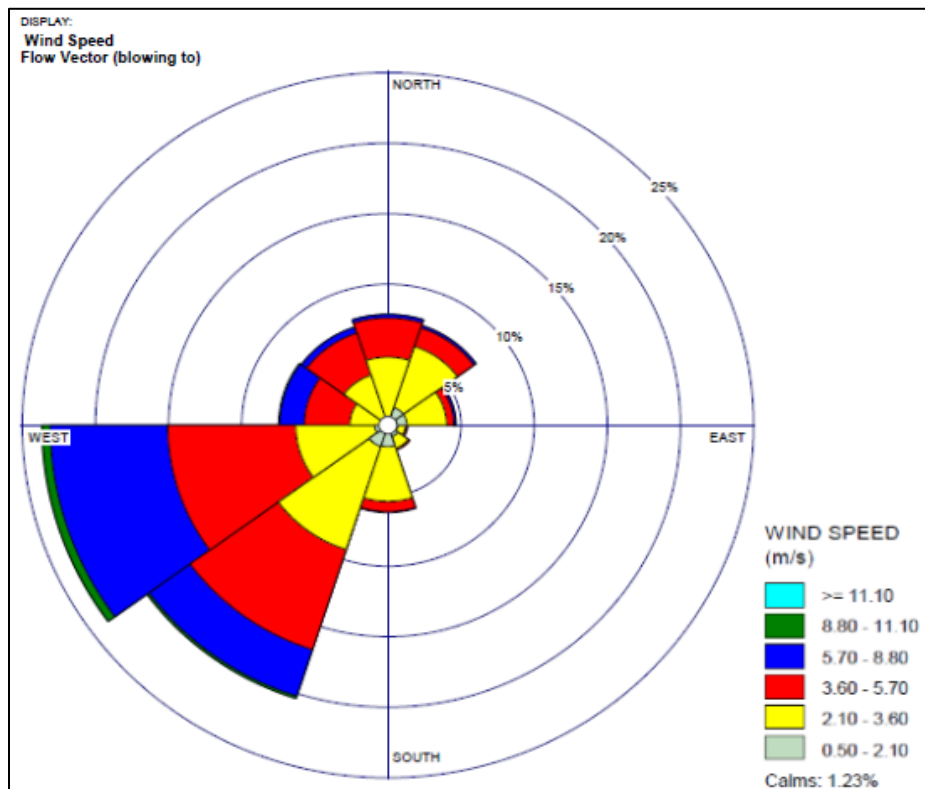


Figure 4-9: Wind-Rose

Figure 4-9 shows the wind blew approximately 23% of the time towards the west at a speed of 0.50-2.10 m/s; about 0.5% of the time, 2.10-3.60 m/s about 4.5% of the time, 3.60-5.70 m/s about 10% of the time, 5.70-8.80 m/s about 12% of the time and 8.80-11.10 m/s about 1% of the time. The wind blew predominantly towards the southwest, blowing approximately 20% of the time at a speed of 0.50-2.10 m/s about 1% of the time, 2.10-3.60 m/s about 8% of the time, 3.60-5.70 m/s about 9% of the time, 5.70-8.80 m/s about 3% of the time and 8.80-11.10 m/s about 0.5% of the time. The wind blew approximately 7.5% of the time towards other directions apart from the southeast where it was less than 5% of the time of assessment. The results show that the wind blew predominantly in the southwest direction. It is expected that the emissions would also move predominantly in the same direction. During the period the data was collected, the average wind speed was 3.46 m/s and calm winds were 1.23%.

4.3.2 Source Emission Rate

The emission rate in mass per unit time (g/s) calculated from the concentration of particulate matter and gaseous emissions obtained in Sections 3.2.1 and 3.2.2 is shown in Table 4-15 – Stack 1, Table 4-16 – Stack 2a and Table 4-17 – Stack 2b.

Table 4-15: Emission Source Data – Cement Factory1 (CF1), Stack 1

CF1, Stack 1 (37S, 273381.45 mE, 9838633.10 mS)				
Pollutant	Emission rates (g/s)			
Total Suspended Particles	0.0567	0.0653	0.0503	0.0574±0.0075
PM ₁₀	0.0482	0.0555	0.0427	0.0488±0.0064
PM _{2.5}	0.0255	0.0294	0.0226	0.0258±0.0034
Sulphur dioxide	0.0646	0.0569	0.0432	0.0549±0.0108
Nitrogen oxides	0.1912	0.1931	0.2321	0.2055±0.0231
Carbon dioxide	276.99	213.93	252.43	247.78±31.79
Carbon monoxide	0.0077	0.0084	0.0065	0.0075±0.0010

Table 4-16: Emission Source Data – Cement Factory 2 (CF2), Stack 2a

CF2, Stack 2a (37S, 273329.86 mE, 9841673.43 mS)				
Pollutant	Emission rates (g/s)			
Total Suspended Particles	0.0540	0.0750	0.0660	0.0650±0.0105
PM ₁₀	0.0459	0.0637	0.0561	0.0552±0.0089
PM _{2.5}	0.0243	0.0337	0.0297	0.0292±0.0047
Carbon dioxide	3.6331	1.8102	1.7873	2.4102±1.0591

Table 4-17: Emission Source Data – Cement Factory 2 (CF2), Stack 2b

CF2, Stack 2b (37S, 273284.21 mE, 9841628.73 mS)				
Pollutant	Emission rates (g/s)			
Total Suspended Particles	0.0925	0.0817	0.0886	0.0876±0.0055
PM ₁₀	0.0786	0.0694	0.0753	0.0744±0.0047
PM _{2.5}	0.0416	0.0367	0.0399	0.0394±0.0025
Carbon dioxide	4.1251	1.9881	1.7885	2.6339±1.2953

The emission rate of particulate matter and gaseous emission directly influences the resulting concentration at the receptor locations. The higher the emission rate the higher the receptor concentration (Westbrook, 1999).

4.3.3 Terrain and Building Data

The elevation of the study area ranged from 1482 m to 1611 m shown in Figure 4-10. The study area is predominantly flat terrain, slopping from the northeast towards the southwest. Flat terrains favour the dispersion of emissions from a point source (Giovannini *et al.*, 2020)

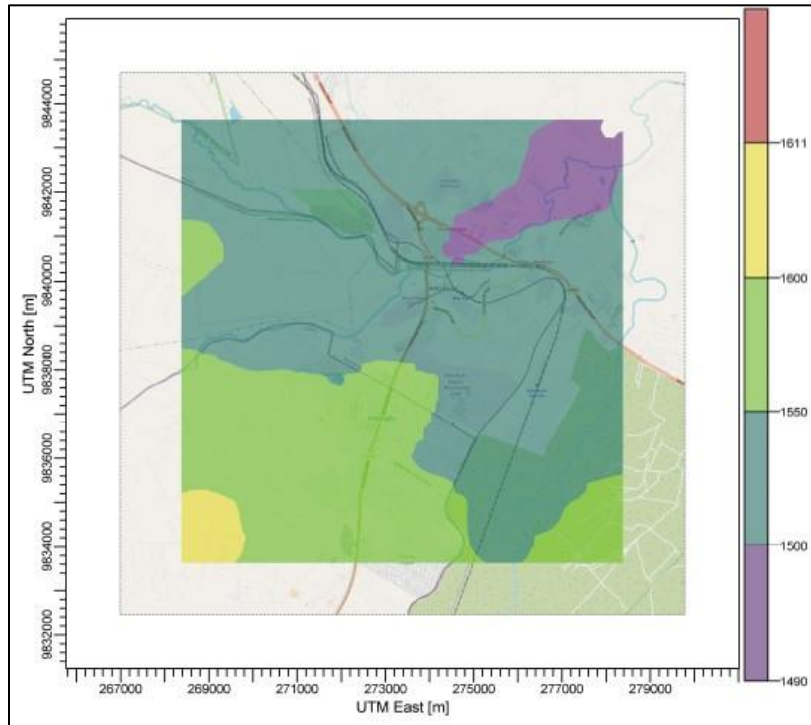


Figure 4-10: Terrain

The building tier heights used in processing the building data are shown in Table 4-18. The tallest building in CF1 had a tier height of 38 m and 35 m in CF2.

Table 4-18: Buildings and Structures Surrounding CF1 and CF2

CF1			CF2		
CF1 Building	Elevation, m	Tier Height, m	CF2 Building	Elevation, m	Tier Height, m
BLD_1	1546.59	15	BLD_1	1510.54	50
BLD_2	1540.02	21.1	BLD_2	1512.35	50
BLD_3	1541.13	25	BLD_3	1513.93	35
BLD_4	1541.28	25	BLD_4	1512.4	35
BLD_5	1540.8	25	BLD_5	1537.4	12
BLD_6	1539.53	25	BLD_6	1540.47	18
BLD_7	1538.82	38	BLD_7	1531.02	33
BLD_8	1538.95	38	BLD_8	1524.12	30
BLD_9	1537.68	3.5	BLD_9	1522.72	35
BLD_10	1539.37	28	BLD_10	1517.29	30
BLD_11	1540.51	12	BLD_11	1529.45	35
BLD_12	1538.58	15	BLD_12	1515.34	30
			BLD_13	1543.72	20
			BLD_14	1516.7	10
			BLD_15	1512.96	15
			BLD_16	1513.29	7

The presence of buildings or any other structure near the elevated stack increases ground-level concentrations of the pollutants near the emission point (Schnelle and Brown, 2001). Wind flowing over buildings or structures creates an eddy current into which the plume is trapped and this causes a downwash effect (Monbureau *et al.*, 2018).

4.4 Dispersion Modelling

The modelling results were expressed as the 1st highest maximum concentration and the concentration at discrete receptors at a flag-pole height of 1.5 m. The point of maximum concentration was recorded at 49.99 m heading 89.88° from CF1 and 117.72 m heading 26.43° from CF2 (Stack 2a). The deposition took place a short distance from the stationary points of both cement factories. The deposition over short distances was likely due to the short stacks in relation to the surrounding buildings and the low stack velocity observed in section 4.1.2.

4.4.1 Total Suspended Particles

The modelling results of Total Suspended Particles for each receptor point were the 1st highest concentration averaged for the annual and 24-hour period shown using contours shown in Figure 4-11 and Figure 4-12 for each of the sample runs.

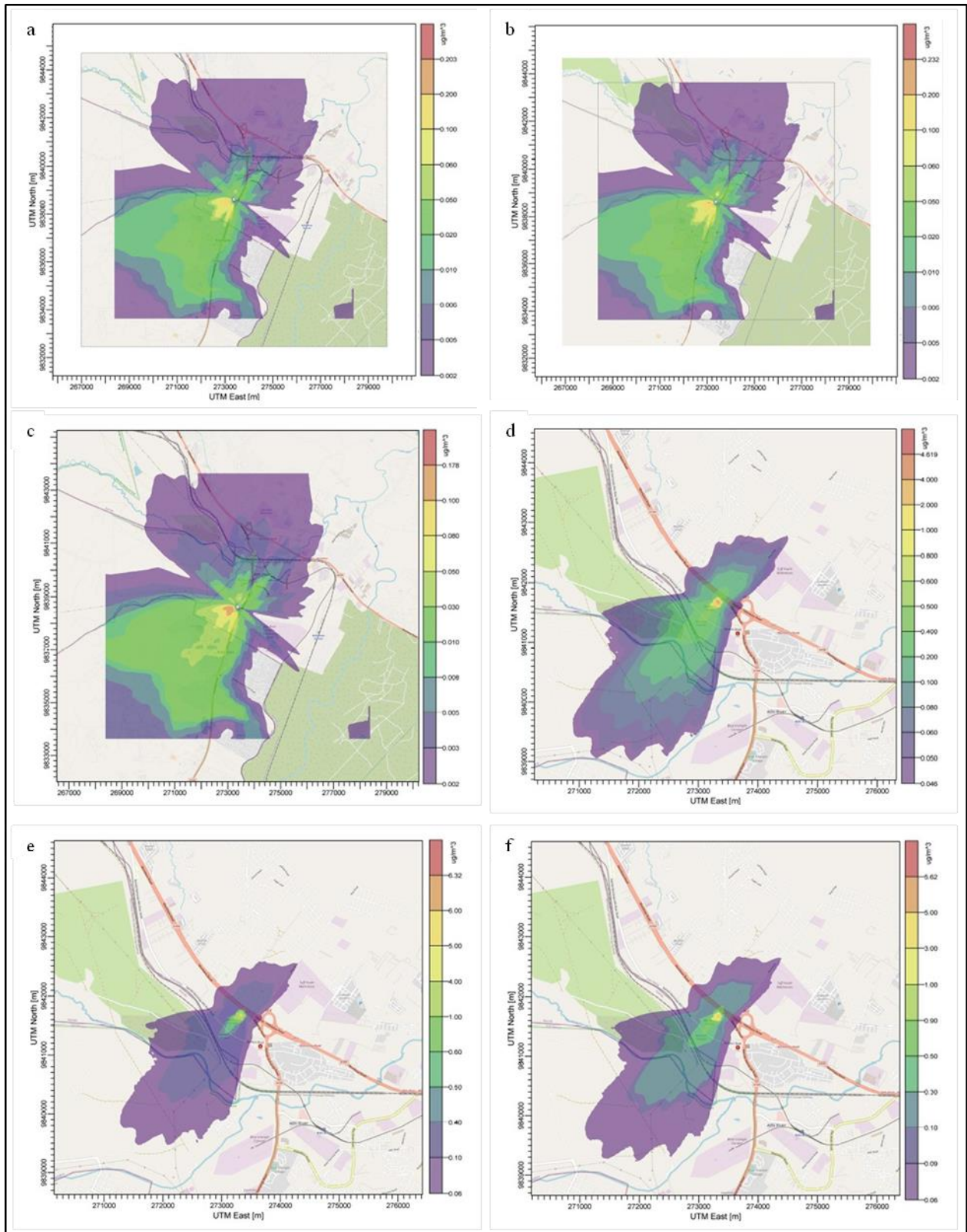


Figure 4-11: Annual ambient concentration of TSP from (a) CF1, S1; (b) CF1, S2; (c) CF1, S3; (d) CF2, S1; (e) CF2, S2; (f) CF2, S3

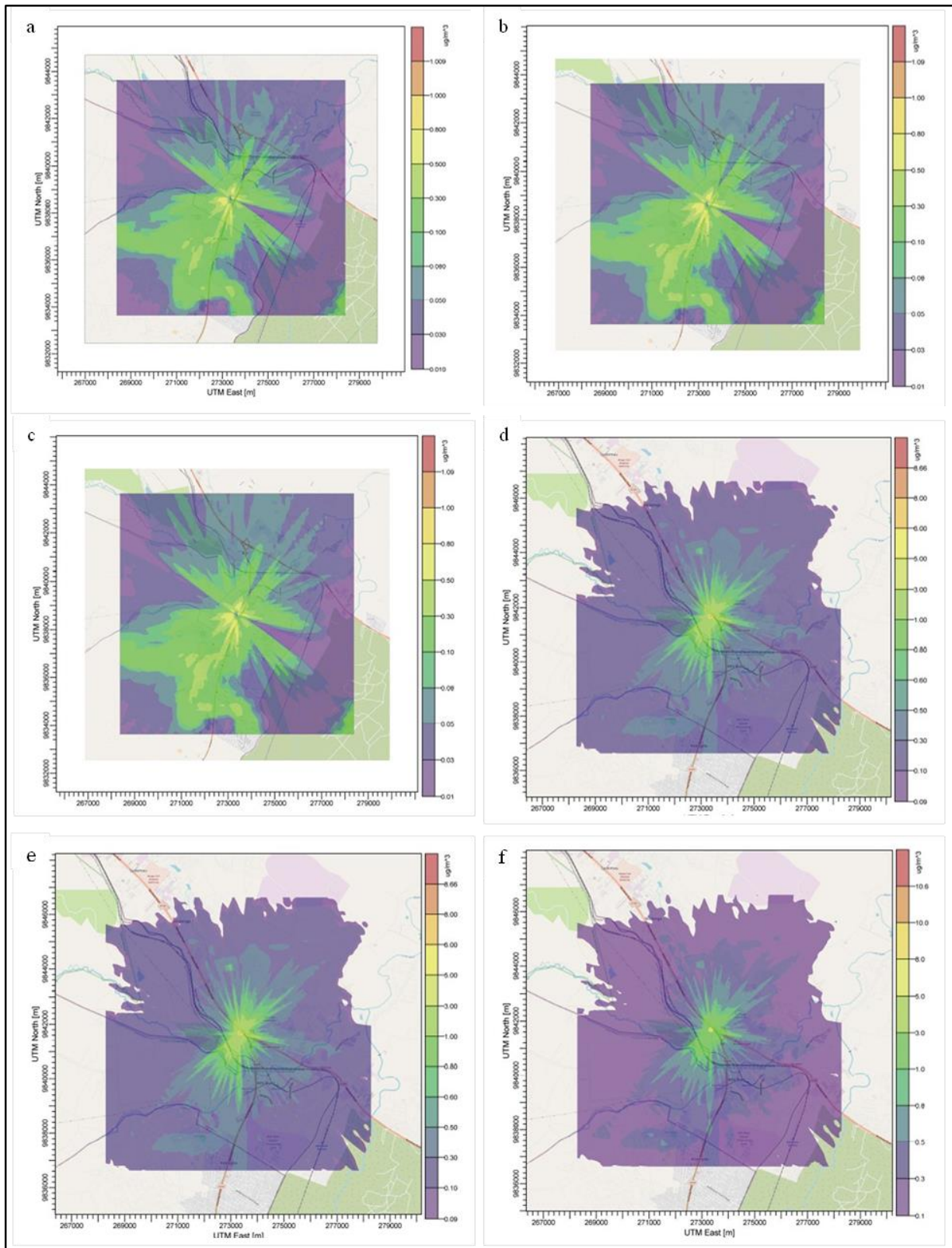


Figure 4-12: 24-hour ambient concentration of TSP from (a) CF1, S1; (b) CF1, S2; (c) CF1, S3; (d) CF2, S1; (e) CF2, S2; (f) CF2, S3

Figure 4-11 and Figure 4-12 show the annual and 24-hour ambient total suspended particle concentrations from CF1 and CF2 predominantly flow towards the southwest from the emission point. The 24-hour ambient total suspended particle concentrations from CF2 are evenly distributed. It is also observed that higher concentrations of Total Suspended Particles are observed around the emission points in both cement factories.

To determine the burden of the contaminant on the receptors, the 1st highest annual and 24-hour maximum concentrations were determined and compared to the standard limits shown in Table 4-19 and Figure 4-13.

Table 4-19: Annual and 24-hour maximum concentration of Total Suspended Particles (TSP)

(µg/m ³)		Sample 1	Sample 2	Sample 3	Average	WHO	NEMA
Annual	CF1	0.203	0.232	0.178	0.205±0.027	Not provided	140
	CF2	4.616	6.319	5.618	5.519±0.8543		
24-hour	CF1	1.009	1.09	0.825	0.975±0.1358		200
	CF2	8.66	11.82	10.55	10.35±1.59		

*WHO –ambient tolerance limit (WHO, 2021), NEMA – Ambient tolerance limits(EMCA, 2014)

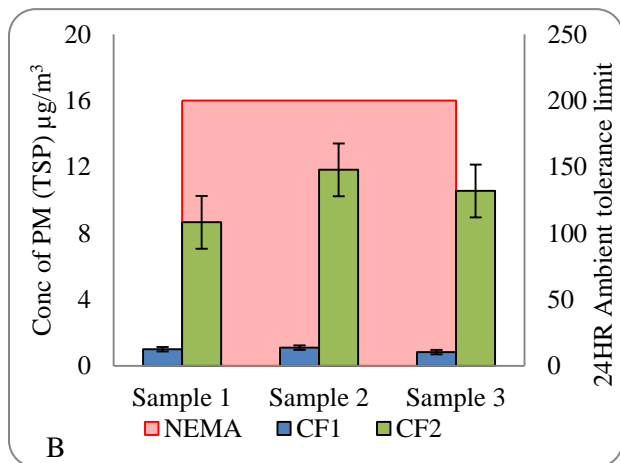
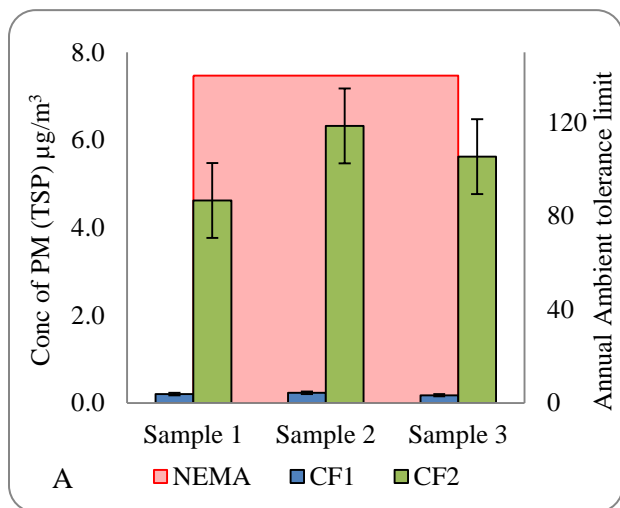


Figure 4-13: A graph of the (A) annual and (B) 24-hour maximum concentration of Total Suspended Particles

The annual average maximum concentration of Total Suspended Particles from CF1 and CF2 were $0.205 \pm 0.027 \mu\text{g}/\text{m}^3$ and $5.519 \pm 0.8543 \mu\text{g}/\text{m}^3$. The 24-hour average maximum concentrations from CF1 and CF2 were $0.975 \pm 0.1358 \mu\text{g}/\text{m}^3$ and $10.35 \pm 1.59 \mu\text{g}/\text{m}^3$.

The ambient 1st highest annual and 24-hour concentration of the Total Suspended Particles at the selected discrete receptors was also determined and the results are shown in Table 4-20.

Table 4-20: Discrete receptor annual and 24-hour average concentration of PM (TSP)

Discrete receptors	CF1		CF2	
	Annual ($\mu\text{g}/\text{m}^3$)	24-hour ($\mu\text{g}/\text{m}^3$)	Annual ($\mu\text{g}/\text{m}^3$)	24-hour ($\mu\text{g}/\text{m}^3$)
A	0.0065 ± 0.0010	0.0707 ± 0.009	0.0059 ± 0.0003	0.3731 ± 0.0414
B	0.0045 ± 0.00075	0.0564 ± 0.0076	0.0322 ± 0.0018	0.9318 ± 0.0982
C	0.0013 ± 0.0002	0.0946 ± 0.0129	0.0030 ± 0.0002	0.2908 ± 0.0297
D	0.0170 ± 0.0023	0.3845 ± 0.0516	0.0206 ± 0.0006	0.4569 ± 0.0194

E	0.0025±0.0004	0.0675±0.0095	0.0072±0.0005	0.2844±0.0321
F	0.0028±0.0004	0.1142±0.0156	0.0046±0.0003	0.2280±0.0258
G	0.0013±0.0002	0.0265±0.0035	0.0094±0.0007	0.3060±0.0332
H	0.0034±0.0005	0.1165±0.0155	0.0055±0.0004	0.2877±0.0340

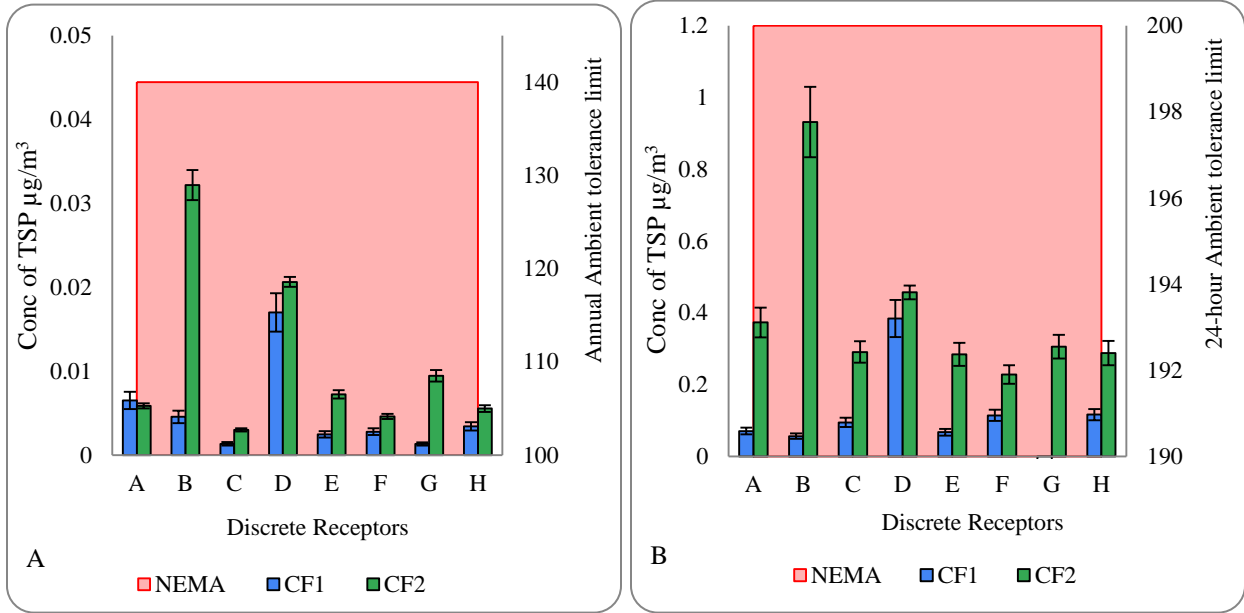


Figure 4-14: The (A) annual and (B) 24-hour discrete receptor concentration of Total Suspended Particles

Both the annual and the 24-hour average maximum concentrations and the concentration at each discrete receptor were below the ambient tolerance limit stipulated under EMCA, 2014. The ambient contribution of Total Suspended Particles from CF2 was 25 times (annual) and 10 times (24-hour) higher than in CF1. This was mainly because CF2 has two stacks in comparison to the one from CF1. Receptor D was the most affected receptor with the emissions from CF1 and receptor B from CF2 as shown in Figure 4-14. This was due to the close distance from the respective cement factories compared to other receptors.

4.4.2 Particulate Matter (PM₁₀)

The modelling results of PM₁₀ for each receptor point were the 1st highest concentration averaged for the annual and 24-hour period shown using contours in Figure 4-15 and Figure 4-16.

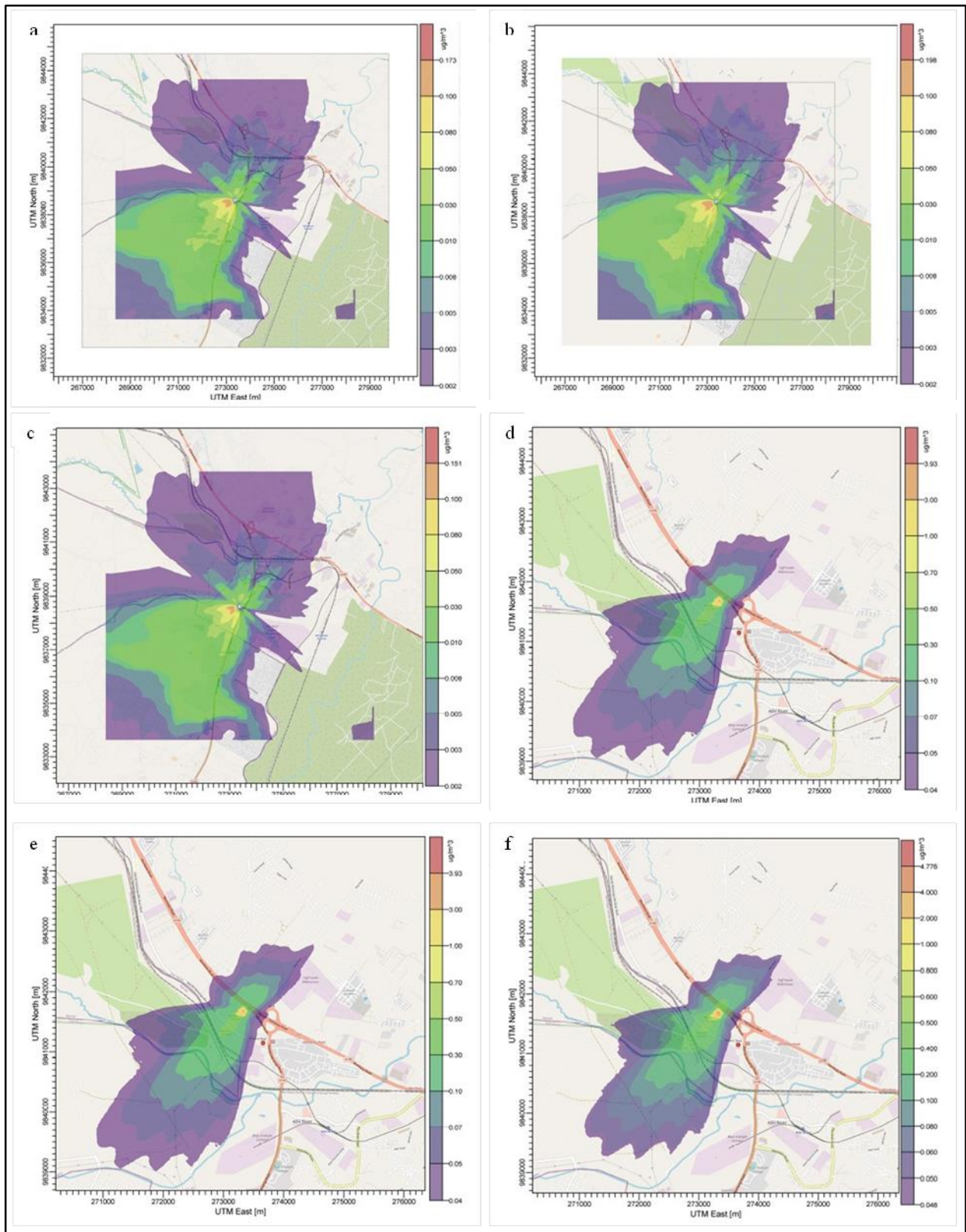


Figure 4-15: Annual ambient concentration of PM₁₀ from (a) CF1, S1; (b) CF1, S2; (c) CF1, S3; (d) CF2, S1; (e) CF2, S2; (f) CF2, S3

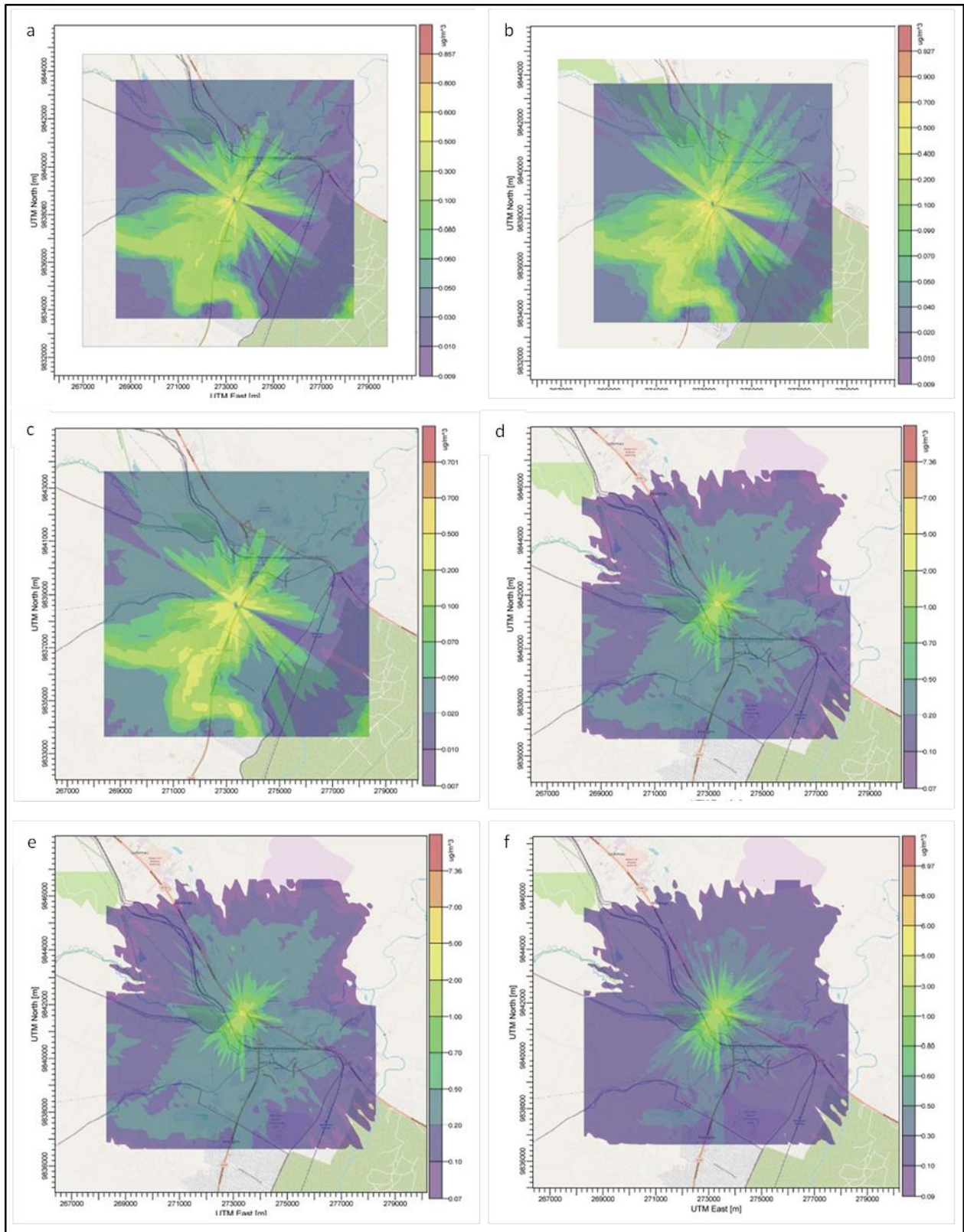


Figure 4-16: 24-hour ambient concentration of PM₁₀ from (a) CF1, S1; (b) CF1, S2; (c) CF1, S3; (d) CF2, S1; (e) CF2, S2; (f) CF2, S3

Higher concentrations of PM₁₀ are observed around the emission points in both cement factories. The annual ambient PM₁₀ concentration from CF1 and CF2 predominantly moves towards the southwest from the emission point. The 24-hour ambient PM₁₀ concentrations are evenly distributed. However, higher concentrations are observed to flow towards the southwest direction from the emission point shown in Figure 4-16.

To determine the burden of PM₁₀ on the receptors, the 1st highest annual and 24-hour maximum concentrations were determined and compared to the standard limits shown in Table 4-21 and Figure 4-17.

Table 4-21: Annual and 24-hour Maximum Concentration of PM₁₀

(µg/m ³)		Sample 1	Sample 2	Sample 3	Average	WHO	NEMA
Annual	CF1	0.173	0.198	0.151	0.174±0.0235	15	50
	CF2	3.926	5.371	4.776	4.691±0.7262		
24-hour	CF1	0.857	0.927	0.701	0.828±0.1157	45	100
	CF2	7.36	10.05	8.97	8.79±1.354		

*WHO air quality guidelines (WHO, 2021), NEMA – Ambient tolerance limits(EMCA, 2014)

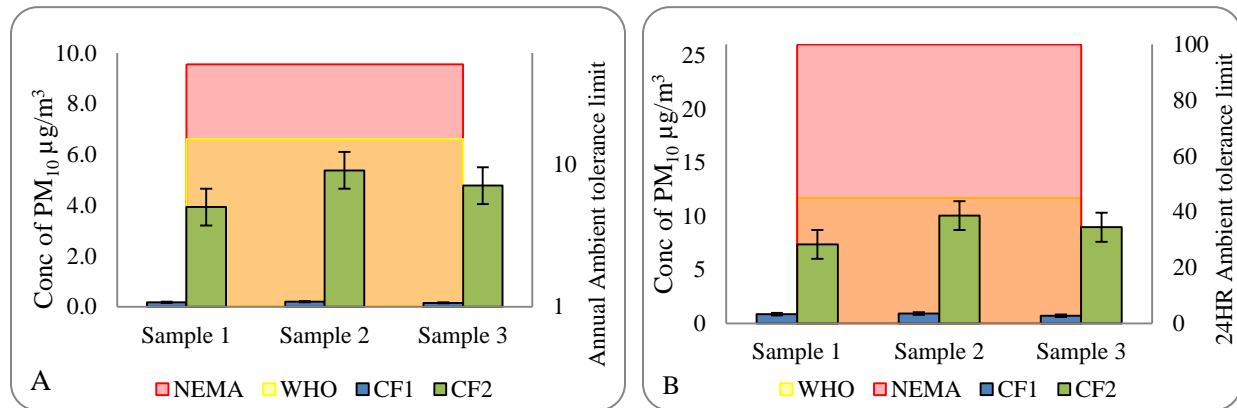


Figure 4-17: A graph of the (A) annual and (B) 24-hour maximum concentration of PM₁₀

The annual average maximum concentration of PM₁₀ for CF1 and CF2 were 0.174±0.0235 µg/m³ and 4.691±0.7262 µg/m³. The 24-hour average maximum concentrations of CF1 and CF2 of the PM₁₀ were 0.828±0.1157 µg/m³ and 8.79±1.354 µg/m³.

The ambient 1st highest annual and 24-hour concentration of the PM₁₀ was also determined at the selected discrete receptors. The results shown in Table 4-22 and Figure 4-18 were compared to the standard limits.

Table 4-22: Discrete receptor annual and 24-hour average concentration of PM₁₀

Discrete receptors	CF1		CF2	
	Annual (µg/m ³)	24-hour (µg/m ³)	Annual (µg/m ³)	Annual (µg/m ³)
A	0.0055±0.0009	0.0601±0.0079	0.0050±0.0003	0.3171±0.0352
B	0.0039±0.0006	0.0479±0.0064	0.0273±0.0015	0.7920±0.0834
C	0.0011±0.0002	0.0804±0.0110	0.0026±0.0002	0.2472±0.0253
D	0.0144±0.0020	0.3268±0.04389	0.0175±0.0005	0.3884±0.01651
E	0.0021±0.0003	0.0574±0.0081	0.0061±0.0004	0.2418±0.0273
F	0.0024±0.0003	0.0971±0.0133	0.0039±0.0003	0.1938±0.0220
G	0.0011±0.0002	0.0225±0.0030	0.0080±0.0006	0.2601±0.0282
H	0.0029±0.0004	0.0990±0.0131	0.0047±0.0003	0.2446±0.0289

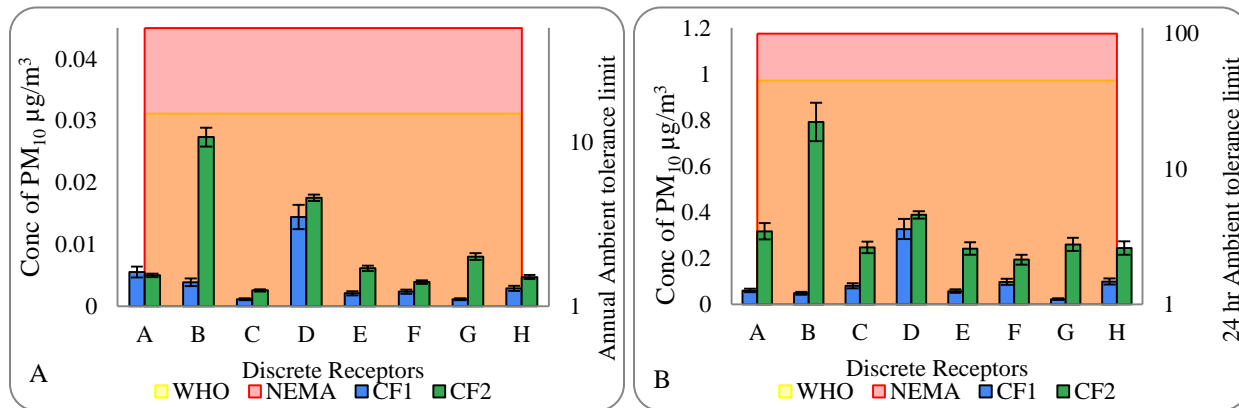


Figure 4-18: The (A) annual and (B) 24-hour discrete receptor concentration of PM₁₀

From Table 4-22 and Figure 4-18, the 24-hour average maximum concentrations and the concentration at each discrete receptor were below the ambient tolerance limit as stipulated under EMCA 2014 and WHO global air quality guidelines, 2021. The ambient contribution of PM₁₀ from CF2 was 25 times (annual) and 10 times (24-hour) higher than in CF1. Receptor D was the most affected receptor with the emissions from CF1 receptor B from CF2 as shown in Figure 4-18.

4.4.3 Particulate Matter (PM_{2.5})

The modelling results of PM₁₀ for each receptor point were the 1st highest concentration averaged for the annual and 24-hour period shown using contours in Figure 4-19 and Figure 4-20.

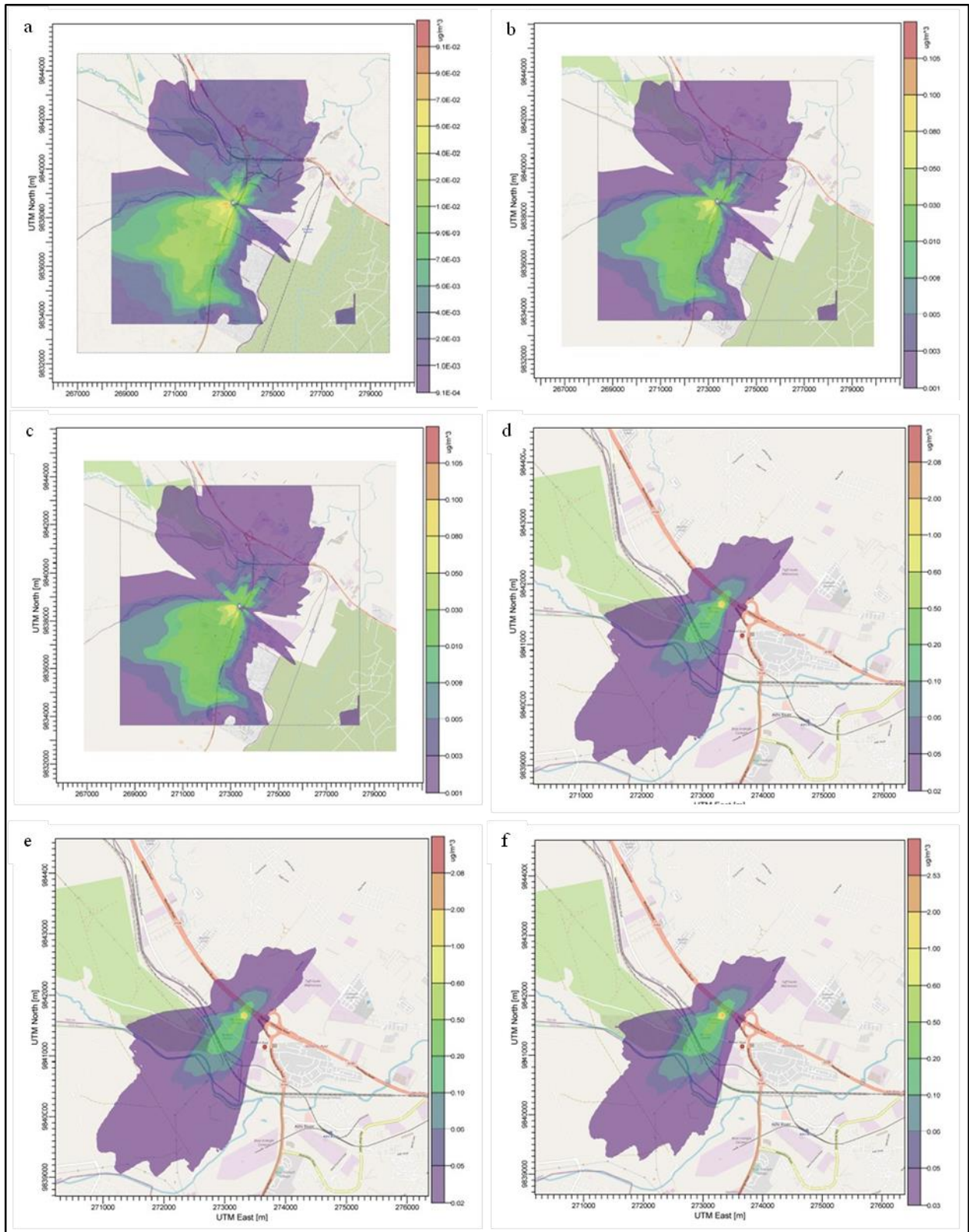


Figure 4-19: Annual ambient concentration of PM_{2.5} from (a) CF1, S1; (b) CF1, S2; (c) CF1, S3; (d) CF2, S1; (e) CF2, S2; (f) CF2, S3

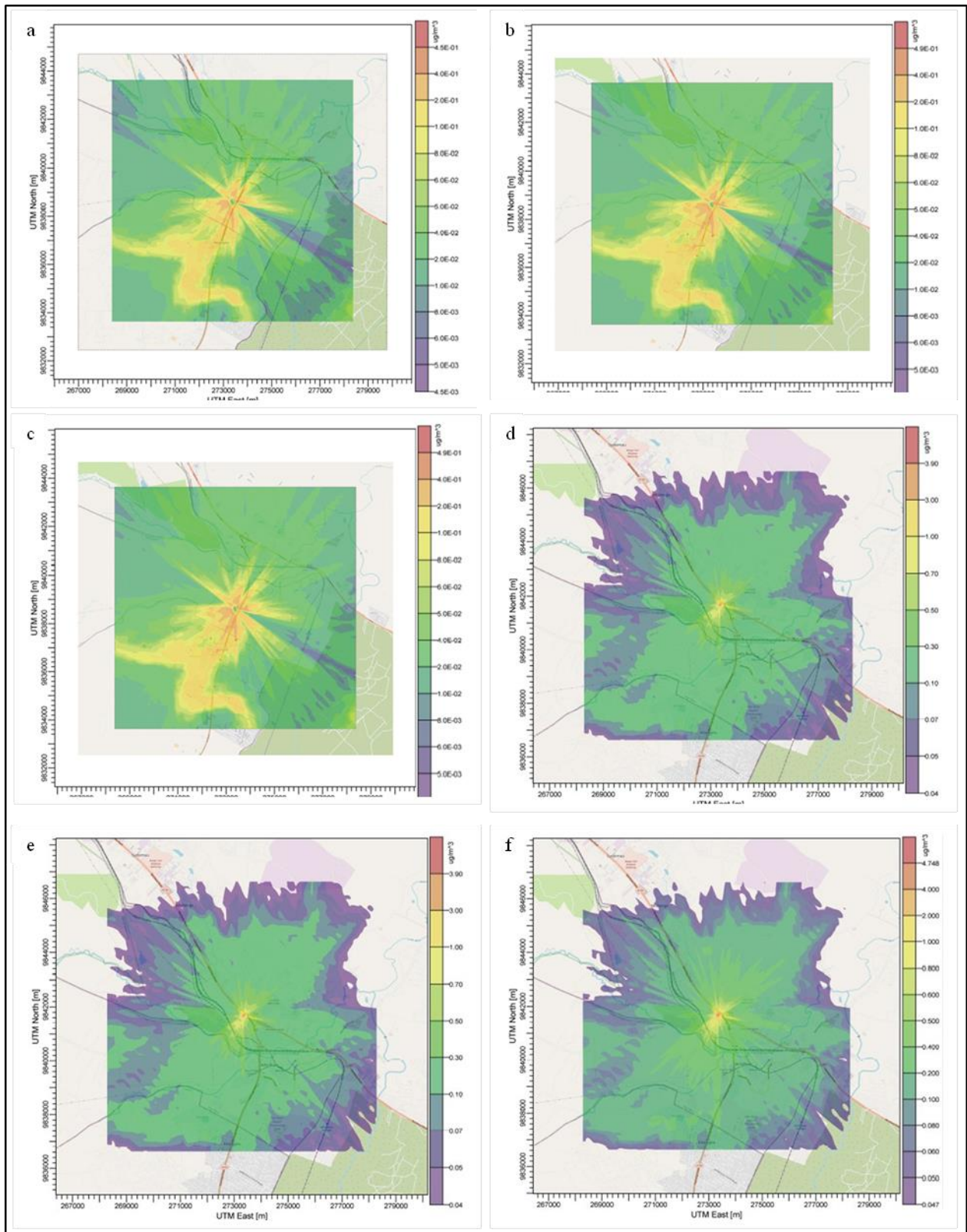


Figure 4-20: 24-hour ambient concentration of PM_{2.5} from (a) CF1, S1; (b) CF1, S2; (c) CF1, S3; (d) CF2, S1; (e) CF2, S2; (f) CF2, S3

Figure 4-19 shows the annual ambient concentration of PM_{2.5} from CF1 and CF2 predominantly moved towards the southwest from the emission point. The 24-hour ambient PM_{2.5} concentration is evenly distributed. However, higher concentrations of PM_{2.5} from CF2 are distributed within the receptors in the 0° to 270° angle (north across to the west) shown in Figure 4-20. It is also observed that higher concentrations of PM_{2.5} are observed around the emission points in both cement factories.

To determine the burden of PM_{2.5} on the receptors, the 1st highest annual and 24-hour maximum concentrations were determined and compared to the standard limits shown in Table 4-23 and Figure 4-21.

Table 4-23: Annual and 24-hour Maximum Concentration of PM_{2.5}

(µg/m ³)		Sample 1	Sample 2	Sample 3	Average	WHO	NEMA
Annual	CF1	0.091	0.105	0.0801	0.332±0.0125	5	Not provided
	CF2	2.079	2.843	2.528	2.483±0.384		
24-hour	CF1	0.454	0.491	0.371	0.439±0.0615	15	
	CF2	3.9	5.32	4.75	4.66±0.715		

*WHO air quality guidelines (WHO, 2021), NEMA – Ambient tolerance limits(EMCA, 2014)

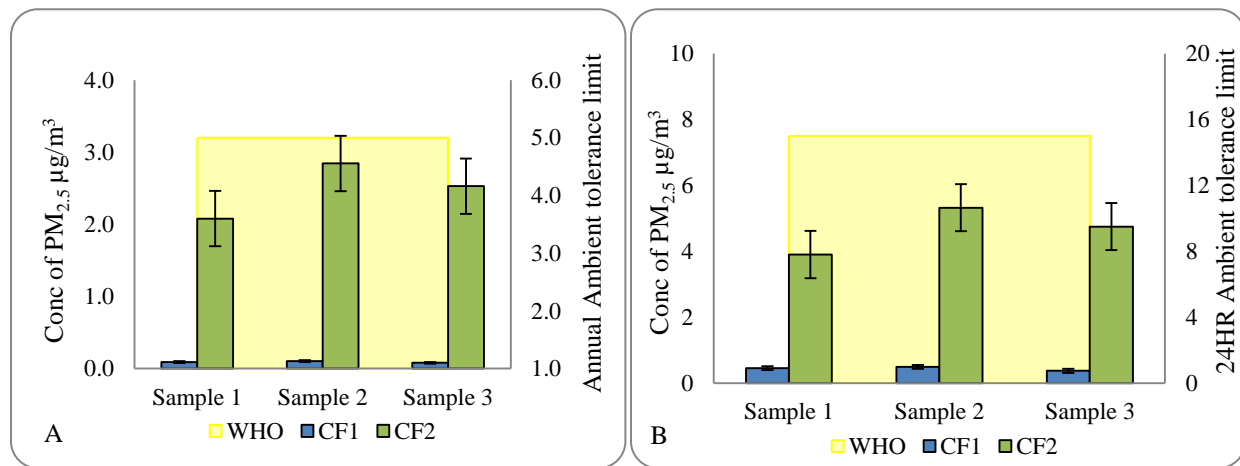


Figure 4-21: The (a) annual and (b) 24-hour maximum concentration of PM_{2.5}

The annual average maximum concentration of PM_{2.5} for CF1 and CF2 were 0.332±0.0125 µg/m³ and 2.483±0.384 µg/m³. The 24-hour average maximum concentrations of CF1 and CF2 of the PM_{2.5} were 0.439±0.0615 µg/m³ and 4.66±0.715 µg/m³.

The ambient 1st highest annual and 24-hour concentration of PM_{2.5} at the selected discrete receptors was also determined and the results are shown in Table 4-24.

Table 4-24: Discrete receptor annual and 24-hour average concentration of PM_{2.5}

Discrete receptors	CF1		CF2	
	Annual (µg/m ³)	24-hour (µg/m ³)	Annual (µg/m ³)	Annual (µg/m ³)
A	0.0029±0.0005	0.0318±0.0042	0.0026±0.0002	0.1679±0.0186
B	0.0020±0.0003	0.0254±0.0034	0.0145±0.0008	0.4193±0.0442
C	0.0006±0.0001	0.0426±0.0058	0.0014±0.0001	0.1309±0.0134
D	0.0076±0.001	0.1730±0.0232	0.0093±0.0003	0.2056±0.0087
E	0.0011±0.0002	0.0304±0.0043	0.0032±0.0002	0.1280±0.0144
F	0.0012±0.0002	0.0514±0.0070	0.0021±0.0001	0.1026±0.0116
G	0.0006±0.0001	0.0119±0.0016	0.0043±0.0003	0.1377±0.0149
H	0.0015±0.0002	0.0524±0.0070	0.0025±0.0002	0.1295±0.0153

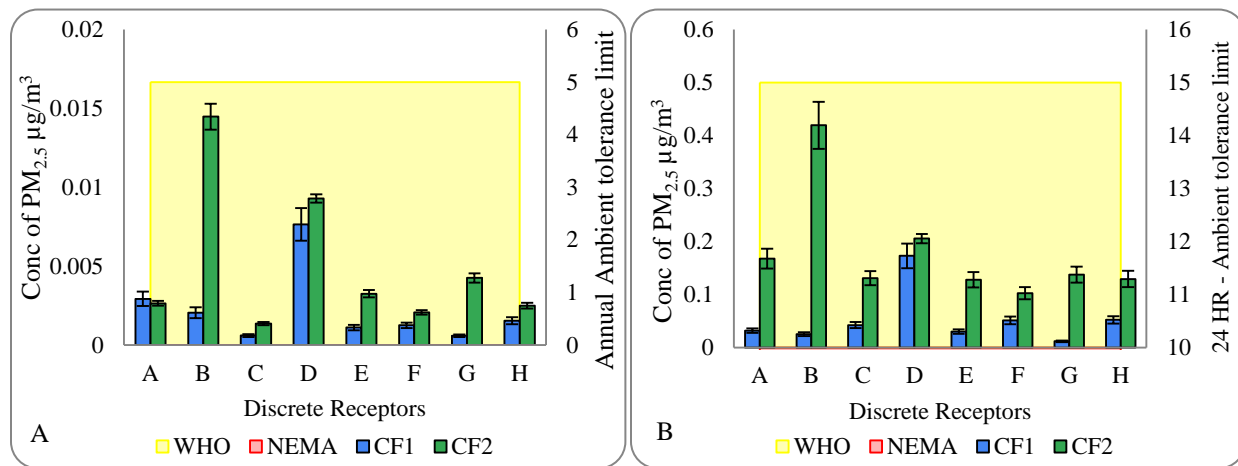


Figure 4-22: The (A) annual and (B) 24-hour discrete receptor concentration of PM_{2.5}

Both the annual and the 24-hour average maximum concentrations and the concentration at each discrete receptor were below the ambient tolerance limit as stipulated under EMCA 2014 and WHO global air quality guidelines, 2021. The ambient contribution of PM_{2.5} from CF2 was 25 times (annual) and 10 times (24-hour) higher than in CF1. Receptor D was the most affected receptor with the emissions from CF1 and receptor B from CF2 as shown in Figure 4-22.

4.4.4 Carbon Dioxide

The modelling results of carbon dioxide for each receptor point were the 1st highest concentration averaged for 8-hour and 1-hour periods shown using contours in Figure 4-23 and Figure 4-24.

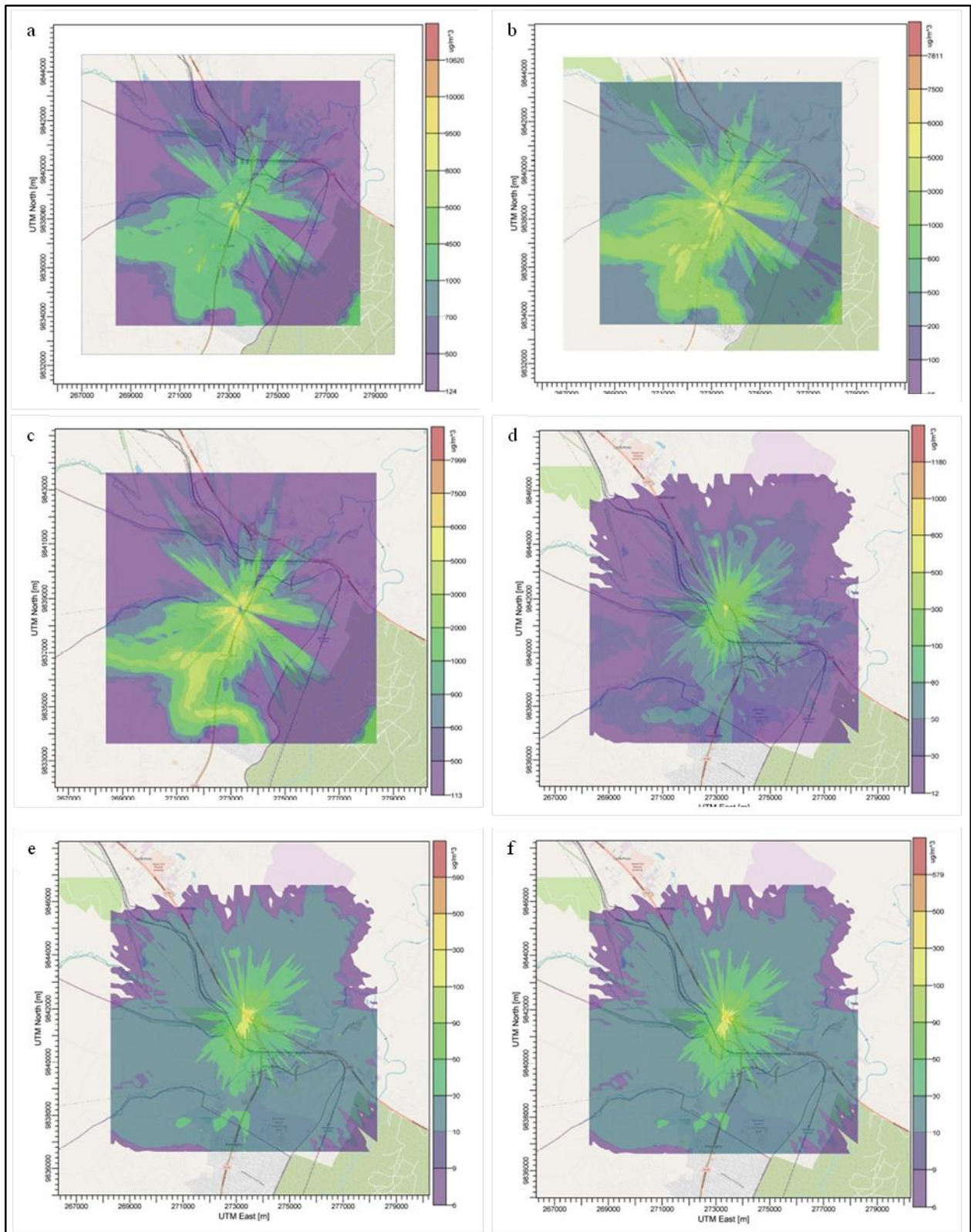


Figure 4-23: 8-hour ambient concentration of carbon dioxide from (a) CF1, S1; (b) CF1, S2; (c) CF1, S3; (d) CF2, S1; (e) CF2, S2; (f) CF2, S3

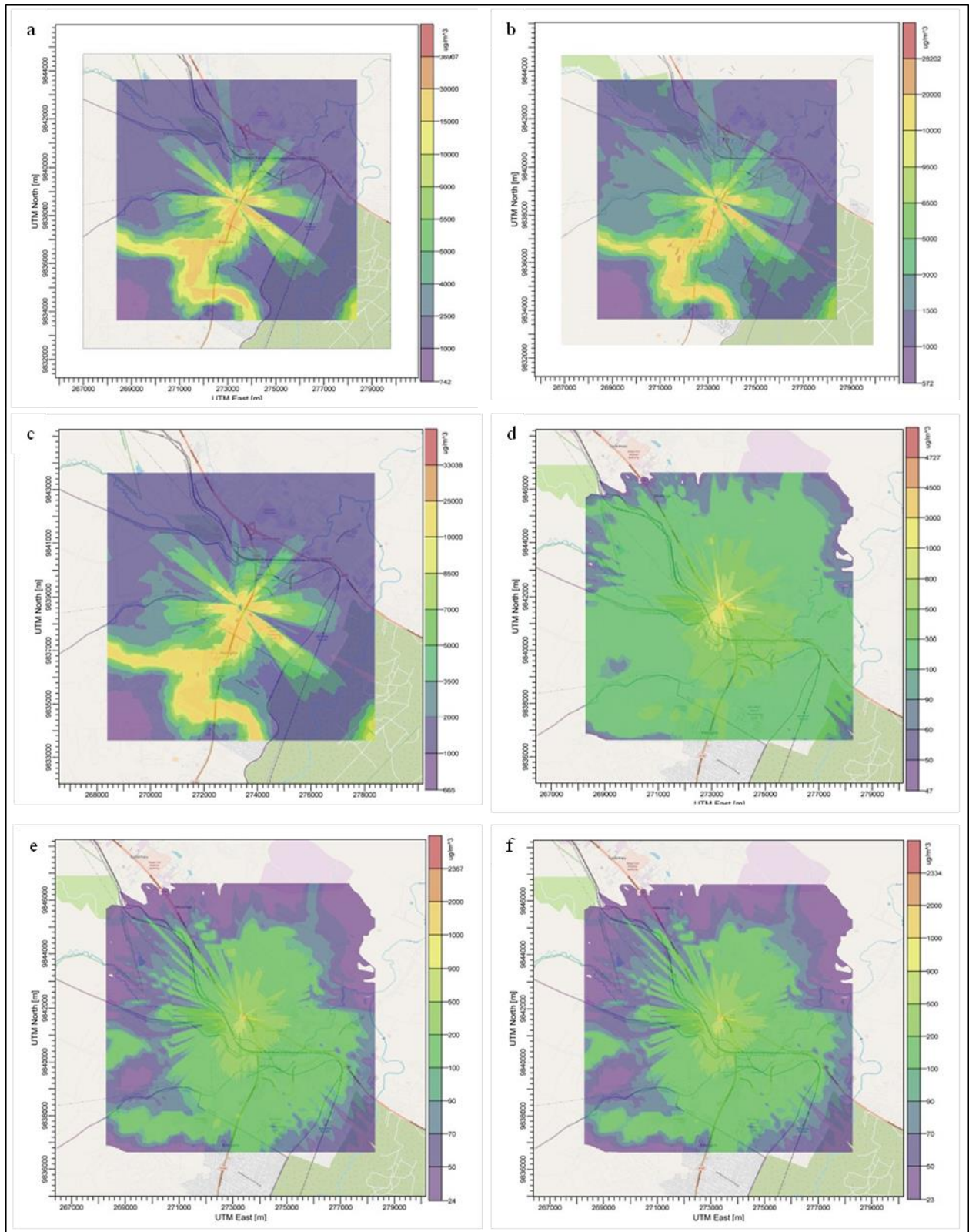


Figure 4-24: 1-hour ambient concentration of carbon dioxide from (a) CF1, S1; (b) CF1, S2; (c) CF1, S3; (d) CF2, S1; (e) CF2, S2; (f) CF2, S3

A higher 8-hour and 1-hour ambient concentration of the contaminants from the emission point is observed around the emission point and towards the south-west direction from the emission point in CF1 shown in Figure 4-19 and Figure 4-20. The concentration of carbon dioxide from CF2 is evenly distributed within the receptors. A lot of factors including meteorological conditions such as wind speed and directions, atmospheric stability and the surrounding buildings affect the dilution and movement of the pollutants in the atmosphere causing the variations.

To determine the burden of carbon dioxide on the receptors, the 1st highest 8-hour and 1-hour maximum concentrations were determined and compared to the standard limits shown in Table 4-25 and Figure 4-25.

Table 4-25: 8-hour and 1-hour Maximum Concentration of carbon dioxide

(mg/m ³)		Sample 1	Sample 2	Sample 3	Average	WHO	NEMA
8-hour	CF1	10.619	7.811	7.998	8.809±1.57	Not provided	2
	CF2	0.571	0.59	0.579	0.58±0.0095		
1-hour	CF1	36.907	28.201	33.038	32.715±4.362		4
	CF2	4.727	2.367	2.334	3.143±1.372		

*WHO air quality guidelines (WHO, 2021), NEMA – Ambient tolerance limits(EMCA, 2014)

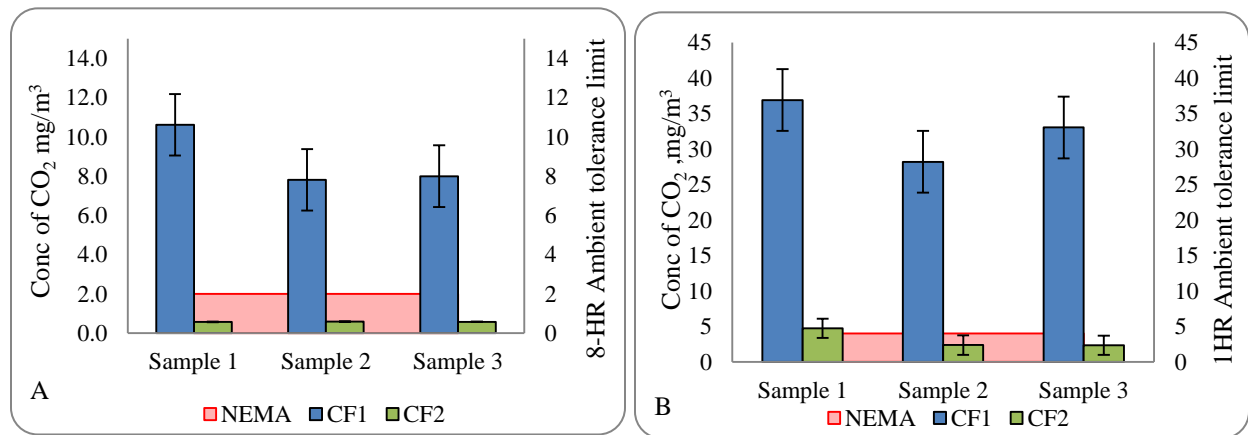


Figure 4-25: The (A) 8-hour and (B) 1-hour maximum concentration of carbon dioxide

The 8-hour average maximum concentration of carbon dioxide for CF1 and CF2 were 8.809±1.57 mg/m³ and 0.58±0.0095 mg/m³ and the 1-hour average maximum concentrations were 32.715±4.362 mg/m³ and 3.143±1.372 mg/m³. The average maximum concentrations from CF1 exceeded the ambient tolerance limit of 2 mg/m³ and 4 mg/m³, as stipulated under EMCA 2014 but were below in CF2. The downwind contribution of carbon dioxide from CF1 was 15 times (8-

hour) and 10 times (1-hour) higher compared to CF2. This is mainly due to the higher emission rate in CF1 as compared to CF2. Emission rates directly influence the ground-level concentration (Westbrook, 1999). The 1st highest 8-hour and 1-hour concentration discrete receptors are shown in Table 4-26 and Figure 4-26.

Table 4-26: Discrete receptor 8-hour and 1-hour average concentration of carbon dioxide

Discrete Receptors	CF1		CF2	
	8-hour (mg/m ³)	1-hour (mg/m ³)	8-hour (mg/m ³)	1-hour (mg/m ³)
A	0.96374±0.149	4.7440±0.745	0.0394±0.017	0.2367±0.105
B	0.58867±0.090	1.6380±0.212	0.0668±0.030	0.3769±0.167
C	0.77559±0.131	4.6891±0.772	0.0262±0.012	0.1382±0.061
D	2.96005±0.399	12.2055±1.654	0.0412±0.019	0.2223±0.105
E	0.55040±0.076	3.1614±0.416	0.0302±0.013	0.1810±0.080
F	1.47737±0.193	7.4697±1.040	0.0239±0.011	0.1451±0.064
G	0.26315±0.034	1.8944±0.245	0.0281±0.013	0.1941±0.087
H	1.50794±0.197	7.4193±1.050	0.0263±0.012	0.1839±0.081

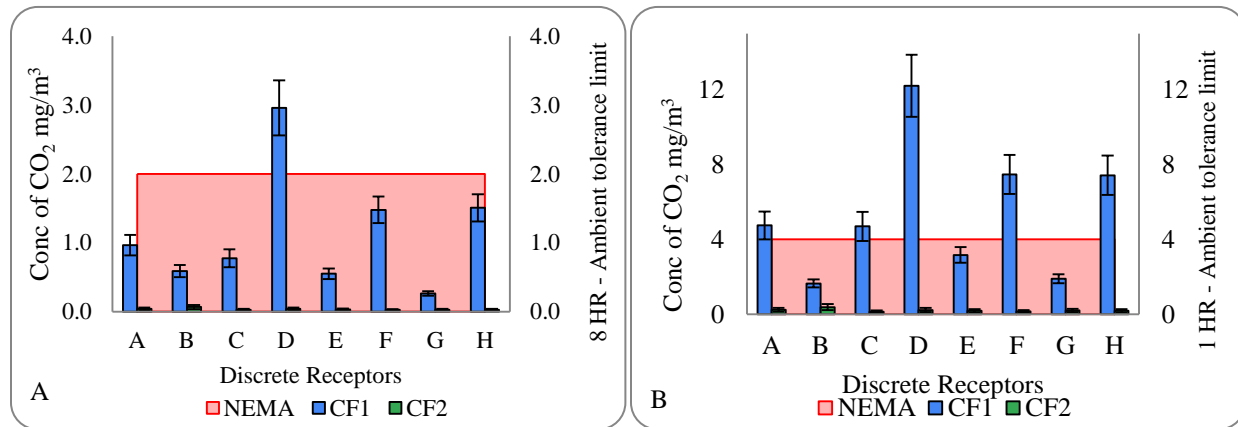


Figure 4-26: The (A) 8-hour and (B) 1-hour discrete receptor concentration of carbon dioxide

The 8-hour ambient concentration of carbon dioxide from CF1 exceeded the ambient tolerance limit at receptor D. The 1-hour ambient concentration of carbon dioxide from CF1 exceeded at receptors A, C, D, F and H.

4.4.5 Carbon Monoxide

The modelling results of carbon monoxide for each receptor point were the 1st highest concentration averaged for 8-hour and 1-hour periods shown using contours in Figure 4-27.

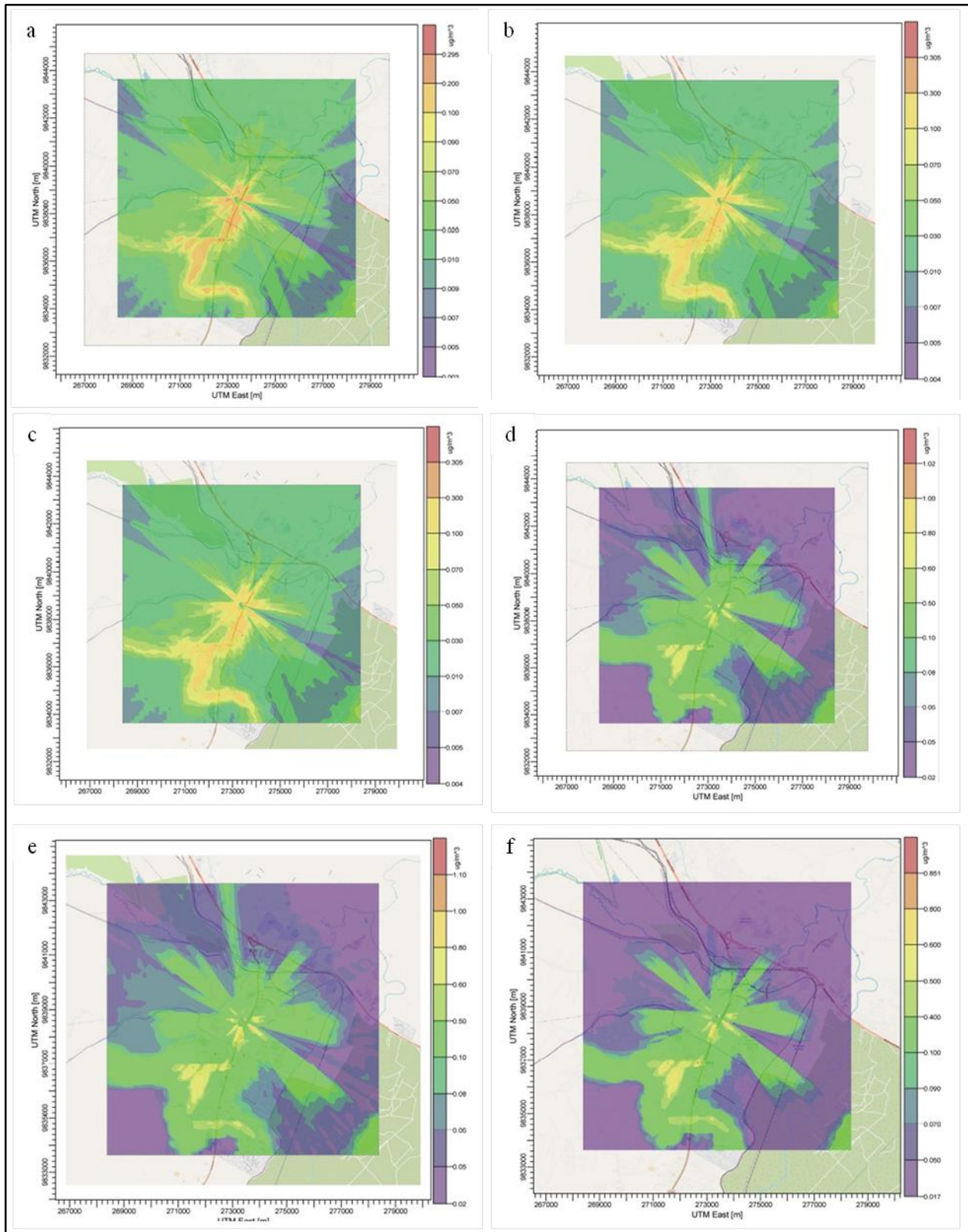


Figure 4-27: 8-hour ambient concentration of CO from (a) CF1, S1; (b) CF1, S2; (c) CF1, S2; and 1-hour ambient concentration of CO from (d) CF1, S1; (e) CF1, S2; (f) CF1, S3

A higher 8-hour and 1-hour ambient concentration of the contaminant from the emission point in CF1 is observed around the emission point and towards the southwest direction from the emission point shown in Figure 4-27. This was mainly caused by the direction of the wind during the study period. The wind predominantly blew towards the southwest. The concentration of carbon monoxide from CF2 was below the detection limit.

To determine the burden of carbon monoxide on the receptors, the 1st highest 8-hour and 1-hour maximum concentrations were determined and compared to the standard limits shown in Table 4-27 and Figure 4-28.

Table 4-27: 8-hour and 1-hour maximum concentration of carbon monoxide

(mg/m ³)	Sample 1	Sample 2	Sample 3	Average	WHO	NEMA
CF1 8-hour	0.00029	0.00031	0.00021	0.00027±0.00005	Not provided	2
CF1 1-hour	0.00102	0.00102	0.00085	0.00096±0.0001	4	4

*WHO air quality guidelines (WHO, 2021), NEMA – Ambient tolerance limits(EMCA, 2014)

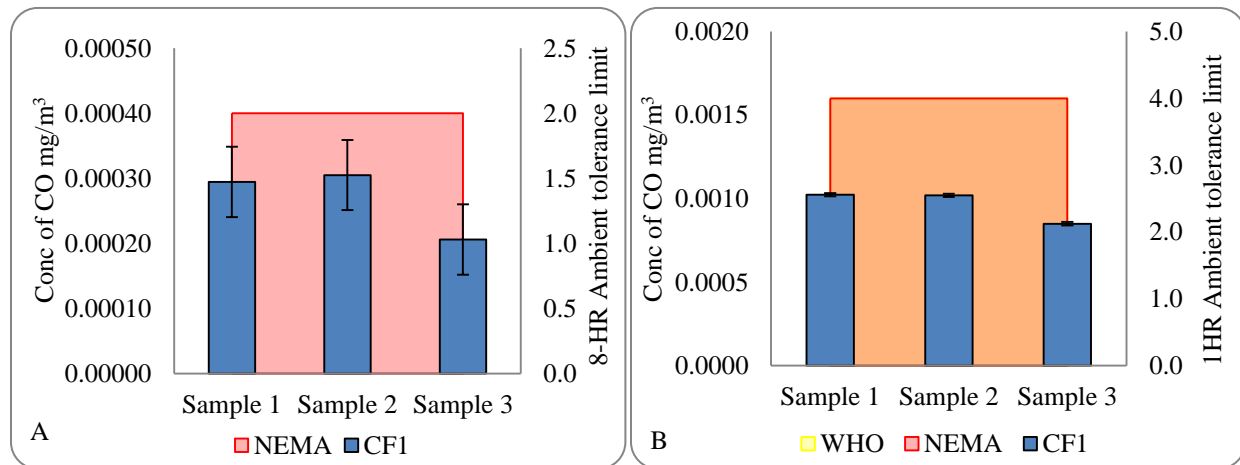


Figure 4-28: The (A) 8-hour and (B) 1-hour maximum concentration of CO

The 8-hour and 1-hour average maximum ambient concentrations of carbon monoxide for CF1 were 0.00027±0.00005 mg/m³ and 0.00096±0.0001 mg/m³.

The ambient 1st highest 8-hour and 1-hour concentrations of the carbon monoxide were also determined at the selected discrete receptors. The results are shown in Table 4-28 and Figure 4-29 below.

Table 4-28: Discrete receptor 8-hour and 1-hour average concentration of carbon monoxide

Discrete Receptors	CF1	
	8-hour (mg/m ³)	1-hour (mg/m ³)
A	0.000029±0.0039	0.000144±0.0193
B	0.000018±0.0036	0.00005±0.0063
C	0.000024±0.004	0.000142±0.0225
D	0.00009±0.0118	0.00037±0.0489
E	0.000017±0.0029	0.000096±0.013
F	0.000045±0.0059	0.000226±0.0294
G	0.000008±0.001	0.000057±0.0073
H	0.000046±0.0058	0.000225±0.0288

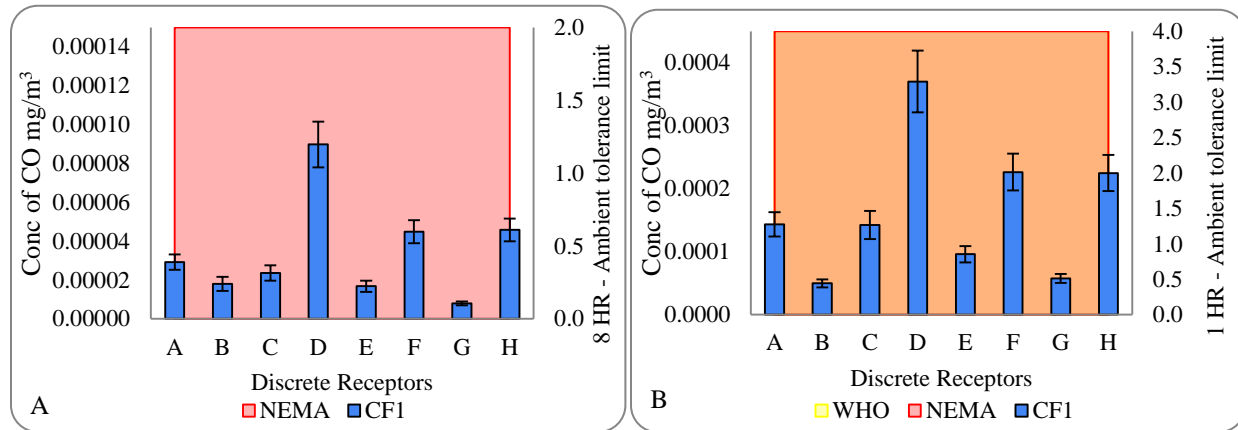


Figure 4-29: The (A) 8-hour and (B) 1-hour discrete receptor concentration of carbon monoxide

The 8-hour and the 1-hour ambient concentrations of carbon monoxide from CF1 were below the ambient tolerance limit of 2 mg/m³ and 4 mg/m³, stipulated under EMCA 2014 and the WHO Global Air Quality Guidelines, 2021. Among the discrete receptors, the receptor exposed to the highest carbon monoxide concentration was receptor D.

4.4.6 Sulphur Dioxide

The modelling results of sulphur dioxide for each receptor point were the 1st highest concentration averaged for the annual and 24-hour period shown using contours in Figure 4-30.

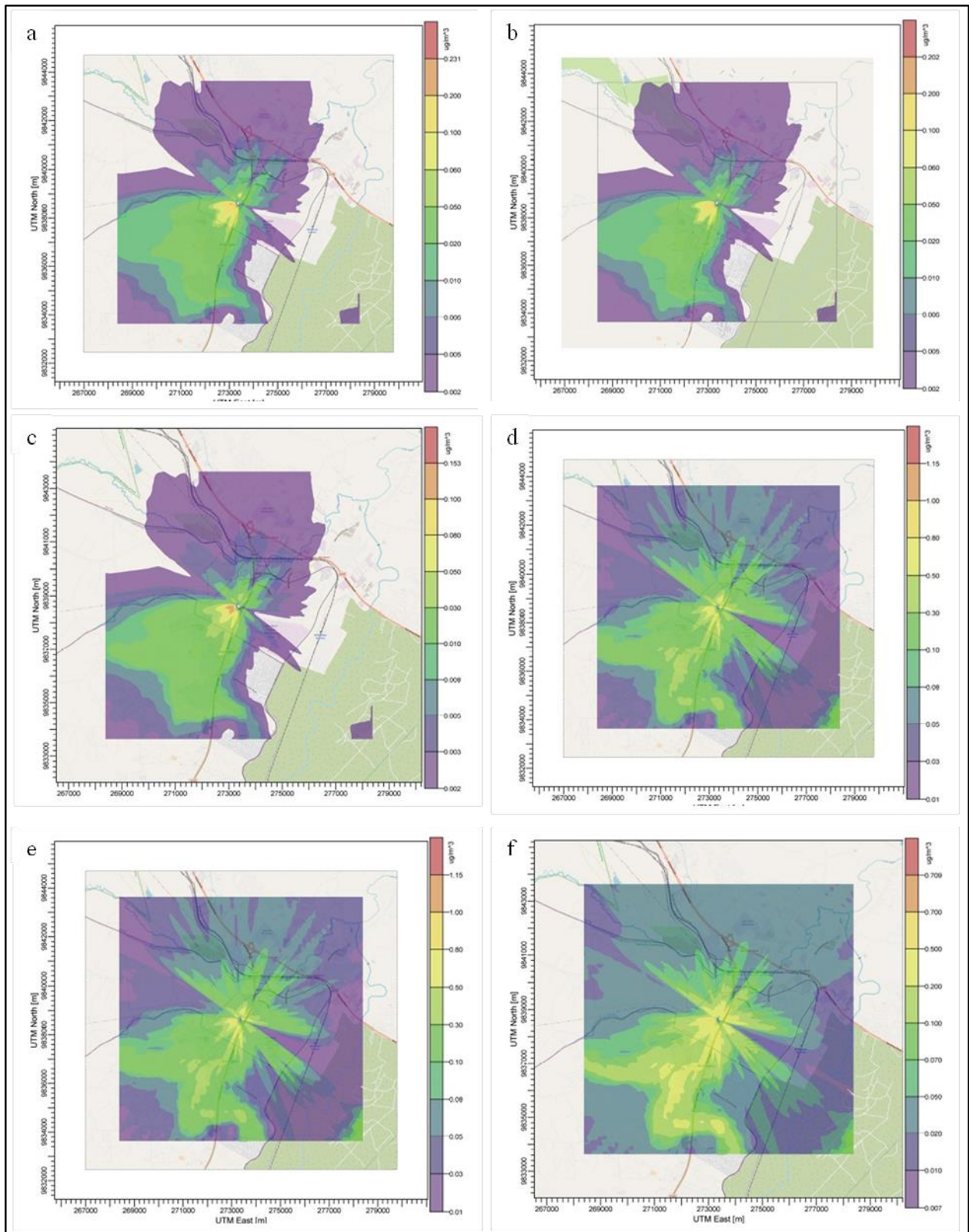


Figure 4-30: Annual ambient concentration of SO₂ from (a) CF1, S1; (b) CF1, S2; (c) CF1, S2; and 24-hour ambient concentration of SO₂ from (d) CF1, S1; (e) CF1, S2; (f) CF1, S2;

A higher annual and 24-hour ambient concentration of the pollutants from the emission point is observed towards the southwest direction from the emission point shown in Figure 4-30. The concentration of sulphur dioxide from CF2 was below the detection limit.

To determine the burden of sulphur dioxide on the receptors, the 1st highest annual and 24-hour maximum concentrations were determined and compared to the standard limits shown in Table 4-29 and Figure 4-31.

Table 4-29: Annual and 24-hour maximum concentration of sulphur dioxide

(mg/m ³)	Sample 1	Sample 2	Sample 3	Average	WHO	NEMA
CF1 Annual	0.231	0.203	0.153	0.196±0.0395	Not provided	60
CF1 24-hour	1.148	0.95	0.709	0.936±0.220	40	80

*WHO air quality guidelines (WHO, 2021), NEMA – Ambient tolerance limits(EMCA, 2014)

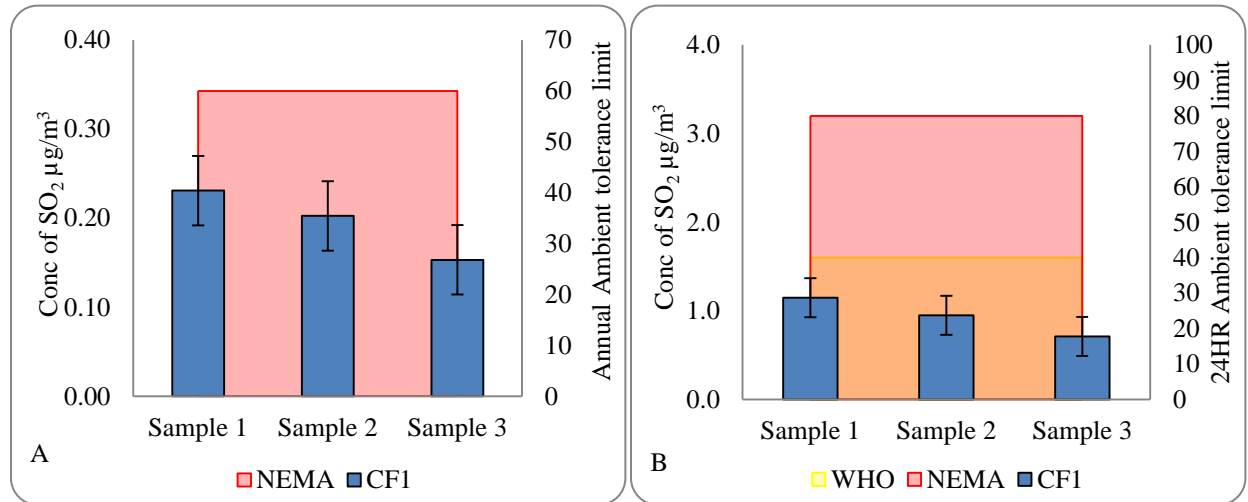


Figure 4-31: A graph of the (A) annual and (B) 24-hour ambient maximum concentration of sulphur dioxide

The annual and 24-hour average maximum ambient concentration of sulphur dioxide for CF1 was 0.196±0.0395 µg/m³ and 0.936±0.220 µg/m³. Downwind dispersion of sulphur dioxide from CF2 was not done because the stack concentration was below the detection limit.

The ambient 1st highest annual and 24-hour concentration of the sulphur dioxide was also determined at the selected discrete receptors. The results are shown in Table 4-30.

Table 4-30: Discrete receptor annual and 24-hour average concentration of sulphur dioxide

Discrete Receptors	CF1	
	Annual $\mu\text{g}/\text{m}^3$	24-hour $\mu\text{g}/\text{m}^3$
A	0.0062±0.0014	0.0679±0.0152
B	0.0044±0.001	0.0539±0.011
C	0.0013±0.0003	0.0906±0.0191
D	0.0163±0.0033	0.3678±0.0757
E	0.0024±0.0005	0.0646±0.0136
F	0.0027±0.0006	0.1093±0.0224
G	0.0013±0.0003	0.0253±0.005
H	0.0033±0.0007	0.1114±0.0224

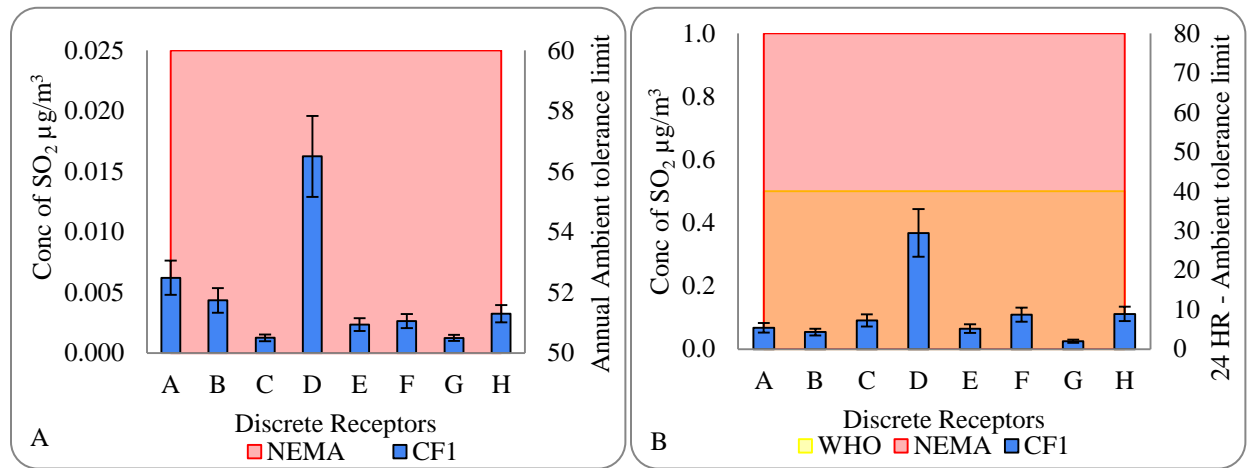


Figure 4-32: The (A) annual and (B) 24-hour discrete receptor ambient concentration of sulphur dioxide

The annual and the 24-hour ambient concentration of sulphur dioxide from CF1 was below the ambient tolerance limit of $60 \mu\text{g}/\text{m}^3$ and $80 \mu\text{g}/\text{m}^3$, stipulated under EMCA 2014 and $40 \mu\text{g}/\text{m}^3$ -24-hour ambient tolerance limit under the WHO Global Air Quality Guidelines, 2021. Among the discrete receptors, the receptor exposed to the highest sulphur dioxide concentration was receptor D. This was likely due to its proximity to the factory compared to other discrete receptors.

4.4.7 Nitrogen Oxides

The modelling results of nitrogen oxides for each receptor point were the 1st highest concentration averaged for the annual and 24-hour period shown using contours in Figure 4-33.

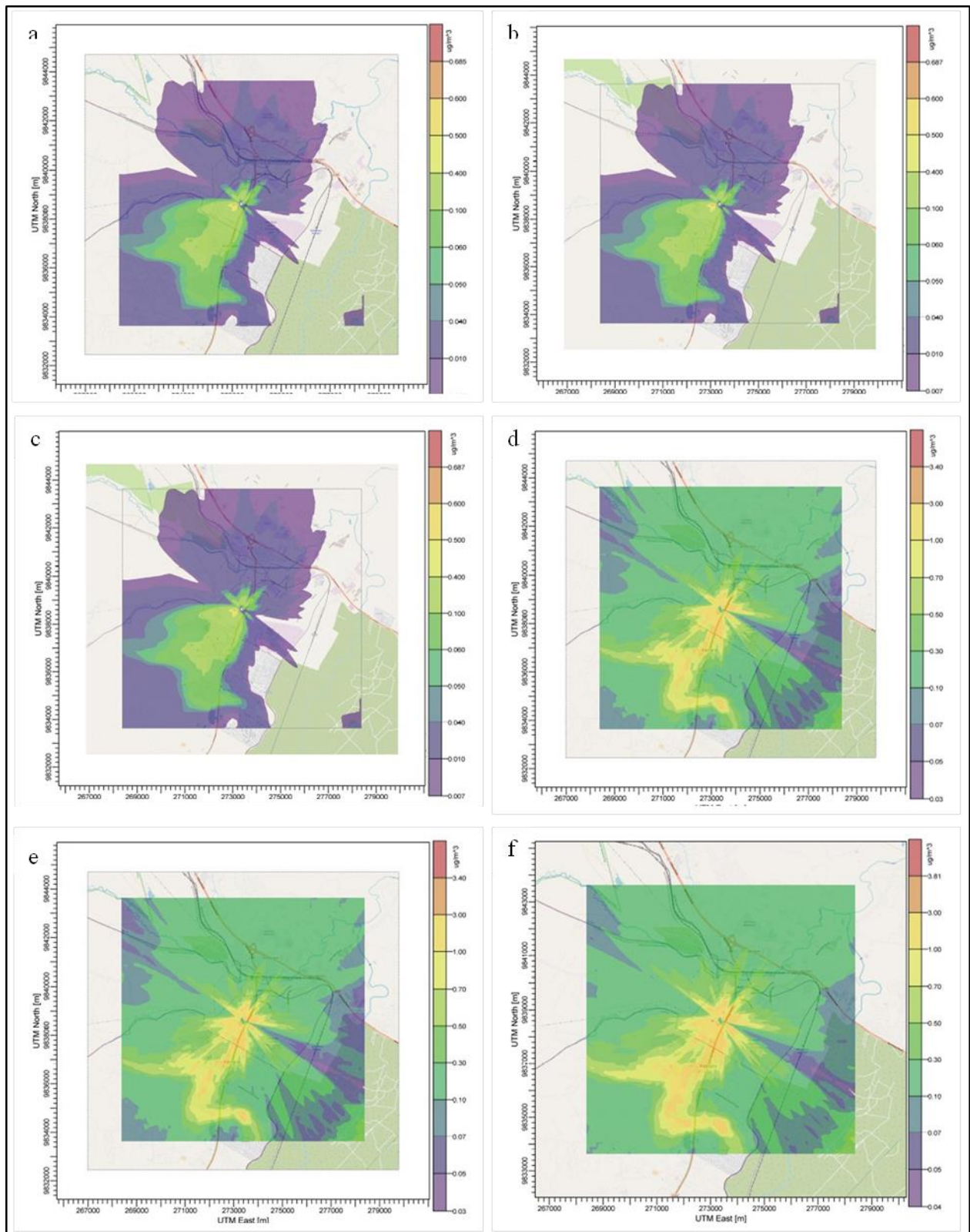


Figure 4-33: Annual ambient concentration of NO_x from (a) CF1, S1; (b) CF1, S2; (c) CF1, S2; and 24-hour ambient concentration of SO_2 from (d) CF1, S1; (e) CF1, S2; (f) CF1, S2;

A higher annual and 24-hour ambient concentration of the contaminants from the emission point is observed around the emission point and towards the southwest direction from the emission point shown in Figure 4-33. The concentration of nitrogen oxides from CF2 was below the detection limit.

To determine the burden of nitrogen oxides on the receptors, the 1st highest annual and 24-hour maximum concentrations were determined and compared to the standard limits shown in Table 4-31 and Figure 4-34.

Table 4-31: Annual and 24-hour maximum concentration of nitrogen oxide

(mg/m ³)	Sample 1	Sample 2	Sample 3	Average	WHO	NEMA
CF1 Annual	0.685	0.688	0.822	0.731±0.0782	10	60
CF1 24-hour	3.4	3.225	3.808	3.478±0.299	25	80

* WHO air quality guidelines (WHO, 2021), NEMA – Ambient tolerance limits(EMCA, 2014)

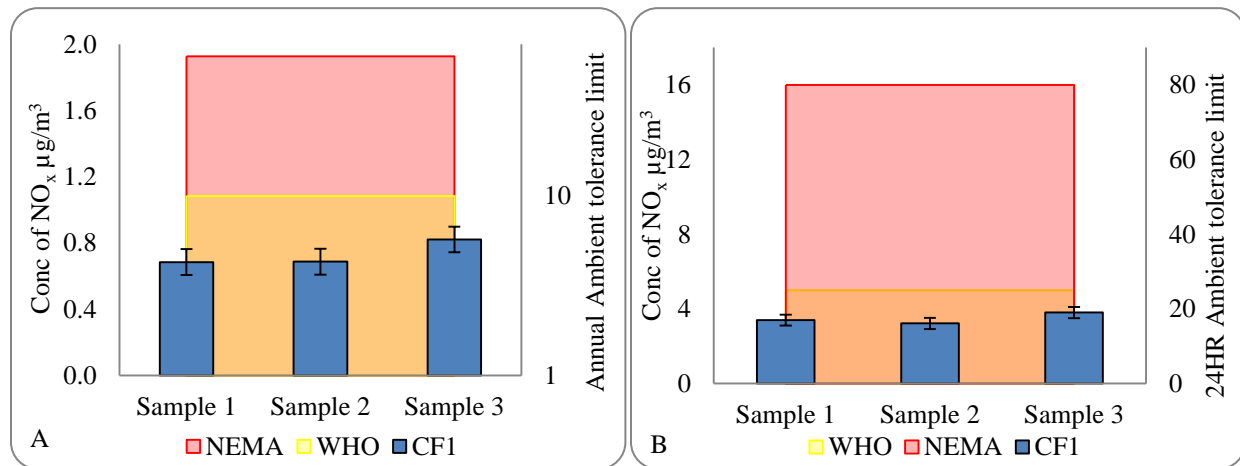


Figure 4-34: The (A) annual and (B) 24-hour maximum ambient concentration of nitrogen dioxide

The annual and 24-hour average maximum concentration of nitrogen oxides for CF1 was 0.731±0.0782 µg/m³ and 3.478±0.299 µg/m³. Downwind dispersion of nitrogen oxides from CF2 was not done because the stack concentration was below the detection limit.

The ambient 1st highest annual and 24-hour concentration of the nitrogen oxides was also determined at the selected discrete receptors and the results are shown in Table 4-32 and Figure 4-35.

Table 4-32: Discrete receptor annual and 24-hour average concentration of nitrogen oxides

Discrete Receptors	CF1	
	Annual $\mu\text{g}/\text{m}^3$	24-hour $\mu\text{g}/\text{m}^3$
A	0.0232±0.0018	0.2528±0.0242
B	0.0162±0.001	0.2016±0.0212
C	0.0047±0.0004	0.3381±0.0335
D	0.0607±0.0063	1.3744±0.1427
E	0.0088±0.0006	0.241±0.0234
F	0.0099±0.0009	0.4082±0.042
G	0.0047±0.0005	0.0946±0.0104
H	0.0122±0.0011	0.4167±0.045

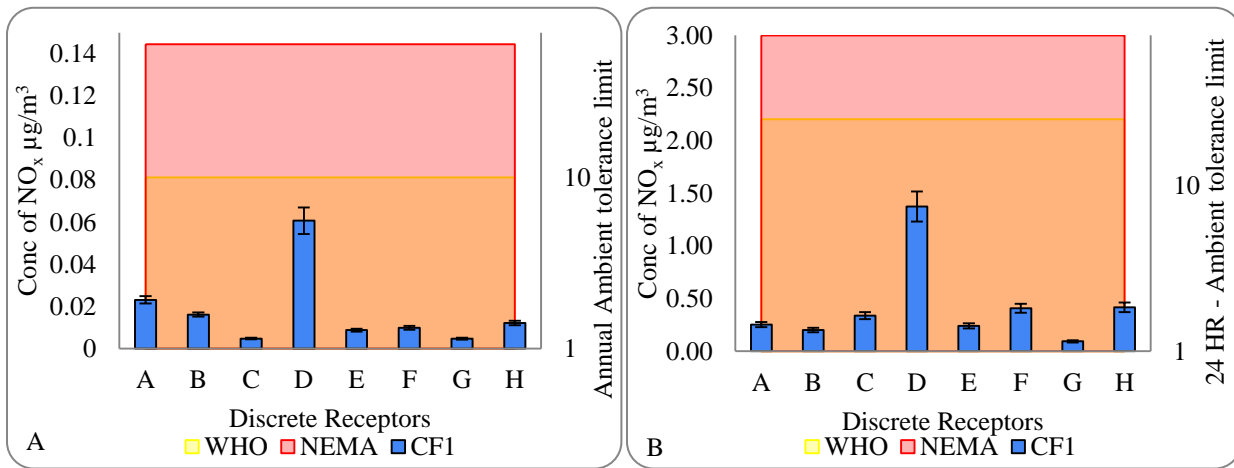


Figure 4-35: The (A) annual (B) 24-hour ambient discrete receptor concentration of nitrogen dioxide

The annual and the 24-hour ambient concentration of nitrogen oxides from CF1 was below the ambient tolerance limit of $60 \mu\text{g}/\text{m}^3$ and $80 \mu\text{g}/\text{m}^3$ stipulated under EMCA 2014 and $10 \mu\text{g}/\text{m}^3$ and $25 \mu\text{g}/\text{m}^3$ stipulated under the WHO Global Air Quality Guidelines, 2021. Among the discrete receptors, the receptor exposed to the highest sulphur dioxide concentration was receptor D due to its proximity to the cement factory.

4.4.8 Effect of Stack Height on Carbon Dioxide Mean Maximum Concentration

The mean maximum concentration of carbon dioxide was determined using the stack heights recommended by the AERMOD model based on the impacts of the emissions on ambient air quality. According to Good Engineering Practises (GEP), the recommended stack heights for Stacks 1, 2a and 2b are 74.02 m, 116.86 m and 92.08 m, from the current stack heights of 35 m, 39 m and 45 m. The results are shown in Table 4-33 and Figure 4-36.

Table 4-33: Effect of stack height on the mean maximum concentration

	8-hour Mean Maximum concentration of Carbon Dioxide (mg/m ³)		1-hour Mean Maximum concentration of Carbon Dioxide (mg/m ³)	
	From current stack heights	From recommended stack heights	From current stack heights	From recommended stack heights
CF1	8.809	1.688	32.715	8.973
CF2	0.58	0.0149	3.143	0.0758

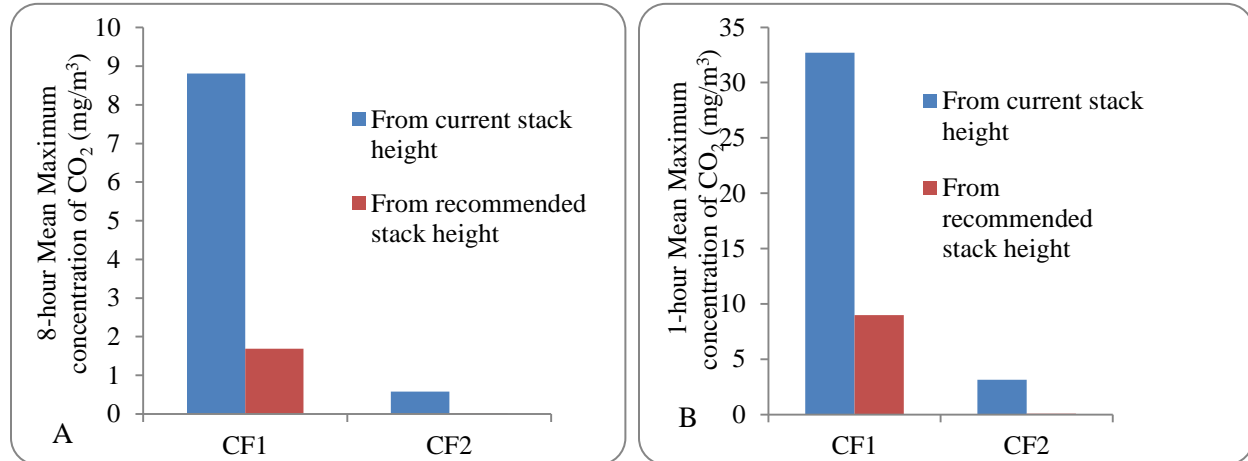


Figure 4-36: Effect of Stack height on (A) 8-hour and (B) 1-hour mean maximum concentration

The results in Table 4-33 shows that the concentration of carbon dioxide reduces to 1.688 mg/m³ from 8.809 mg/m³ and 0.0149 mg/m³ from 0.58 mg/m³ in CF1 and CF2 if the recommended stack heights were installed. The 1-hour mean maximum concentration would also reduce to 8.973 mg/m³ from 32.715 mg/m³ and 0.0758 mg/m³ from 3.143 mg/m³ in CF1 and CF2. The results show that a tall stack height significantly ($P < 0.05$) reduces the mean maximum concentration. The 8-hour and 1-hour concentrations from CF1 were reduced by a factor of 5 and 3 and 38 and 41 from CF2.

CHAPTER FIVE

5 CONCLUSIONS AND RECOMMENDATIONS

5.1 Conclusions

The source concentration of particulate matter (TSP, PM₁₀ and PM_{2.5}) was released at a greater proportion in Stack 2b (approximately 38%) compared to Stacks 1 and 2a. However, there was an insignificant difference ($P>0.05$) in the source concentrations of particulate matter (TSP, PM₁₀ and PM_{2.5}) from the three stationary points.

The source concentration of gaseous emissions accounted for over 90% of the total emissions released from the stationary points and 10% of particulate matter during the time of the study. In addition, the concentration of carbon dioxide was significantly higher ($P<0.05$) in CF1 than in CF2.

The cement production process affects the type and concentration of emissions released from the stack. The grinding stage was responsible for the release of particulate matter from both cement factories and the drying stage was responsible for the release of gaseous emissions from Stack 1 in CF1. The drying stage was also responsible for the production of high concentrations (above permissible limits) in CF1.

The peak maximum concentration of the dispersed particulate matter and gaseous emissions were significantly different ($P<0.05$) in the two cement factories.

The dispersion of particulate matter and gaseous emissions from CF1 resulted in higher concentrations being observed in the southwest direction from the emission source while the emissions from CF2 were evenly distributed in all directions from the emission points.

The distance of the receptor from the emission source determines the ground-level concentration measured at the receptor. The further the receptor is to the emission point, the less the overall exposure to the emissions released.

The emission rate of the dispersed particulate matter and gaseous emissions directly influences the ground-level concentration of the emissions. The higher emission rate of carbon dioxide from CF1 (>200 g/s) compared to other gaseous emissions in CF2 (<4.5 g/s) resulted in a higher impact of carbon dioxide in the areas surrounding the cement factory.

The elevation of the point of emission has a direct influence on the extent of dispersion of particulate matter and gaseous emissions. Increasing stack height affects the distance pollutants travel before deposition takes place and reduces the overall ground-level concentration. There

would be a significant decrease ($P < 0.05$) in the peak maximum concentration of carbon dioxide if the elevation of the point of emissions were to be increased as shown in Table 4-33 and Figure 4-36.

5.2 Recommendations

- A carbon-reducing technology such as carbon capture and carbon dioxide absorption (K_2CO_3 –wet scrubbers) can be introduced in CF1 Stack 1 to reduce the carbon dioxide released.
- Application of flue gas recycling. In addition to reducing the emission rate, flue gas recycling also acts as a pre-heater.
- The use of alternative sources of energy such as hydropower, solar and wind energy is also recommended as they result in lower emission rates compared to fossil fuels
- To reduce ground-level concentration, it is recommended that the stack height should be at least 2.5 times the height of the tallest building or structure surrounding it.
- The standard limits under the Air Quality Regulations, 2014 should be reviewed and the limits not provided included in the regulation
- During the planning and operation phase, the manufacturers and environmental agencies should ensure that the emissions released from an emission source are as low as possible, within the recommended national standard limits to reduce both health and environmental-related effects on the surrounding ecosystem.

References

- Abd-Alla, G. H. (2002). Using exhaust gas recirculation in internal combustion engines: a review. *Energy Conversion and Management*, **43**(8), 1027–1042. [https://doi.org/10.1016/S0196-8904\(01\)00091-7](https://doi.org/10.1016/S0196-8904(01)00091-7).
- Ali, M. B., Saidur, R., & Hossain, M. S. (2011). A review on emission analysis in cement industries. *Renewable and Sustainable Energy Reviews*, **15**(5), 2252–2261. <https://doi.org/10.1016/J.RSER.2011.02.014>.
- Ali, M. C., Yang, Q., Fine, A. A., Jin, W., Zhang, Z., Xing, H., & Ren, Q. (2015). Efficient removal of both basic and non-basic nitrogen compounds from fuels by deep eutectic solvents. *Green Chemistry*, **18**(1), 157–164. <https://doi.org/10.1039/C5GC01823D>.
- Ali, N., Abbas, J., Anwer, M., Alwi, S., & Anjum, M. (2015). The Greenhouse Gas Emissions Produced by Cement Production and Its Impact on Environment: A Review of Global Cement Processing. *International Journal of Research (IJR)*, **2**(2), 488–500.
- Altun, D., Benzer, H., Aydogan, N., & Gerold, C. (2017). Operational parameters affecting the vertical roller mill performance. *Minerals Engineering*, **103–104**, 67–71. <https://doi.org/10.1016/J.MINENG.2016.08.015>.
- Anderson, J. O., Thundiyil, J. G., & Stolbach, A. (2012). Clearing the Air: A Review of the Effects of Particulate Matter Air Pollution on Human Health. *Journal of Medical Toxicology*, **8**(2), 166–175. <https://doi.org/10.1007/S13181-011-0203-1/TABLES/5>.
- Apex Instruments. (2016, April 4). *Isokinetic Sampling*. Apex Instruments. <https://www.apexinst.com/product-category/isokinetic>.
- Aramide, F. O., & Seidu, S. O. (2013). Production of Refractory Lining for Diesel Fired Rotary Furnace, from Locally Sourced Kaolin and Potter's Clay. *Journal of Minerals and Materials Characterization and Engineering*, **2013**(03), 75–79. <https://doi.org/10.4236/JMMCE.2013.13014>.
- Bai, X., Chen, H., & Oliver, B. (2022). The health effects of traffic-related air pollution: A review focused on the health effects of going green. *Chemosphere*, 289. <https://doi.org/10.1016/j.chemosphere.2021.133082>.
- Barratt, R. (2001). *Atmospheric dispersion modelling : an introduction to practical applications*. Earthscan Ltd.
- Beard, H. R., Farley, K. R., Crane, S. R., & Marchant, W. N. (1979). *Gas Analysis Procedures*

- Applicable to Flue Gas Desulfurization by the Citrate Process.* Dept. of the Interior, Bureau of Mines.
- Bhargava, akshey. (2016, April). *Effect of Stack Exit Velocity and Gas Temperature on Plume rise using different equations.*
- Blaszczak, R. (1999). *Nitrogen Oxides (NOx): Why and How They Are Controlled | CICA | US EPA-456/F-99-006R.*
- Boningari, T., & Smirniotis, P. G. (2016). Impact of nitrogen oxides on the environment and human health: Mn-based materials for the NOx abatement. *Current Opinion in Chemical Engineering*, **13**, 133–141. <https://doi.org/10.1016/J.COCHE.2016.09.004>.
- Brusca, S., Famoso, F., Lanzafame, R., Mauro, S., Garrano, A. M. C., & Monforte, P. (2016). Theoretical and Experimental Study of Gaussian Plume Model in Small Scale System. *Energy Procedia*, **101**, 58–65. <https://doi.org/10.1016/J.EGYPRO.2016.11.008>.
- Carson, J. E., & Moses, H. (2012). The Validity of Several Plume Rise Formulas. *Journal of the Air Pollution Control Association*, **19**(11), 862–866. <https://doi.org/10.1080/00022470.1969.10469350>.
- Chen, G., Zhang, W., Li, S., Williams, G., Liu, C., Morgan, G. G., Jaakkola, J. J. K., & Guo, Y. (2017). Is short-term exposure to ambient fine particles associated with measles incidence in China? A multi-city study. *Environmental Research*, **156**, 306–311. <https://doi.org/10.1016/J.ENVRES.2017.03.046>.
- Chen, H., Oliver, B. G., Pant, A., Olivera, A., Poronnik, P., Pollock, C. A., & Saad, S. (2022). Effects of air pollution on human health – Mechanistic evidence suggested by in vitro and in vivo modelling. *Environmental Research*, **212**(Part C), 113378. <https://doi.org/10.1016/j.envres.2022.113378>.
- Chen, T. M., Gokhale, J., Shofer, S., & Kuschner, W. G. (2007). Outdoor Air Pollution: Nitrogen Dioxide, Sulfur Dioxide, and Carbon Monoxide Health Effects. *The American Journal of the Medical Sciences*, **333**(4), 249–256. <https://doi.org/10.1097/MAJ.0B013E31803B900F>.
- Chmielewski, A. G. (1999). Environmental Effects of Fossil Fuel Combustion. *INTERACTIONS: ENERGY/ENVIRONMENT*, 56–74.
- Ciobanu, C., Istrate, I. A., Tudor, P., Voicu, G., Ciolli, M., Ionescu, G., & Tchounwou, P. B. (2021). Dust Emission Monitoring in Cement Plant Mills: A Case Study in Romania. *International Journal of Environmental Research and Public Health 2021, Vol. 18, Page*

- 9096, 18(17), 9096. <https://doi.org/10.3390/IJERPH18179096>.
- Craig, S. J., & McMahon, J. F. (1996). The effects of draft control on combustion. *ISA Transactions*, 35(4), 345–349. [https://doi.org/10.1016/S0019-0578\(96\)00043-2](https://doi.org/10.1016/S0019-0578(96)00043-2).
- Dean, S. W. (2001). Natural Atmospheres: Corrosion. In *Encyclopedia of Materials: Science and Technology* (2nd ed., pp. 5930–5938). Elsevier. <https://doi.org/10.1016/B0-08-043152-6/01033-0>.
- deSouza, P. (2018). Every breath you take: Who is monitoring air quality in Kenya? *The Elephant*, 1–18.
- deSouza, P. (2020). Air pollution in Kenya: a review. *Air Quality, Atmosphere & Health* 2020 13:12, 13(12), 1487–1495. <https://doi.org/10.1007/S11869-020-00902-X>.
- Devi, K. S., Lakshmi, V. V., & Alakanandana, A. (2017). Impacts Of Cement Industry On Environment-An Overview. *Asia Pacific Journal of Research ISSN*, 1(57), 2347–4793.
- Duncan, B. N., Prados, A. I., Lamsal, L. N., Liu, Y., Streets, D. G., Gupta, P., Hilsenrath, E., Kahn, R. A., Nielsen, J. E., Beyersdorf, A. J., Burton, S. P., Fiore, A. M., Fishman, J., Henze, D. K., Hostetler, C. A., Krotkov, N. A., Lee, P., Lin, M., Pawson, S., ... Ziemba, L. D. (2014). Satellite data of atmospheric pollution for U.S. air quality applications: Examples of applications, summary of data end-user resources, answers to FAQs, and common mistakes to avoid. *Atmospheric Environment*, 94, 647–662. <https://doi.org/10.1016/J.ATMOSENV.2014.05.061>.
- El-Azazy, M. (2019). Introductory Chapter: Infrared Spectroscopy - A Synopsis of the Fundamentals and Applications. *Infrared Spectroscopy - Principles, Advances, and Applications*, 1–10. <https://doi.org/10.5772/INTECHOPEN.82210>.
- EMCA. (2014). *Legal Notice No.34 E Environmental Management and Co-Ordination Act (No 8 Of 1999) The Environmental Management and Co-Ordination (Air Quality) Regulations, 2014*. NEMA.
- EPA. (2017a). *Method 10-Determination of Carbon Monoxide Emissions from Stationary Sources (Instrumental Analyzer Procedure) 1.0 Scope and Application*.
- EPA. (2017b). *Method 3a-Determination of Oxygen and Carbon Dioxide Concentrations in Emissions from Stationary Sources (Instrumental Analyzer Procedure) 1.0 Scope and Application*.
- EPA. (2017c). *Method 6C-Determination of Sulfur Dioxide Emissions from Stationary Sources*

- (Instrumental Analyzer Procedure) 1.0 Scope and Application.
- EPA. (2017d). Method 3 - Gas Analysis for the Determination of Dry Molecular Weight. *Air Emission Measurement Center (EMC)*, 1–9.
- EPA. (2017e). Method 2-Determination of Stack Gas Velocity and Volumetric Flow Rate (Type S Pitot Tube). *Air Emission Measurement Center (EMC)*, 1–22.
- EPA. (2017f). Method 4-Determination Of Moisture Content In Stack Gases. *Air Emission Measurement Center (EMC)*.
- EPA. (2018). Air Emissions Monitoring Guidance Note #2 (AG2). *Environment Protection Agency Office of Environmental Enforcement (OEE) Air*, 1–79.
- EPA. (2020a). *Method 7e-Determination of Nitrogen Oxides Emissions from Stationary Sources (Instrumental Analyzer Procedure) 1.0 Scope And Application*.
- EPA. (2020b, December 7). *Method 5 - Determination of Particulate Matter Emissions from Stationary Sources*. Air Emission Measurement Center (EMC).
- Eshikumo, S. M., & Odock, S. O. (2017). Green Manufacturing and Operational Performance of a Firm: Case of Cement Manufacturing in Kenya. *International Journal of Business and Social Science*, *8*(4), 106–120.
- Etim, M. A., Babaremu, K., Lazarus, J., & Omole, D. (2021). Health Risk and Environmental Assessment of Cement Production in Nigeria. *Atmosphere*, *12*(9), 1111. <https://doi.org/10.3390/ATMOS12091111/S1>.
- Finlayson-Pitts, B. J., & Pitts, J. N. (2012). Atmospheric Chemistry of Tropospheric Ozone Formation: Scientific and Regulatory Implications. *Air and Waste Management Association*, *43*(8), 1091–1100. <https://doi.org/10.1080/1073161X.1993.10467187>.
- Florides, G. A., & Christodoulides, P. (2009). Global warming and carbon dioxide through sciences. *Environment International*, *35*(2), 390–401. <https://doi.org/10.1016/J.ENVINT.2008.07.007>.
- Francis, W., & Peters, M. C. (1980). Prevention of Atmospheric Pollution by Industrial Gases. In *Fuels and Fuel Technology* (pp. 651–660). Pergamon. <https://doi.org/10.1016/B978-0-08-025249-0.50111-7>.
- Gandhi, A., Patel, P., & Bagale, G. (2017). A Study on Acid Rain: Effects and Control Measures. *International Journal of Innovative Research in Science, Engineering and Technology*, *6*(4), 5538–5543. <https://doi.org/10.15680/IJRSET.2017.0604061>.

- Geršl, J., Knotek, S., Belligoli, Z., Dwight, R. P., Robinson, R. A., & Coleman, M. D. (2018). Flow rate measurement in stacks with cyclonic flow – Error estimations using CFD modelling. *Measurement*, **129**, 167–183.
- Giovannini, L., Ferrero, E., Karl, T., Rotach, M. W., Staquet, C., Castelli, S. T., & Zardi, D. (2020). Atmospheric Pollutant Dispersion over Complex Terrain: Challenges and Needs for Improving Air Quality Measurements and Modeling. *Atmosphere 2020*, **Vol. 11**, Page 646, *11*(6), 646. <https://doi.org/10.3390/ATMOS11060646>.
- Gupta, R. K., Majumdar, D., Trivedi, J. V., & Bhanarkar, A. D. (2012). Particulate matter and elemental emissions from a cement kiln. *Fuel Processing Technology*, **104**, 343–351. <https://doi.org/10.1016/J.FUPROC.2012.06.007>.
- Han, L., Cai, S., Gao, M., Hasegawa, J. Y., Wang, P., Zhang, J., Shi, L., & Zhang, D. (2019). Selective Catalytic Reduction of NO_x with NH₃ by Using Novel Catalysts: State of the Art and Future Prospects. *Chemical Reviews*, **119**(19), 10916–10976. https://doi.org/10.1021/ACS.CHEMREV.9B00202/ASSET/IMAGES/MEDIUM/CR9B00202_0044.GIF.
- Horak, F., Studnicka, M., Gartner, C., Spengler, J. D., Tauber, E., Urbanek, R., Veiter, A., & Frischer, T. (2002). Particulate matter and lung function growth in children: a 3-yr follow-up study in Austrian school children. *European Respiratory Journal*, **19**(5), 838–845. <https://doi.org/10.1183/09031936.02.00512001>.
- Hu, H., & Xu, K. (2020). Physicochemical technologies for HRP_s and risk control. In *High-Risk Pollutants in Wastewater* (pp. 169–207). Elsevier. <https://doi.org/10.1016/B978-0-12-816448-8.00008-3>.
- Ibrahim, H. G., Okasha, A. Y., Elatrash, M. S., & Al-Meshragi, M. A. (2012). Emissions of SO₂, NO_x and PMs from Cement Plant in Vicinity of Khoms City in Northwestern Libya. *Journal of Environmental Science and Engineering*, **1**, 620–628.
- Jafarinejad, S. (2022). Control and treatment of sulfur compounds specially sulfur oxides (SO_x) emissions from the petroleum industry: A review. *Chemistry International*, **2**(4), 242–253.
- Jankovic, A., Valery, W., & Davis, E. (2004). Cement grinding optimisation. *Minerals Engineering*, **17**(11–12), 1075–1081. <https://doi.org/10.1016/J.MINENG.2004.06.031>.
- Javed, T. M., Irfan, N., & Gibbs, B. M. (2007). Control of combustion-generated nitrogen oxides by selective non-catalytic reduction. *Journal of Environmental Management*, **83**(3), 251–289.

- <https://doi.org/10.1016/J.JENVMAN.2006.03.006>.
- Jittra, N., Pinthong, N., & Thepanondh, S. (2015). Performance Evaluation of AERMOD and CALPUFF Air Dispersion Models in Industrial Complex Area: *Air, Soil and Water Research*, **8**, 87–95. <https://doi.org/10.4137/ASWR.S32781>.
- Johnson, J. B. (2022). An Introduction to Atmospheric Pollutant Dispersion Modelling. *Environmental Sciences Proceedings*. <https://doi.org/10.3390/ecas2022-12826>.
- Kääntee, U., Zevenhoven, R., Backman, R., & Hupa, M. (2004). Cement manufacturing using alternative fuels and the advantages of process modelling. *Fuel Processing Technology*, **85**(4), 293–301. [https://doi.org/10.1016/S0378-3820\(03\)00203-0](https://doi.org/10.1016/S0378-3820(03)00203-0).
- Kakali, G., & Tsivilis, S. (1993). The effect of inter-grinding and separate grinding of cement raw mix on the burning process. *Cement and Concrete Research*, **23**(3), 651–662. [https://doi.org/10.1016/0008-8846\(93\)90016-3](https://doi.org/10.1016/0008-8846(93)90016-3).
- Kampa, M., & Castanas, E. (2008). Human health effects of air pollution. *Environmental Pollution*, **151**(2), 362–367. <https://doi.org/10.1016/J.ENVPOL.2007.06.012>.
- Karagulian, F., Belis, C. A., Dora, C. F. C., Prüss-Ustün, A. M., Bonjour, S., Adair-Rohani, H., & Amann, M. (2015). Contributions to cities' ambient particulate matter (PM): A systematic review of local source contributions at global level. *Atmospheric Environment*, **120**, 475–483. <https://doi.org/10.1016/J.ATMOSENV.2015.08.087>.
- Khalil, M. A. K., & Rasmussen, R. A. (1992). The global sources of nitrous oxide. *Journal of Geophysical Research: Atmospheres*, **97**(D13), 14651–14660. <https://doi.org/10.1029/92JD01222>.
- Kiano, E. K. (2018). *Economic analysis of health effects of industrial air pollution in Kenya: a case of Webuye and its environs*.
- Kim, A.-Y., Kim, J., Ko, M.-S., & Kim, K.-W. (2010). Acid Rain Impact on Phytoavailability of Heavy Metals in Soils. *Geosystem Engineering*, **13**(4), 133–138. <https://doi.org/10.1080/12269328.2010.10541320>.
- Koz. (2021, June 30). *Best Combustion Analyzer (Ultimate Guide) – Forensics Detectors*. <https://www.forensicsdetectors.com/blogs/articles/what-are-combustion-analyzers>.
- Kuo, Y. M., Kuan, W. Y., Lin, S. L., Yin, L. Te, & Hsieh, Y. K. (2019). Air Pollution Characteristics of Reclamation of Refuse Derived Fuel (RDF) Recovered from Cutting Oil Waste. *Aerosol and Air Quality Research*, **19**(11), 2576–2584.

- <https://doi.org/10.4209/AAQR.2019.09.0481>.
- Kurane, I. (2010). The Effect of Global Warming on Infectious Diseases. *Osong Public Health and Research Perspectives*, *1*(1), 4–9. <https://doi.org/10.1016/j.phrp.2010.12.004>
- Kweku, D., Bismark, O., Maxwell, A., Desmond, K., Danso, K., Oti-Mensah, E., Quachie, A., & Adormaa, B. (2018). Greenhouse Effect: Greenhouse Gases and Their Impact on Global Warming. *Journal of Scientific Research and Reports*, *17*(6), 1–9. <https://doi.org/10.9734/JSRR/2017/39630>.
- Kwiatkowski, S., Polat, M., Yu, W., & Johnson, M. S. (2019). Industrial Emissions Control Technologies: Introduction. *Encyclopedia of Sustainability Science and Technology*, 1–35. https://doi.org/10.1007/978-1-4939-2493-6_1083-1.
- Lee, H. K., Khaine, I., Kwak, M. J., Jang, J. H., Lee, T. Y., Lee, J. K., Kim, I. R., Kim, W. Il, Oh, K. S., & Woo, S. Y. (2017). The relationship between sulphur dioxide exposure and plant physiology: A mini-review. *Horticulture, Environment, and Biotechnology*, *58*(6), 523–529. <https://doi.org/10.1007/S13580-017-0053-0>.
- Lee, S., Russell, A. G., & Baumann, K. (2007). Source apportionment of fine particulate matter in the Southeastern United States. *Journal of the Air and Waste Management Association*, *57*(9), 1123–1135. <https://doi.org/10.3155/1047-3289.57.9.1123>.
- Li, X., Jin, L., & Kan, H. (2019). Air pollution: a global problem needs local fixes. *Nature* *2021* *570*:7762, *570*(7762), 437–439. <https://doi.org/10.1038/d41586-019-01960-7>.
- Longhurst, J., Barnes, J., Chatterton, T., De Vito, L., Everard, M., Hayes, E., Prestwood, E., & Williams, B. (2018). Analysing air pollution and its management through the lens of the UN sustainable development goals: A review and assessment. *WIT Transactions on Ecology and the Environment*, *230*, 3–14. <https://doi.org/10.2495/AIR180011>.
- Makri, A., & Stilianakis, N. I. (2008). Vulnerability to air pollution health effects. *International Journal of Hygiene and Environmental Health*, *211*(3–4), 326–336. <https://doi.org/10.1016/J.IJHEH.2007.06.005>.
- Manahan, S. (2017). Environmental chemistry, Tenth edition. In *Environmental Chemistry, Tenth Edition* (10th ed.). CRC Press.
- Manisalidis, I., Stavropoulou, E., Stavropoulos, A., & Bezirtzoglou, E. (2020). Environmental and Health Impacts of Air Pollution: A Review. *Frontiers in Public Health*, *8*. <https://doi.org/10.3389/fpubh.2020.00014>.

- Mansoor, K., Parkins, G., Wilson, L., White, J., Shiflett, B. S., Ajmeri, A., Zeid, F., University, M., & Edwards, J. C. (2019). Carbon Monoxide: A Rare Cause of Myocardial Ischemia. *Marshall Journal of Medicine*, *5*(1), 8–13. <https://doi.org/10.33470/2379-9536.1203>.
- Marangu, J. M. (2020). Physico-chemical properties of Kenyan made calcined Clay -Limestone cement (LC3). *Case Studies in Construction Materials*, *12*, e00333. <https://doi.org/10.1016/J.CSCM.2020.E00333>.
- McDermott, H. (2004). Instruments with Sensors for Specific Chemicals. In *AIR MONITORING FOR TOXIC EXPOSURES* (2nd ed., pp. 295–324). A JOHN WILEY & SONS, INC., PUBLICATION.
- Mohajan, H. (2018). Acid Rain is a Local Environment Pollution but Global Concern. *Open Science Journal of Analytical Chemistry*, *5*(5), 47–55.
- Monbureau, E. M., Heist, D. K., Perry, S. G., Brouwer, L. H., Foroutan, H., & Tang, W. (2018). Enhancements to AERMOD's Building Downwash Algorithms based on Wind-Tunnel and Embedded-LES Modeling. *Atmospheric Environment (Oxford, England: 1994)*, *179*, 330. <https://doi.org/10.1016/J.ATMOSENV.2018.02.022>.
- Najjar, Y. (2011). Gaseous Pollutants Formation and Their Harmful Effects on Health and Environment. *Ashdin Publishing Innovative Energy Policies*, *1*. <https://doi.org/10.4303/iep/E101203>.
- Ndetei, C. J. (2010). *Noise Assessment and H2S Dispersion At Olkaria Geothermal Power Plant, Kenya* (Issue 23).
- Nicklin, D., & Darabkhani, H. G. (2022). Feasibility of Using Isokinetic Sampling Techniques to Extract a Representative Sample from Processes in the United Kingdom. *Atmosphere 2022, Vol. 13, Page 1585*, *13*(10), 1585. <https://doi.org/10.3390/ATMOS13101585>.
- Nyairo, B., & Onyancha, D. (2018). Modeling H2S Dispersion from Proposed Menengai Geothermal Powerplant. *Shodhshauryam, International Scientific Refereed Research Journal © 2018 SISRRJ*, *1*(4), 2581–6306.
- Obaidullah, M. (2016, January). *Formation, measurement and analysis of emissions from stack gas*. Centre for Energy Studies, BUET.
- Okoji, A. I., Babatunde, D. E., Anozie, A. N., & Omoleye, J. A. (2018). Thermodynamic Analysis of Raw Mill in Cement Industry Using Aspen Plus Simulator. *IOP Conference Series: Materials Science and Engineering*, *413*(1), 012048. [94](https://doi.org/10.1088/1757-</p>
</div>
<div data-bbox=)

899X/413/1/012048.

- Omanga, E., Ulmer, L., Berhane, Z., & Gatari, M. (2014). Industrial air pollution in rural Kenya: community awareness, risk perception and associations between risk variables. *BMC Public Health* 2014 14:1, **14**(1), 1–14. <https://doi.org/10.1186/1471-2458-14-377>.
- Onoja, U., Dibua, U., & Enete, A. (2011). Climate Change: Causes, Effects and Mitigation Measures - A review. *Global Journal of Pure and Applied Sciences*, **17**(4), 469–479.
- Papageorgiou, A., Tzouvalas, G., & Tsimas, S. (2005). Use of inorganic setting retarders in cement industry. *Cement and Concrete Composites*, **27**(2), 183–189. <https://doi.org/10.1016/J.CEMCONCOMP.2004.02.005>.
- Pareek, P., & Sankhla, V. S. (2021). Review on vertical roller mill in cement industry & its performance parameters. *Materials Today: Proceedings*, **44**, 4621–4627. <https://doi.org/10.1016/J.MATPR.2020.10.916>.
- Pastuszka, J. S. (2016). *Synergic influence of gaseous, particulate, and biological pollutants on human health*. CRC Press.
- Patel, M. (2022). *Advancing flue-gas flow monitoring techniques*. Control Engineering. [https://www.controleng.com/articles/advancing-flue-gas-flow-monitoring-techniques/#:~:text=Process conditions of flue gas in stack&text=Process temperature of 130 to,second \(m%2Fs\)](https://www.controleng.com/articles/advancing-flue-gas-flow-monitoring-techniques/#:~:text=Process conditions of flue gas in stack&text=Process temperature of 130 to,second (m%2Fs)).
- Paykani, A., Saray, R. K., Shervani-Tabar, M. T., & Mohammadi-Kousha, A. (2012). Effect of exhaust gas recirculation and intake pre-heating on performance and emission characteristics of dual fuel engines at part loads. *Journal of Central South University of Technology (English Edition)*, **19**(5), 1346–1352. <https://doi.org/10.1007/S11771-012-1148-5>.
- Peters, R. L. (1990). Effects of global warming on forests. *Forest Ecology and Management*, **35**(1–2), 13–33. [https://doi.org/10.1016/0378-1127\(90\)90229-5](https://doi.org/10.1016/0378-1127(90)90229-5).
- Pongprueksa, P., & Chatchupong, T. (2016). High Resolution Land Cover Data for Thailand's Air Quality Impact Assessment. *High Resolution Land Cover Data for Thailand's Air Quality Impact Assessment*. <https://doi.org/10.13140/RG.2.1.4427.8642>.
- Price, H. (2019). Air analysis | Field portable instruments for the measurement of airborne hazards. In *Encyclopedia of Analytical Science* (3rd ed., pp. 40–43). Elsevier. <https://doi.org/10.1016/B978-0-12-409547-2.12680-0>.
- Rahman, F. A., Aziz, M. M. A., Saidur, R., & Bakar, W. A. W. A. (2018). A review of methods

- for measuring the gas emission for combustion analysis in industrial sector. *AIP Conference Proceedings*, **2030**(1), 020291-1-020291–020298. <https://doi.org/10.1063/1.5066932>.
- Rajabloo, T., Valee, J., Marenne, Y., Coppens, L., & Ceuninck, W. De. (2023). Carbon capture and utilization for industrial applications. *Energy Reports*, **9**(2), 111–116. <https://doi.org/https://doi.org/10.1016/j.egy.2022.12.009>.
- Raub, J. A., Mathieu-Nolf, M., Hampson, N. B., & Thom, S. R. (2000). Carbon monoxide poisoning — a public health perspective. *Toxicology*, **145**(1), 1–14. [https://doi.org/10.1016/S0300-483X\(99\)00217-6](https://doi.org/10.1016/S0300-483X(99)00217-6).
- Samet, J., Zeger, S., Dominici, F., Curriero, F., Coursac, I., Dockery, D., Schwartz, J., & Zanobetti, A. (2000). The National Morbidity, Mortality, and Air Pollution Study. Part II: Morbidity and mortality from air pollution in the United States. *Research Report (Health Effects Institute)*, **94**, 71–79.
- Santolero, J. (2003). Hazardous Waste Incineration. In *Encyclopedia of Physical Science and Technology (Third Edition)* (pp. 223–244). Academic Press. <https://doi.org/10.1016/B0-12-227410-5/00308-2>.
- Schnelle, Jr., K. B., & Brown, C. A. (2001). *Air Pollution Control Technology Handbook* (F. Kreith (ed.); 1st ed.). CRC Press. <https://doi.org/10.1201/9781420036435>.
- Schweitzer, L., & Noblet, J. (2018). Water Contamination and Pollution. In B. Török & T. Dransfield (Eds.), *Green Chemistry: An Inclusive Approach* (pp. 261–290). Elsevier. <https://doi.org/10.1016/B978-0-12-809270-5.00011-X>.
- Sen, R., Mandal, A. K., Goswami, S., & Chakraborty, B. (2023). Prediction of Particulate Matter (PM_{2.5}) Across India Using Machine Learning Methods. *Proceedings of International Conference on Data Science and Applications*, **553**, 545–556. https://doi.org/10.1007/978-981-19-6634-7_38.
- Sharma, A. K., & Balyan, P. (2020). Air pollution and COVID-19: Is the connect worth its weight? *Indian Journal of Public Health*, **64**(6), 134. https://doi.org/10.4103/IJPH.IJPH_466_20.
- Shinwari, M. W., Zhitomirsky, D., Deen, I. A., Selvaganapathy, P. R., Jamal Deen, M., & Landheer, D. (2010). Microfabricated reference electrodes and their biosensing applications. *Sensors (Basel, Switzerland)*, **10**(3), 1679–1715. <https://doi.org/10.3390/S100301679>.
- Thurston, G. D. (2008). *Outdoor Air Pollution: Sources, Atmospheric Transport, and Human Health Effects*. 700–712. <https://doi.org/10.1016/B978-012373960-5.00275-6>.

- Turner, D. B. (1994). *Workbook of atmospheric dispersion estimates: an introduction to dispersion modeling* (2nd ed.). Lewis Publishers.
- Tuvjargal, N., Enkhsetseg, L., Shagjjamba, D., & Zuzaan, P. (2019). Morphological study of PM_{2.5} by SEM-EDS in Ulaanbaatar. *IOP Conference Series: Materials Science and Engineering*, **704**(1), 23–28. <https://doi.org/10.1088/1757-899X/704/1/012012>.
- Ukaogo, P. O., Ewuzie, U., & Onwuka, C. V. (2020). Environmental pollution: causes, effects, and the remedies. In *Microorganisms for Sustainable Environment and Health* (pp. 419–429). Elsevier. <https://doi.org/10.1016/B978-0-12-819001-2.00021-8>.
- Umar, S. A., Babawuro, A. Y., Jimoh, M., Salami, E., & Raisuddin Khan, M. (2006). Control of particulate matter (pm) emissions from industrial plant using ANFIS based controller. *ARPN Journal of Engineering and Applied Sciences*, **11**(1), 404–409.
- Vaart, D. R. V. Der, Vatvuk, W. M., & Wehe, A. H. (2012). Thermal and Catalytic Incinerators for the Control of VOCs. *Journal of the Air & Waste Management Association*, **41**(1), 92–98. <https://doi.org/10.1080/10473289.1991.10466828>.
- Vakkilainen, E. K. (2017). Solid Biofuels and Combustion. In *Steam Generation from Biomass* (pp. 18–56). Butterworth-Heinemann. <https://doi.org/10.1016/B978-0-12-804389-9.00002-2>.
- Vallero, D. (2014). Fundamentals of air pollution. In *Fundamentals of Air Pollution, Fifth Edition* (fifth). Elsevier Science. <https://doi.org/10.1016/B978-0-12-401733-7.01001-X>.
- Vallero, D. A. (2019). Thermal reactions. In *Air Pollution Calculations* (pp. 207–218). Elsevier. <https://doi.org/10.1016/B978-0-12-814934-8.00009-0>.
- van Doremalen, N., Bushmaker, T., Morris, D. H., Holbrook, M. G., Gamble, A., Williamson, B. N., Tamin, A., Harcourt, J. L., Thornburg, N. J., Gerber, S. I., Lloyd-Smith, J. O., de Wit, E., & Munster, V. J. (2020). Aerosol and Surface Stability of SARS-CoV-2 as Compared with SARS-CoV-1. *New England Journal of Medicine*, **382**(16), 1564–1567. https://doi.org/10.1056/NEJMC2004973/SUPPL_FILE/NEJMC2004973_DISCLOSURES.PDF.
- Visser, A. De. (2013). AERMOD AND AERMET: A detailed description. In *Air Dispersion Modeling A foundation and Application* (pp. 491–513). John Wiley & Sons, Ltd. <https://doi.org/10.1002/9781118723098.CH14>.
- Westbrook, J. (1999). Air Dispersion Models: Tools to Assess Impacts from Pollution Sources on

- JSTOR. *Natural Resources & Environment*, **13**(4), 546–551.
- WHO. (2019). *Air pollution*. https://www.who.int/health-topics/air-pollution#tab=tab_1.
- WHO. (2021). *WHO global air quality guidelines: particulate matter (PM_{2.5} and PM₁₀), ozone, nitrogen dioxide, sulfur dioxide and carbon monoxide*.
- Yadav, I. C., & Devi, N. L. (2019). Biomass burning, regional air quality, and climate change. *Encyclopedia of Environmental Health*, 386–391. <https://doi.org/10.1016/B978-0-12-409548-9.11022-X>.
- Yang, J., Tang, T., Jiang, Y., Karavalakis, G., Durbin, T. D., Wayne Miller, J., Cocker, D. R., & Johnson, K. C. (2021). Controlling emissions from an ocean-going container vessel with a wet scrubber system. *Fuel*, **304**, 121323. <https://doi.org/10.1016/J.FUEL.2021.121323>.
- Yang, M. C., Wang, J. Z., & Sun, T. Y. (2018). EMD-Based Preprocessing with a Fuzzy Inference System and a Fuzzy Neural Network to Identify Kiln Coating Collapse for Predicting Refractory Failure in the Cement Process. *International Journal of Fuzzy Systems*, **20**(8), 2640–2656. <https://doi.org/10.1007/S40815-018-0510-7/METRICS>.
- Zade, S., & Ingole, N. W. (2015). Air Dispersion Modelling to Assess Ambient Air Quality Impact Due to Carbon Industry. *International Journal of Research Studies in Science, Engineering and Technology*, **2**(7), 53.
- Zandaryaa, S., & Buekens, A. (2009). Control of Sulphur Dioxide. *Pollution Control Technology*, *II*, 124–152.
- Zaporozhets, A. (2019). Analysis of control system of fuel combustion in boilers with oxygen sensor. *Periodica Polytechnica Mechanical Engineering*, **64**(4), 241–248. <https://doi.org/10.3311/PPME.12572>.
- Zhang, J. J., Wei, Y., & Fang, Z. (2019). Ozone pollution: A major health hazard worldwide. *Frontiers in Immunology*, **10**(OCT), 2518.

Appendix

Appendix I: Gaseous emissions – Cement Factory 1, Stack 1, Sample 1



Memory		1
Model		E6000-5SC
Serial number		1218
Client		Cement Factory 1
Client address		Stack 1

Operator		Jermaine
Altitude	ft	100
Air relative humidity	%	50
Fuel		---

Number		1	2	3
Date		5/4/2022	5/4/2022	5/4/2022
Time		0900hrs	0910hrs	0920hrs
O2	%	19.77	19.81	19.85
CO	mg/m3	0.77	1.04	0.47
CO2	%	1.1	1.4	2.6
Eff. tot	%	---	---	---
Loss tot	%	---	---	---
T gas	°C	83	127.8	125.8
T air	°C	26.1	28.9	19.4
?T	°C	111.4	101.7	102.5
Exc. air	%	231	210	221
Eff. cond	%	---	---	---
Eff. cond (LHV)	%	---	---	---
Eff. sens (LHV)	%	---	---	---
Loss sens (LHV)	%	---	---	---
Loss sens	%	---	---	---
NO	mg/m3	3.21	2.2	7.12
SO2	mg/m3	6.98	7.92	4.27
NOx	mg/m3	20.19	17.88	18.69
PI	%	0.24	0.77	5.71
Pressure	mmHg	-1.163	-1.163	-0.27
Draft	mmHg	-1.163	-1.163	-0.27
CxHy	%	0	0	0
H2S-L	mg/m3	0	0	0
H2S-L (0%)	mg/m3	0	0	0
NOx (0%)	mg/m3	20.19	17.88	18.69

Velocity		
Velocity	m/s	23.1
Gas		air
Density	kg/m3	1.09
Altitude	ft	100
T air	°C	49.8
K Pitot		1

Appendix II: Gaseous emissions – Cement Factory 2, Stack 2a, Sample 1



Memory		1
Model		E6000-5SC
Serial number		1218
Client		Cement Factory 2
Client address		Stack 2a

Operator		Jermaine
Altitude	ft	100
Air relative humidity	%	50
Fuel		---

Number		1	2	3
Date		11/4/2022	11/4/2022	11/4/2022
Time		0900hrs	0910hrs	0920hrs
O2	%	19.77	19.81	20.36
CO	mg/m3	0	0	0
CO2	%	0.01	0.02	0.03
Eff. tot	%	---	---	---
Loss tot	%	---	---	---
T gas	°C	71.3	60.32	79.1
T air	°C	27.9	23.9	25.1
?T	°C	61	52.9	62
Exc. air	%	314	398	401
Eff. cond	%	---	---	---
Eff. cond (LHV)	%	---	---	---
Eff. sens (LHV)	%	---	---	---
Loss sens (LHV)	%	---	---	---
Loss sens	%	---	---	---
NO	mg/m3	0	0	0
SO2	mg/m3	0	0	0
NOx	mg/m3	0	0	0
PI	%	4.12	5.2	3.1
Pressure	mmHg	-0.131	0.141	0.221
Draft	mmHg	-0.131	0.141	0.221
CxHy	%	0	0	0
H2S-L	mg/m3	0	0	0
H2S-L (0%)	mg/m3	0	0	0
NOx (0%)	mg/m3	0	0	0

Velocity		
Velocity	m/s	21.4
Gas		air
Density	kg/m3	0.991
Altitude	ft	100
T air	°C	56.2
K Pitot		1

Appendix III: Gaseous emissions – Cement Factory 2, Stack 2b, Sample 1



Memory		1
Model		E6000-5SC
Serial number		1218
Client		Cement Factory 2
Client address		Stack 2b

Operator		Jermaine
Altitude	ft	100
Air relative humidity	%	50
Fuel		---

Number		1	2	3
Date		12/4/2022	12/4/2022	12/4/2022
Time		1331hrs	1342hrs	1350hrs
O2	%	19.77	19.81	20.36
CO	mg/m3	0	0	0
CO2	%	0.01	0.03	0.01
Eff. tot	%	---	---	---
Loss tot	%	---	---	---
T gas	°C	70	68.4	72.1
T air	°C	30.1	27.1	23.2
?T	°C	55.7	61.9	62
Exc. air	%	543	453	651
Eff. cond	%	---	---	---
Eff. cond (LHV)	%	---	---	---
Eff. sens (LHV)	%	---	---	---
Loss sens (LHV)	%	---	---	---
Loss sens	%	---	---	---
NO	mg/m3	0	0	0
SO2	mg/m3	0	0	0
NOx	mg/m3	0	0	0
PI	%	5.41	0.43	0.71
Pressure	mmHg	-0.271	-0.271	-0.271
Draft	mmHg	-0.271	-0.271	-0.271
CxHy	%	0	0	0
H2S-L	mg/m3	0	0	0
H2S-L (0%)	mg/m3	0	0	0
NOx (0%)	mg/m3	0	0	0

Velocity		
Velocity	m/s	31.5
Gas		air
Density	kg/m3	0.981
Altitude	ft	100
T air	°C	54.1
K Pitot		1

Appendix IV: Gaseous emissions – Cement Factory 1, Stack 1, Sample 2



Memory		1
Model		E6000-5SC
Serial number		1218
Client		Cement Factory 1
Client address		Stack 1

Operator		Jermaine
Altitude	ft	100
Air relative humidity	%	50
Fuel		---

Number		1	2	3
Date		12/7/2022	12/7/2022	12/7/2022
Time		1015hrs	1027hrs	1040hrs
O2	%	19.41	19.56	19.53
CO	mg/m3	0.91	0.52	1.0
CO2	%	1.9	2	0.9
Eff. tot	%	---	---	---
Loss tot	%	---	---	---
T gas	°C	83	127.8	125.8
T air	°C	26.1	28.9	19.4
?T	°C	111.4	101.7	102.5
Exc. air	%	231	210	221
Eff. cond	%	---	---	---
Eff. cond (LHV)	%	---	---	---
Eff. sens (LHV)	%	---	---	---
Loss sens (LHV)	%	---	---	---
Loss sens	%	---	---	---
NO	mg/m3	2.91	2.88	2.94
SO2	mg/m3	7.11	2.98	6.44
NOx	mg/m3	15.21	19.73	21.19
PI	%	0.24	0.77	5.71
Pressure	mmHg	1.009	1.009	1.821
Draft	mmHg	1.009	1.009	1.821
CxHy	%	0	0	0
H2S-L	mg/m3	0	0	0
H2S-L (0%)	mg/m3	0	0	0
NOx (0%)	mg/m3	15.21	19.73	21.19

Velocity		
Velocity	m/s	19.81
Gas		air
Density	kg/m3	1.11
Altitude	ft	100
T air	°C	51
K Pitot		1

Appendix V: Gaseous emissions – Cement Factory 2, Stack 2a, Sample 2



Memory		2
Model		E6000-5SC
Serial number		1218
Client		Cement Factory 2
Client address		Stack 2a

Operator		Jermaine
Altitude	ft	100
Air relative humidity	%	50
Fuel		---

Number		1	2	3
Date		21/7/2022	21/7/2022	21/7/2022
Time		0915hrs	0924hrs	0941hrs
O2	%	19.41	19.56	20.64
CO	mg/m3	0	0	0
CO2	%	0.01	0.01	0.01
Eff. tot	%	---	---	---
Loss tot	%	---	---	---
T gas	°C	84.91	87.32	71.61
T air	°C	26.99	26.15	26.49
?T	°C	43	41	46
Exc. air	%	287	294	264
Eff. cond	%	---	---	---
Eff. cond (LHV)	%	---	---	---
Eff. sens (LHV)	%	---	---	---
Loss sens (LHV)	%	---	---	---
Loss sens	%	---	---	---
NO	mg/m3	0	0	0
SO2	mg/m3	0	0	0
NOx	mg/m3	0	0	0
PI	%	2.91	2.68	2.49
Pressure	mmHg	-1.912	-1.085	0.021
Draft	mmHg	-1.912	-1.085	0.021
CxHy	%	0	0	0
H2S-L	mg/m3	0	0	0
H2S-L (0%)	mg/m3	0	0	0
NOx (0%)	mg/m3	0	0	0

Velocity		
Velocity	m/s	15.93
Gas		air
Density	kg/m3	1.12
Altitude	ft	100
T air	°C	57
K Pitot		1

Appendix VI: Gaseous emissions – Cement Factory 2, Stack 2b, Sample 2



Memory		2
Model		E6000-5SC
Serial number		1218
Client		Cement Factory 2
Client address		Stack 2b

Operator		Jermaine
Altitude	ft	100
Air relative humidity	%	50
Fuel		---

Number		1	2	3
Date		22/7/2022	22/7/2022	22/7/2022
Time		0835hrs	0846hrs	0859hrs
O2	%	19.41	19.56	20.64
CO	mg/m3	0	0	0
CO2	%	0.01	0.01	0.01
Eff. tot	%	---	---	---
Loss tot	%	---	---	---
T gas	°C	70	71.6	68.4
T air	°C	29.9	24.1	21.7
?T	°C	40.9	40.9	41.6
Exc. air	%	335	329	371
Eff. cond	%	---	---	---
Eff. cond (LHV)	%	---	---	---
Eff. sens (LHV)	%	---	---	---
Loss sens (LHV)	%	---	---	---
Loss sens	%	---	---	---
NO	mg/m3	0	0	0
SO2	mg/m3	0	0	0
NOx	mg/m3	0	0	0
PI	%	3.59	3.33	3.91
Pressure	mmHg	0.063	0.063	0.063
Draft	mmHg	0.063	0.063	0.063
CxHy	%	0	0	0
H2S-L	mg/m3	0	0	0
H2S-L (0%)	mg/m3	0	0	0
NOx (0%)	mg/m3	0	0	0

Velocity		
Velocity	m/s	30.92
Gas		air
Density	kg/m3	0.995
Altitude	ft	100
T air	°C	42.7
K Pitot		1

Appendix VII: Gaseous emissions – Cement Factory 1, Stack 1, Sample 3



Memory		1
Model		E6000-5SC
Serial number		1218
Client		Cement Factory 1
Client address		Stack 1

Operator		Jermaine
Altitude	ft	100
Air relative humidity	%	50
Fuel		---

Number		1	2	3
Date		20/9/2022	20/9/2022	20/9/2022
Time		1217hrs	1229hrs	1240hrs
O2	%	19.01	19.24	19.65
CO	mg/m3	0.81	0.41	0.64
CO2	%	1.6	1.7	1.2
Eff. tot	%	---	---	---
Loss tot	%	---	---	---
T gas	°C	113.2	119.3	112.4
T air	°C	22.9	29.4	27.1
?T	°C	115.2	192.1	104.2
Exc. air	%	441	412	391
Eff. cond	%	---	---	---
Eff. cond (LHV)	%	---	---	---
Eff. sens (LHV)	%	---	---	---
Loss sens (LHV)	%	---	---	---
Loss sens	%	---	---	---
NO	mg/m3	4.11	4.19	2.05
SO2	mg/m3	4.41	4.13	3.82
NOx	mg/m3	25.91	19.23	21.22
PI	%	0.24	0.77	5.71
Pressure	mmHg	-1.103	-1.163	-0.131
Draft	mmHg	-1.103	-1.163	-0.131
CxHy	%	0	0	0
H2S-L	mg/m3	0	0	0
H2S-L (0%)	mg/m3	0	0	0
NOx (0%)	mg/m3	25.91	19.23	21.22

Velocity		
Velocity	m/s	22.1
Gas		air
Density	kg/m3	1.1
Altitude	ft	100
T air	°C	44.78
K Pitot		1

Appendix VIII: Gaseous emissions – Cement Factory 2, Stack 2a, Sample 3



Memory		3
Model		E6000-5SC
Serial number		1218
Client		Cement Factory 2
Client address		Stack 2a

Operator		Jermaine
Altitude	ft	100
Air relative humidity	%	50
Fuel		---

Number		1	2	3
Date		6/9/2022	6/9/2022	6/9/2022
Time		1210hrs	1224hrs	1336hrs
O2	%	19.01	19.24	18.48
CO	mg/m3	0	0	0
CO2	%	0.01	0.01	0.01
Eff. tot	%	---	---	---
Loss tot	%	---	---	---
T gas	°C	81.54	79.99	74.76
T air	°C	23.58	24.33	24.19
?T	°C	54	57	61
Exc. air	%	305	281	396
Eff. cond	%	---	---	---
Eff. cond (LHV)	%	---	---	---
Eff. sens (LHV)	%	---	---	---
Loss sens (LHV)	%	---	---	---
Loss sens	%	---	---	---
NO	mg/m3	0	0	0
SO2	mg/m3	0	0	0
NOx	mg/m3	0	0	0
PI	%	2.94	2.89	2.88
Pressure	mmHg	0.034	0.026	0.185
Draft	mmHg	0.034	0.026	0.185
CxHy	%	0	0	0
H2S-L	mg/m3	0	0	0
H2S-L (0%)	mg/m3	0	0	0
NOx (0%)	mg/m3	0	0	0

Velocity		
Velocity	m/s	19.84
Gas		air
Density	kg/m3	0.97
Altitude	ft	100
T air	°C	54
K Pitot		1

Appendix IX: Gaseous emissions – Cement Factory 2, Stack 2b, Sample 3



Memory		3
Model		E6000-5SC
Serial number		1218
Client		Cement Factory 2
Client address		Stack 2b

Operator		Jermaine
Altitude	ft	100
Air relative humidity	%	50
Fuel		---

Number		1	2	3
Date		7/9/2020	7/9/2020	7/9/2020
Time		0852hrs	0905hrs	0914hrs
O2	%	19.01	19.24	18.48
CO	mg/m3	0	0	0
CO2	%	0.01	0.01	0.01
Eff. tot	%	---	---	---
Loss tot	%	---	---	---
T gas	°C	65	67.4	72.1
T air	°C	30.1	34.1	23.2
?T	°C	62	63.9	62
Exc. air	%	375	358	336
Eff. cond	%	---	---	---
Eff. cond (LHV)	%	---	---	---
Eff. sens (LHV)	%	---	---	---
Loss sens (LHV)	%	---	---	---
Loss sens	%	---	---	---
NO	mg/m3	0	0	0
SO2	mg/m3	0	0	0
NOx	mg/m3	0	0	0
PI	%	4.71	4.44	4.03
Pressure	mmHg	0.087	0.081	0.098
Draft	mmHg	0.087	0.081	0.098
CxHy	%	0	0	0
H2S-L	mg/m3	0	0	0
H2S-L (0%)	mg/m3	0	0	0
NOx (0%)	mg/m3	0	0	0

Velocity		
Velocity	m/s	23.7
Gas		air
Density	kg/m3	1.138
Altitude	ft	100
T air	°C	59.4
K Pitot		1

Appendix X: Cement Factory 1 – Stack 1 average data

	Apr-22				Jul-22				Sep-22			
	Run 1	Run 2	Sun 3	Sample 1 (Avg)	Run 1	Run 2	Sun 3	Sample 1 (Avg)	Run 1	Run 2	Sun 3	Sample 1 (Avg)
Plant ID	CF1				CF1				CF1			
Stack ID	Stack 1				Stack 1				Stack 1			
Sampling Date	5-Apr-22				12-Jul-22				20-Sep-22			
Stack Height	35				35				35			
Stack Diameter	1.8				1.8				1.8			
Nozzle Diameter	10				10				10			
Traverses	12				12				12			
Start Time	0800hrs	1115hrs	1400hrs		0833hrs	1105hrs	1400hrs		0813hrs	1230hrs	1505hrs	
End Time	0900hrs	1215hrs	1500hrs		0935hrs	1205hrs	1500hrs		0913hrs	1330hrs	1605hrs	
Ambient Temp	18.4	18.9	24.5	20.6	18.5	24.1	21.6	21.4	15.8	17.1	19.9	17.6
Bar. Press. (mm Hg)	764.3	764.3	764.3	764.3	760.6	760.6	760.6	760.6	764.3	764.3	764.3	764.3
Sampling Time	60	60	60	60	60	60	60	60	60	60	60	60
P _g (mm H ₂ O)	0.109	0.142	0.118	0.123	0.333	0.281	0.349	0.321	0.291	0.222	0.441	0.318
T _{s (avg)} (°C)	61.98	58.31	58.68	59.66	61.94	64.41	63.80	63.38	65.94	56.06	62.03	61.34
ΔP (mm Hg)	1.23	1.23	1.30	1.250	1.26	1.27	1.30	1.278	1.37	1.30	1.32	1.328
√ΔP (mm Hg)	1.11	1.11	1.11	1.108	1.12	1.13	1.13	1.128	1.17	1.14	1.15	1.151
ΔH (mm H ₂ O)	27.91	24.42	29.17	27.17	29.14	31.56	25.80	28.83	31.38	27.73	25.65	28.25
Gas Volume (m ³)	0.965	0.994	0.942	0.967	0.842	0.931	1.161	0.978	0.993	1.058	1.033	1.028
T _{m (avg)} (°C)	33.65	37.21	30.27	33.71	37.26	35.04	32.80	35.03	33.66	38.02	33.11	34.93
Exit Temp. (°C)	11.28	13.59	11.88	12.25	12.39	11.36	12.75	12.17	15.82	16.13	17.79	16.58
Filter Temp. (°C)	123.2	122.7	123.8	123.3	126.9	123.9	124.3	125.0	121.0	122.1	122.7	121.9
Liquid collected (g)	33.9	35.0	36.1	35.0	22.9	15.0	25.1	21.0	19.2	19.8	21.9	20.3
PM Mass (g)	0.0050	0.0048	0.0055	0.0051	0.0061	0.0055	0.0061	0.0059	0.0049	0.0048	0.0043	0.0047
Oxygen (%)	19.77	19.81	19.85	19.81	19.41	19.56	19.53	19.50	19.01	19.24	19.65	19.30
Carbon monoxide (mg/m ³)	0.77	1.04	0.47	0.76	0.91	0.52	1	0.81	0.81	0.41	0.64	0.62
Carbon dioxide (%)	1.1	1.4	2.6	1.7	1.9	2	0.9	1.6	1.6	1.7	1.2	1.5
Nitrogen oxides (mg/m ³)	20.19	17.88	18.69	18.92	15.21	19.73	21.19	18.71	25.91	19.23	21.22	22.12
Sulphur dioxide (mg/m ³)	6.98	7.92	4.27	6.39	7.11	2.98	6.44	5.51	4.41	4.13	3.82	4.12

Appendix XI: Cement Factory 2 – Stack 2a average data

	Apr-22				Jul-22				Sep-22			
	Run 1	Run 2	Sun 3	Sample 1 (Avg)	Run 1	Run 2	Sun 3	Sample 1 (Avg)	Run 1	Run 2	Sun 3	Sample 1 (Avg)
Plant ID	CF2				CF2				CF2			
Stack ID	Stack 2a				Stack 2a				Stack 2a			
Sampling Date	11-Apr-22				21-Jul-22				6-Sep-22			
Stack Height (m)	39				39				39			
Stack Diameter (m)	1.5				1.5				1.5			
Nozzle Diameter (mm)	8				8				8			
Traverses	12				12				12			
Start Time	0815hrs	1117hrs	1400hrs		0831hrs	1141hrs	1400hrs		0800hrs	1115hrs	1425hrs	
End Time	0915hrs	1217hrs	1500hrs		0931hrs	1241hrs	1500hrs		0900hrs	1215hrs	1525hrs	
Ambient Temp	17.4	24.0	27.6	23.0	15.0	18.4	17.6	17.0	19.0	22.1	21.9	21.0
Bar. Press. (mm Hg)	680.5	680.5	680.5	680.5	680.5	680.5	680.5	680.5	680.5	680.5	680.5	680.5
Sampling Time	60	60	60	60	60	60	60	60	60	60	60	60
P _g , (mm H ₂ O)	0.133	0.121	0.124	0.126	0.102	0.067	0.113	0.094	0.125	0.113	0.143	0.127
T _{s (avg)} (°C)	64.03	64.51	65.36	64.63	62.41	65.79	64.25	64.15	75.96	74.47	63.40	71.28
ΔP (mm Hg)	2.700	2.225	3.595	2.840	4.102	1.906	2.413	2.807	2.793	2.920	2.665	2.793
√ΔP (mm Hg)	1.685	1.686	1.681	1.684	1.672	1.676	1.676	1.675	1.672	1.914	1.427	1.671
ΔH (mm H ₂ O)	25.11	25.92	28.22	26.42	26.86	28.24	29.66	28.25	30.38	25.66	26.71	27.58
Gas Volume (m ³)	0.915	0.994	1.161	1.023	1.011	0.970	0.932	0.971	1.014	1.095	0.858	0.989
T _{m (avg)} (°C)	36.91	40.05	28.56	35.175	38.62	36.87	34.99	36.825	37.20	39.30	35.20	37.233
Exit Temp. (°C)	14.09	13.20	20.09	15.792	12.49	11.59	15.93	13.333	12.47	15.17	14.11	13.917
Filter Temp. (°C)	120.7	117.9	135.1	124.5	122.0	123.3	122.3	122.5	129.0	126.9	127.6	127.8
Liquid collected (g)	30.80	32.99	31.91	31.90	33.91	33.95	33.96	33.94	32.80	32.78	32.79	32.79
PM Mass (g)	0.0051	0.0048	0.0024	0.0041	0.0053	0.0054	0.0055	0.0054	0.0050	0.0052	0.0042	0.0048
Oxygen (%)	19.77	19.81	20.36	19.98	19.41	19.56	20.64	19.87	19.01	19.24	18.48	18.91
Carbon monoxide (mg/m ³)	0	0	0	0	0	0	0	0	0	0	0	0
Carbon dioxide (%)	0.01	0.02	0.03	0.02	0.01	0.01	0.01	0.01	0.01	0.01	0.01	0.01
Nitrogen oxides (mg/m ³)	0	0	0	0	0	0	0	0	0	0	0	0
Sulphur dioxide (mg/m ³)	0	0	0	0	0	0	0	0	0	0	0	0

Appendix XII: Cement Factory 2 – Stack 2b average data

	Apr-22				Jul-22				Sep-22			
	Run 1	Run 2	Sun 3	Sample 1 (Avg)	Run 1	Run 2	Sun 3	Sample 1 (Avg)	Run 1	Run 2	Sun 3	Sample 1 (Avg)
Plant ID	CF2				CF2				CF2			
Stack ID	Stack 2b				Stack 2b				Stack 2b			
Sampling Date	12-Apr-22				22-Jul-22				7-Sep-22			
Stack Height (m)	45				45				45			
Stack Diameter (m)	1.5				1.5				1.5			
Nozzle Diameter (mm)	8				8				8			
Traverses	12				12				12			
Start Time	0800hrs	1117hrs	1355hrs		0820hrs	1135hrs	1400hrs		0800hrs	1115hrs	1425hrs	
End Time	0900hrs	1217hrs	1455hrs		0920hrs	1235hrs	1500hrs		0900hrs	1215hrs	1525hrs	
Ambient Temp	17.4	22.0	20.6	20.0	15.0	19.2	22.8	19.0	19.7	20.5	18.3	19.5
Bar. Press. (mm Hg)	680.5	680.5	680.5	680.5	680.5	680.5	680.5	680.5	680.5	680.5	680.5	680.5
Sampling Time	60	60	60	60	60	60	60	60	60	60	60	60
P _g (mm H ₂ O)	-0.12	-0.12	-0.12	-0.120	-0.12	-0.12	-0.12	0.094	-0.12	-0.12	-0.12	0.127
T _{s (avg)} (°C)	69.26	71.95	67.17	69.458	61.90	63.38	76.77	67.350	71.23	68.94	68.21	69.458
ΔP (mm Hg)	4.44	4.77	1.89	3.703	2.71	4.61	2.99	3.436	4.92	2.27	1.13	2.773
√ΔP (mm Hg)	1.92	1.92	1.93	1.923	1.84	1.85	1.86	1.852	1.67	1.68	1.64	1.665
ΔH (mm H ₂ O)	28.38	28.20	30.18	28.917	30.22	29.69	21.34	27.083	35.09	31.52	34.14	33.583
Gas Volume (m ³)	1.260	1.142	1.132	1.178	1.327	1.007	1.242	1.192	0.846	1.040	1.240	1.042
T _{m (avg)} (°C)	41.10	39.29	31.76	37.38	39.20	37.64	35.68	37.51	38.69	36.38	39.00	38.03
Exit Temp. (°C)	16.44	13.44	13.64	14.51	12.83	11.67	16.00	13.50	14.43	12.16	12.92	13.17
Filter Temp. (°C)	124.3	126.5	125.1	125.3	132.8	133.7	132.8	133.1	135.6	135.6	138.8	136.7
Liquid collected (g)	33.31	33.30	33.28	33.30	31.90	31.93	31.98	31.94	40.60	40.62	40.63	40.62
M ₂ -M ₁ (g)	0.0068	0.0064	0.0078	0.0070	0.0065	0.0066	0.0064	0.0065	0.0069	0.0070	0.0064	0.0068
Oxygen (%)	19.77	19.81	20.36	19.98	19.41	19.56	20.64	19.87	19.01	19.24	18.48	18.91
Carbon monoxide (mg/m ³)	0	0	0	0	0	0	0	0	0	0	0	0
Carbon dioxide (%)	0.01	0.03	0.01	0.02	0.01	0.01	0.01	0.01	0.01	0.01	0.01	0.01
Nitrogen oxides (mg/m ³)	0	0	0	0	0	0	0	0	0	0	0	0
Sulphur dioxide (mg/m ³)	0	0	0	0	0	0	0	0	0	0	0	0

Appendix XIII: Particulate matter run summaries – Cement Factory 1 Stack 1

Cement Factory 1 Stack 1				
Calculations	Sample 1	Sample 2	Sample 3	Average
US EPA Method	5	5	5	
Stack ID	Stack 1	Stack 1	Stack 1	
Sampling date	5/24/2022	5/25/2022	5/26/2022	
Sampling time	1100hrs	1130hrs	1115hrs	
Set up data				
Barometric pressure (mmHg)	764.3	764.3	764.3	
Calibrated nozzle diameter (mm)	10	10	10	
Probe heat setting (°C)	123.25	125	121.917	
Leak rate (m ³ /min)	≤0.002	≤0.002	≤0.002	
Static pressure (mmH ₂ O)	0.123	0.321	0.318	
Absolute Stack pressure (mmHg)	764.31	764.32	764.32	
Test Results				
Total sampling time	60	60	60	60
Stack temperature (°C)	59.658	63.383	61.342	61.461
Average velocity head, ΔP (mmH ₂ O)	1.233	1.275	1.342	1.283
Average vΔP	1.108	1.128	1.151	1.129
Average orifice pressure, ΔH (mmH ₂ O)	27.167	28.83	28.25	28.082
Total volume sampled (m ³)	0.967	0.978	1.028	0.991
Dry gas meter (DGM) temperature (°C)	33.708	35.033	34.933	34.558
Exit Temperature (°C)	12.25	12.167	16.583	13.667
Area of nozzle, (mm ²)	0.785	0.785	0.785	0.785
Molecular weight, dry basis (g/gmol)	29.064	28.988	29.012	29.021
Molecular weight, wet basis (g/gmol)	28.533	28.667	28.716	28.639
Moisture content, B _{ws}	0.048	0.029	0.027	0.035
Calculated results				
Volume of gas corrected, V _{std} (dsm ³)	0.9264	0.9329	0.9809	0.9468
Calculated Stack Velocity (m/s)	3.972	4.057	4.123	4.051
Volumetric flow rate, actual Q _a (m ³ /min)	606.442	619.374	629.550	618.455
Volumetric flow rate, standard Q _s (sm ³ /min)	500.515	505.537	516.979	507.677
Volumetric flow rate, dry standard Q _{std} (dsm ³ /min)	476.482	490.788	503.081	490.117
Particulate matter concentration (g)	0.005	0.006	0.005	0.005
Dry Standard Particulate Conc. C _d , (mg/Nm ³)	5.613	6.324	4.791	5.576
Normal Wet particulate Concentration, C _w , (mg/Nm ³)	5.344	6.140	4.663	5.382
Dry Standard PM ₁₀ Conc. C _d , (mg/Nm ³)	4.771	5.376	4.073	4.740
Dry Standard PM _{2.5} Conc. C _d , (mg/Nm ³)	2.526	2.846	2.156	2.509
Particulate Emission Rate, E (g/s)	0.057	6.324	0.065	2.149
Percentage isokinetic %I	97.755	95.574	98.036	97.122
Normal (N) = Normal conditions of pressure (760mmHg and temperature (0°C or 273 K) without any moisture				

Appendix XIV: Particulate matter run summaries – Cement Factory 2 Stack 2a

Cement Factory 2 Stack 2a				
Calculations	Sample 1	Sample 2	Sample 3	Average
US EPA Method	5	5	5	
Stack ID	Stack 2a	Stack 2a	Stack 2a	
Sampling date	6/6/2022	6/7/2022	6/8/2022	
Sampling time	1400hrs	1200hrs	1312hrs	
Set up data				
Barometric pressure (mmHg)	680.5	680.5	680.5	
Calibrated nozzle diameter (mm)	8	8	8	
Probe heat setting (°C)	124.542	122.508	127.83	
Leak rate (m ³ /min)	≤0.002	≤0.003	≤0.004	
Static pressure (mmH ₂ O)	0.126	0.094	0.127	
Absolute Stack pressure (mmHg)	680.51	680.51	680.51	
Test Results				
Total sampling time	60	60	60	60
Stack temperature (°C)	64.633	64.15	71.275	66.686
Average velocity head, ΔP (mmH ₂ O)	2.84	2.807	2.7925	2.813
Average vΔP	1.684	1.675	1.6709	1.677
Average orifice pressure, ΔH (mmH ₂ O)	26.417	28.25	27.583	27.417
Total volume sampled (m ³)	1.023	0.971	0.989	0.994
Dry gas meter (DGM) temperature (°C)	35.175	36.825	37.233	36.411
Exit Temperature (°C)	15.792	13.333	13.917	14.347
Area of nozzle, (mm ²)	0.503	0.503	0.503	0.503
Molecular weight, dry basis (g/gmol)	28.802	28.796	28.758	28.786
Molecular weight, wet basis (g/gmol)	28.297	28.231	28.222	28.250
Moisture content, B _{ws}	0.047	0.052	0.050	0.050
Calculated results				
Volume of gas corrected, V _{std} (dsm ³)	0.8685	0.8199	0.8340	0.8408
Calculated Stack Velocity (m/s)	6.472	6.441	6.493	6.469
Volumetric flow rate, actual Q _a (m ³ /min)	686.232	682.879	688.483	685.865
Volumetric flow rate, standard Q _s (sm ³ /min)	496.840	495.119	488.853	493.604
Volumetric flow rate, dry standard Q _{std} (dsm ³ /min)	473.616	469.191	464.475	469.094
Particulate matter concentration (g)	0.004	0.005	0.005	0.005
Dry Standard Particulate Conc. C _d , (mg/Nm ³)	4.721	6.586	5.755	5.687
Normal Wet particulate Concentration, C _w , (mg/Nm ³)	4.500	6.241	5.468	5.403
Dry Standard PM ₁₀ Conc. C _d , (mg/Nm ³)	4.013	5.598	4.892	4.834
Dry Standard PM _{2.5} Conc. C _d , (mg/Nm ³)	2.124	2.964	2.590	2.559
Particulate Emission Rate, E (g/s)	0.054	6.586	0.075	2.238
Percentage isokinetic %I	100.038	95.340	97.964	97.780
Normal (N) = Normal conditions of pressure (760mmHg and temperature (0°C or 273 K) without any moisture				

Appendix XV: Particulate matter run summaries – Cement Factory 2 Stack 2b

Cement Factory 2 Stack 2b				
Calculations	Sample 1	Sample 2	Sample 3	Average
US EPA Method	5	5	5	
Stack ID	Stack 2b	Stack 2b	Stack 2b	
Sampling Date	6/14/2022	6/15/2022	6/16/2022	
Sampling time	0900hrs	0900hrs	1100hrs	
Set up data				
Barometric pressure (mmHg)	680.5	680.5	680.5	
Calibrated nozzle diameter (mm)	8	8	8	
Probe heat setting (°C)	125.342	133.083	136.67	
Leak rate (m ³ /min)	≤0.002	≤0.002	≤0.002	
Static pressure (mmH ₂ O)	-0.12	-0.12	-0.12	
Absolute Stack pressure (mmHg)	680.49	680.49	680.49	
Test Results				
Total sampling time	60	60	60	60
Stack temperature (°C)	68.075	67.35	69.4584	68.294
Average velocity head, ΔP (mmH ₂ O)	3.7025	3.4358	2.773	3.304
Average vΔP	1.9232	1.8524	1.6649	1.814
Average orifice pressure, ΔH (mmH ₂ O)	28.917	27.0833	33.583	29.861
Total volume sampled (m ³)	1.178	1.192	1.042	1.137
Dry gas meter (DGM) temperature (°C)	37.383	37.508	38.025	37.639
Exit Temperature (°C)	14.508	13.5	13.167	13.725
Area of nozzle, (mm ²)	0.503	0.503	0.503	0.503
Molecular weight, dry basis (g/gmol)	28.802	28.796	28.758	28.786
Molecular weight, wet basis (g/gmol)	28.339	28.357	28.131	28.276
Moisture content, B _{ws}	0.043	0.041	0.058	0.047
Calculated results				
Volume of gas corrected, V _{std} (dsm ³)	0.9930	1.0043	0.8765	0.9579
Calculated Stack Velocity (m/s)	7.424	7.141	6.463	7.009
Volumetric flow rate, actual Q _a (m ³ /min)	787.117	757.104	685.305	743.176
Volumetric flow rate, standard Q _s (sm ³ /min)	564.116	543.762	489.165	532.348
Volumetric flow rate, dry standard Q _{std} (dsm ³ /min)	539.942	521.616	460.665	507.408
Particulate matter concentration (g)	0.007	0.007	0.007	0.007
Dry Standard Particulate Conc. C _d , (mg/Nm ³)	7.050	6.472	7.758	7.093
Normal Wet particulate Concentration, C _w , (mg/Nm ³)	6.748	6.208	7.306	6.754
Dry Standard PM ₁₀ Conc. C _d , (mg/Nm ³)	5.992	5.501	6.594	6.029
Dry Standard PM _{2.5} Conc. C _d , (mg/Nm ³)	3.172	2.912	3.491	3.192
Particulate Emission Rate, E (g/s)	0.092	6.472	0.082	2.215
Percentage isokinetic %I	100.328	105.043	103.807	103.060
Normal (N) = Normal conditions of pressure (760mmHg and temperature (0°C or 273 K) without any moisture				

Appendix XVI: Particulate matter calculation equations

ISOKINETIC SAMPLING EQUATIONS			
Absolute Pressure of stack gas, P_s		Molecular weight of wet gas, M_s	
Barometric Pressure, P _{bar}	mm Hg	$M_s = M_d(1 - B_{ws}) + 18(B_{ws})$	g/g.mol
Stack Static Pressure, P _g	mm H ₂ O		
mmHg to mmH ₂ O conversion factor	13.6	Stack gas velocity, V_s	
$P_s = P_{bar} + \frac{P_g}{13.6}$	mm Hg	Pitot tube velocity constant, K _p	
		Average coefficient, C _p	
		√ΔP	
Gas moisture volume, V_{wc(std)}		Average stack temperature, T _{s(avg)}	°C
Mass of moisture collected, m _w	g	$v_s = K_p C_p (\sqrt{\Delta P})_{avg} \sqrt{\frac{T_{s(avg)}}{P_s M_s}}$	m/s
$V_{wc(std)} = K_2(M_w)$	m ³		
		Actual flow of stack gas, Q_a	
Dry gas volume, V_{m(std)}		Area of stack, A _s	m ²
Gas meter volume reading, ΔV	m ³	$Q_a = 60 v_s A_s$	m ³ /min
Gas meter correction factor, Y			
Dry Gas Meter (DGM) Temperature, T _{m(avg)}	°C	Standard flow rate, Q_s	
Meter pressure differential across orifice meter, ΔP	mm H ₂ O	Conversion factor (K/mm.Hg), K _s	
$V_{m(std)} = K_2 Y \Delta V_m \left(\frac{P_{bar} + \frac{\Delta H}{13.6}}{T_m} \right)$	m ³	$Q_s = K_s v_s A_s \frac{P_s}{T_s}$	m ³ /min
Total volume collected, V _{m(stw)}	m ³		
$V_{matw} = V_{wc(std)} + V_{m(std)}$	m ³	Dry standard total flow of stack gas, Q_{std}	
		$Q_{std} = K_s (1 - B_{ws}) v_s A_s \frac{P_s}{T_s}$	m ³ /min
Gas volume metered at O₂ ref. cond. V_{mstd@O₂ref}		Percentage Isokinetic, I%	
O ₂ reference condition		Nozzle diameter, D _n	m
O ₂ reference factor $O_{2\ ref} = \frac{21 - O_{2\ reference}}{21 - O_{2\ measured}}$		Nozzle area, A _n	m ²
$V_{m(std)@O_{2ref}} = V_{m(std)} O_{2\ ref}$	m ³	Total sampling time	mins
		$\%I = \frac{K_4 T_s V_{mstd}}{P_s v_s A_n \theta (1 - B_{ws})}$	%
Molecular weight of dry gas, M_d		Particulate concentration	
O ₂	%	$C_{dry} = \frac{M_p}{V_{m(std)}} \times 1000$	
CO ₂	%	$C_{wet} = \frac{M_p}{V_{wc(std)} + V_{m(std)}} \times 1000$	
CO	%	$C_{corrected} = (C_{dry}) \cdot (O_{2\ ref})$	
N ₂ % (N ₂ = 100 - (%O ₂ + %CO ₂ + %CO))	%		
$M_d = 0.32(\%O_2) + 0.44(\%CO_2) + 0.28(\%CO + \%N_2)$	g/g.mol	Emission rate	
Moisture content, B_{ws}		$E = \frac{Q_a \times C_{dry}}{10^3}$	g/s
$B_{ws} = \frac{V_{wc(std)}}{V_{wc(std)} + V_{m(std)}}$	%		

Appendix XVII: Statistical analysis (P-test)

STACK													
Null hypothesis: No significance difference between the value													
STACK EMISSION CONCENTRATION													
		TSP			PM10			PM2.5			CO2		
		Stack 1	Stack 2a	Stack 2b	Stack 1	Stack 2a	Stack 2b	Stack 1	Stack 2a	Stack 2b	Stack 1	Stack 2a	Stack 2b
		5.613	4.721	7.05	4.771	4.013	5.992	2.526	2.124	3.172	27404.3	317.65	314.45
		6.324	6.586	6.472	5.376	5.598	5.501	2.846	2.964	2.912	20724.1	159.05	157.56
		4.791	5.755	7.758	4.073	4.892	6.594	2.156	2.59	3.491	24058.5	155.76	156.59
P value	S1 and S2a	0.881	No significant difference		0.882	No significant difference		0.882	No significant difference		0.006	Significant difference	
	S2 and S2b	0.107	No significant difference		0.107	No significant difference		0.107	No significant difference		0.987	No significant difference	
	S1 and S2b	0.060	No significant difference		0.060	No significant difference		0.061	No significant difference		0.006	Significant difference	
		Annual TSP			Annual PM10			Annual PM2.5			8-hour CO2		
		CF1	CF2		CF1	CF2		CF1	CF2		CF1	CF2	
		0.203	4.616		0.173	3.926		0.091	2.079		10.619	0.571	
		0.232	6.319		0.198	5.371		0.105	2.843		7.811	0.59	
		0.178	5.618		0.151	4.776		0.0801	2.528		7.998	0.579	
P value	CF1 and CF2	0.008	Significant difference		0.008	Significant difference		0.008	Significant difference		0.012	Significant difference	
		24-hour TSP			24-hour PM10			24-hour PM2.5			1-hour CO2		
		CF1	CF2		CF1	CF2		CF1	CF2		CF1	CF2	
		1.009	8.66		0.857	7.36		0.454	3.9		36.907	4.727	
		1.09	11.82		0.927	10.05		0.491	5.32		28.201	2.367	
		0.825	10.55		0.701	8.97		0.371	4.75		33.038	2.334	
P value	CF1 and CF2	0.009	Significant difference		0.009	Significant difference		0.009	Significant difference		0.004	Significant difference	

Appendix XVIII: Discrete receptor sample run (Annual and 24-hour concentrations)

		ANNUAL CONCENTRATION						24-HOUR CONCENTRATION					
		Cement Factory 1			Cement Factory 2			Cement Factory 1			Cement Factory 2		
		Run 1	Run 2	Run 3	Run 1	Run 2	Run 3	Run 1	Run 2	Run 3	Run 1	Run 2	Run 3
PM (TSP) µg/m ³	A	0.0066	0.0075	0.0055	0.0055	0.0061	0.0060	0.0724	0.0791	0.0607	0.3277	0.4089	0.3827
	B	0.0046	0.0053	0.0038	0.0301	0.0333	0.0332	0.0561	0.0641	0.0490	0.8222	1.0116	0.9616
	C	0.0013	0.0015	0.0011	0.0028	0.0032	0.0031	0.0949	0.1074	0.0816	0.2582	0.3164	0.2979
	D	0.0169	0.0193	0.0147	0.0199	0.0210	0.0210	0.3833	0.4366	0.3334	0.4346	0.4704	0.4656
	E	0.0025	0.0028	0.0021	0.0066	0.0076	0.0074	0.0673	0.0770	0.0580	0.2493	0.3122	0.2917
	F	0.0028	0.0032	0.0024	0.0042	0.0048	0.0047	0.1136	0.1301	0.0989	0.1998	0.2506	0.2335
	G	0.0013	0.0015	0.0011	0.0087	0.0100	0.0097	0.0262	0.0301	0.0231	0.2700	0.3355	0.3124
	H	0.0034	0.0039	0.0029	0.0051	0.0058	0.0057	0.1157	0.1324	0.1015	0.2508	0.3177	0.2948
PM ₁₀ µg/m ³	A	0.0056	0.0064	0.0046	0.0047	0.0052	0.0051	0.0616	0.0673	0.0516	0.2785	0.3475	0.3253
	B	0.0039	0.0045	0.0032	0.0256	0.0283	0.0282	0.0477	0.0545	0.0416	0.6989	0.8599	0.8174
	C	0.0011	0.0013	0.0010	0.0023	0.0027	0.0026	0.0806	0.0913	0.0694	0.2195	0.2690	0.2532
	D	0.0144	0.0164	0.0125	0.0170	0.0178	0.0178	0.3258	0.3711	0.2834	0.3695	0.3999	0.3958
	E	0.0021	0.0024	0.0017	0.0056	0.0065	0.0063	0.0572	0.0655	0.0493	0.2119	0.2654	0.2480
	F	0.0024	0.0027	0.0020	0.0036	0.0041	0.0040	0.0966	0.1106	0.0841	0.1699	0.2130	0.1985
	G	0.0011	0.0013	0.0010	0.0074	0.0085	0.0082	0.0223	0.0256	0.0196	0.2295	0.2852	0.2655
	H	0.0029	0.0033	0.0025	0.0043	0.0050	0.0048	0.0983	0.1125	0.0863	0.2132	0.2700	0.2506
PM _{2.5} µg/m ³	A	0.0030	0.0034	0.0025	0.0025	0.0027	0.0027	0.0326	0.0356	0.0273	0.1475	0.1840	0.1722
	B	0.0021	0.0024	0.0017	0.0135	0.0150	0.0149	0.0252	0.0289	0.0220	0.3700	0.4552	0.4327
	C	0.0006	0.0007	0.0005	0.0012	0.0014	0.0014	0.0427	0.0483	0.0367	0.1162	0.1424	0.1340
	D	0.0076	0.0087	0.0066	0.0090	0.0094	0.0094	0.1725	0.1965	0.1500	0.1956	0.2117	0.2095
	E	0.0011	0.0013	0.0009	0.0030	0.0034	0.0033	0.0303	0.0347	0.0261	0.1122	0.1405	0.1313
	F	0.0013	0.0014	0.0011	0.0019	0.0022	0.0021	0.0511	0.0585	0.0445	0.0899	0.1128	0.1051
	G	0.0006	0.0007	0.0005	0.0039	0.0045	0.0043	0.0118	0.0135	0.0104	0.1215	0.1510	0.1406
	H	0.0015	0.0018	0.0013	0.0023	0.0026	0.0026	0.0520	0.0596	0.0457	0.1129	0.1430	0.1327
SO ₂ µg/m ³	A	0.0075	0.0065	0.0047				0.0825	0.0689	0.0522			
	B	0.0052	0.0046	0.0032				0.0638	0.0559	0.0421			
	C	0.0015	0.0013	0.0010				0.1080	0.0936	0.0702			
	D	0.0193	0.0168	0.0127				0.4364	0.3804	0.2867			
	E	0.0028	0.0025	0.0018				0.0767	0.0671	0.0499			
	F	0.0032	0.0028	0.0020				0.1294	0.1134	0.0851			
	G	0.0015	0.0013	0.0010				0.0298	0.0262	0.0199			
	H	0.0039	0.0034	0.0025				0.1317	0.1154	0.0873			
NO _x µg/m ³	A	0.0221	0.0221	0.0252				0.2442	0.2341	0.2801			
	B	0.0155	0.0156	0.0174				0.1890	0.1897	0.2261			
	C	0.0045	0.0045	0.0052				0.3198	0.3177	0.3768			
	D	0.0571	0.0571	0.0679				1.2922	1.2918	1.5391			
	E	0.0084	0.0084	0.0095				0.2270	0.2279	0.2679			
	F	0.0094	0.0093	0.0109				0.3831	0.3849	0.4566			
	G	0.0044	0.0044	0.0053				0.0883	0.0890	0.1067			
	H	0.0115	0.0116	0.0134				0.3898	0.3917	0.4687			

Appendix XIX: Discrete receptor sample run (8-hour and 1-hour concentrations)

		8-HOUR CONCENTRATION						1-HOUR CONCENTRATION					
		Cement Factory 1			Cement Factory 2			Cement Factory 1			Cement Factory 2		
		Run 1	Run 2	Run 3	Run 1	Run 2	Run 3	Run 1	Run 2	Run 3	Run 1	Run 2	Run 3
CO ₂ µg/m ³	A	1114.5	817.0	959.7	59.65	29.67	29.03	5502.7	4014.4	4714.9	357.9	178.0	174.2
	B	692.4	533.1	540.6	101.24	50.20	48.89	1837.3	1414.9	1661.8	569.4	283.2	278.1
	C	922.2	669.5	735.1	39.64	19.69	19.18	5533.0	4017.2	4517.1	209.0	104.0	101.6
	D	3348.9	2552.0	2979.2	63.40	31.04	29.20	13828.2	10521.5	12266.9	343.0	167.5	156.4
	E	635.7	488.6	526.8	45.63	22.65	22.21	3573.3	2740.6	3170.2	273.8	135.9	133.3
	F	1664.0	1278.6	1489.5	36.21	17.97	17.52	8485.3	6407.0	7517.0	219.4	109.1	106.7
	G	294.9	227.2	267.4	42.63	21.16	20.61	2123.3	1635.2	1924.8	294.1	146.1	142.2
	H	1693.6	1301.4	1528.9	39.70	19.75	19.36	8441.3	6343.6	7473.1	277.9	138.3	135.5
CO µg/m ³	A	0.0309	0.0319	0.0247				0.1526	0.1569	0.1215			
	B	0.0192	0.0208	0.0139				0.0510	0.0553	0.0428			
	C	0.0256	0.0262	0.0189				0.1534	0.1570	0.1164			
	D	0.0929	0.0997	0.0768				0.3835	0.4112	0.3161			
	E	0.0176	0.0191	0.0136				0.0991	0.1071	0.0817			
	F	0.0461	0.0500	0.0384				0.2353	0.2504	0.1937			
	G	0.0082	0.0089	0.0069				0.0589	0.0639	0.0496			
	H	0.0470	0.0509	0.0394				0.2341	0.2479	0.1926			